A novel cell and gene therapy approach for Friedreich's ataxia

A thesis submitted for the degree of Doctor of Philosophy by

Enas Shaban

January 2020

Abstract

Friedreich's ataxia (FA) is an autosomal-recessive, neurodegenerative incapacitating disease that mainly affects the nervous system and heart, and has a significant effect on the life of affected individuals. FA is closely correlated with the frequency of large normal FXN alleles (>12 GAA motifs) in the population. It is characterised clinically by early onset (usually in childhood or adolescence) spinocerebellar ataxia, dysarthria, proximal weakness, sensory loss, and cardiomyopathy, and leads to dependence on a wheelchair and reduced life expectancy to usually between 40-50 years. It is caused by GAA expansions repeated in the first intron of the frataxin gene on chromosome 9. Trinucleotide expansions repeat in the gene and consequently cause an abnormal conformation in the DNA which leads to decreased transcription of the frataxin gene and therefore to reduced expression of the frataxin protein. Frataxin is a mitochondrial protein required for iron haemostasis and iron-sulphur cluster (Fe-S) formation and it plays an essential role in the protection of cells from oxidative damage. Decreased levels result in reduced iron-sulphur group creation, mitochondrial iron build-up, cytosolic iron diminution, oxidative stress and mitochondrial dysfunction. Several studies have shown that replacement of the frataxin can restore mitochondrial function. The main hypothesis of this research project is that a tissue-penetrating version of frataxin could be delivered to diseased tissues by genetically modified patient-derived haematopoietic stem cells. Therapeutic stem cells should be able to survive in the bone marrow for many years and migrate from their niche to differentiate into different cell lineages within various tissues, so the resultant delivery of frataxin would be continuous and long-term. To validate this strategy, we have generated frataxin fused to tissue penetrating peptides encoded by lentiviral vectors that we have used to infect human cell lines. We confirmed that the different frataxin peptides were secreted by HEK 293T cells and differentiated primary human haematopoietic stem cells. Importantly, supernatants containing the therapeutic peptides rescued the apoptotic phenotype and the aconitase activity deficit of fibroblasts isolated from Friedreich's patients cells. We have therefore validated a new cell and gene therapy approach that has the potential to provide a permanent cure for the disease.

Acknowledgements

I would like to extend my deepest gratitude to my supervisor Professor Arturo Sala, for accepting me as his student and for his guidance throughout my PhD.

I would like to extend my appreciation to Dr. Predrag Slijepcevic for all of his support and help. I am also very grateful to Dr. Mark Pook and Dr. Sahar Al-Mahdawi for their continual support.

I am truly grateful to Saqlain Suleman, Marianne Henry, Mursal Sherzai and Hajar Mikaeili Neil for their continual support, advice, and help.

I am blessed with a wonderful family whom I would like to thank very much for providing me with support every step of the way, especially my mum, Mrs. Badeia Elbishti and dad, Professor. Abdulfatah Shaban, my sisters, Dr. Nehal, Dr. Naila, and Dr. Aya and my brother Dr. Abduladem.

I am eternally grateful for my loving children and little angels, my daughter Basant and my son, Mohamedamen, and my husband Mohamed for believing in me and constantly encouraging me.

Table of Contents

Table of Figures

Table of Tables

Declaration

I hereby declare that the research presented in this thesis is my own work, except where otherwise specified, and has not been submitted for any other degree.

Enas Shaban

List of Abbreviations

APTX	Aprataxin
ATP	Adenosine triphosphate
AV	Aortic valve
BP	Base pair
cDNA	Complementary DNA
DMEM	Dulbecco's modified eagle's medium
DMSO	Dimethyl sulfoxide
DNA	Deoxyribonucleic acid
DRG	Dorsal root ganglion
DTT	Dithiothreitol
EC	Electrocardiogram
ECL	Enhanced chemiluminescent
EDTA	Ethylene diamine-tetra acetic
FBS	Foetal bovine serum
FRDA	Friedreich's ataxia
FXN	Frataxin
hFXN	Human frataxin
GAA	Guanine-adenine-adenine
H_2O	Water
H_2O_2	Hydrogen peroxide
HDAC	Histone deacetylase
IMS	Industrial methylated spirit
iPS	Induced pluripotent stem cells
iPSCs	Induced pluripotent stem cells
ISC	Iron-sulphur cluster

LA	Left atrium
LL	Lower limb
LV	Left ventricle
LVOT	Left ventricular outflow tract
MBP	Major Basic Protein
MOI	Multiplicity of infection
MPP	Mitochondrial processing peptidase
mRNA	Messenger RNA
mt-DNA	Mitochondrial DNA
MV	Mitral valve
NaCl	Sodium chloride
$NaHCO_3$	Sodium bicarbonate
OD	Optical density
PAGE	Polyacrylamide gel electrophoresis
PBS	Phosphate buffered saline
Pen/Strep	Penicillin and streptomycin
ROS	Reactive oxygen species
X g	Revolutions per minute
RT	Room temperature
SACS	Sacsin
SEM	Standard error of the mean
SETX	Senataxin
TAE	Tris-acetic acid
TE	Tris-EDTA
TNR	Trinucleotide repeat
TTPA	α-tocopherol transfer protein

Ml	Millilitre
µM	Micro molar

Chapter 1.

Introduction and literature review

Although Friedreich's ataxia is a rare disease, it is the most common cause of hereditary ataxias (Schulz *et al.*, 2009a). It is an autosomal-recessive, neurodegenerative debilitating illness that has a significant effect on the life of affected individuals, and affects the nervous system and heart (Bidichandani, Ashizawa and Patel, 1998). The clinical features of the disease include progressive gait and limb ataxia, muscular weakness, dysarthria, lower-limb areflexia, diminished vibration sense, a positive extensor plantar response (Schulz *et al.*, 2009), hypertrophic cardiomyopathy and diabetes (Harding, 1981).

1.1 Epidemiology

The highest prevalence of the disease is reported in Western Europe (1/30,000 in northwest Spain and Ireland), North Africa, the Middle East, and India (Schulz *et al.*, 2009). The prevalence of the disease is closely correlated to the frequency of large normal frataxin alleles (>12 GAA motifs) in the general population (Schulz *et al.*, 2009) and is rare in East Asia (Schulz *et al.*, 2009a).

Table 1-1. Frataxin allele distribution in healthy controls (Schulz et al., 2009a).

Reference	Allele frequencies			Ethnicity
	Short (<12 GAA repeats [%])	Long normal (>12 GAA repeats [%]	Expanded (>60 GAA repeats [%])	
Epplen et al. (1997)	83	16a	0.6	European (German)
Cossee et al. (1997)	83	17b	0.6	European (French)
Mukerji et al. (2000)	89	11	Not reported	Indian
Labuda et al. (2000)	88	12	Not reported	European
Labuda et al. (2000)	83	17	Not reported	African American

Labuda et al. (2000)	88	12	Not reported	Sub-Saharan African
Juvonen et al. (2002)	81	19c	0.3	European (French)
17–58 GAA repeats. B. 16–34 GAA repeats. C. 16–27 GAA repeats. D. 13–21 GAA repeats.				

The frequency of expanded alleles in control individuals can be used to estimate the incidence of Friedreich's ataxia (Schulz *et al.*, 2009a)(Table 1). The carriers of heterozygous mutation decline in frequency from south to north-east across Europe, from 1:78 in France to 1:89 in Germany and 1:500 in Finland; therefore the predictable prevalence of Friedreich's ataxia will be 4.2/100,000 in France, 3.1/100,000 in Germany and 0.13/100,000 in Finland (Schulz *et al.*, 2009a). It is also expected that the prevalence will be 4.7/100,000 in Spain, 1.8/100,000 in the UK, between 0.5/100,000 and 1/100,00 in Denmark, 1/100,000 in Norway. 0.23/100,000 in Sweden and 0.13/100,000 in Finland (Cossee *et al.*, 1997).

1.2 Pathology

The main affected areas in Friedreich's ataxia are the dorsal root ganglion, the posterior column of the spinal cord, the corticospinal tracts and the heart (Koppen, 2019) (Figure 1-1). Degenerative changes usually start in the dorsal root ganglia (Bürk, 2017). The loss of sensory ganglion cells and degeneration of their axons in peripheral dorsal roots and the posterior column deprive the cerebellum of the sensory input that is considered crucial for movement coordination (Bürk, 2017). There is also a loss of transsynaptic neurons in the dorsal nuclei of Clarke and degeneration of the dorsal spinocerebellar tract (Bürk, 2017) (Figure 1-2).

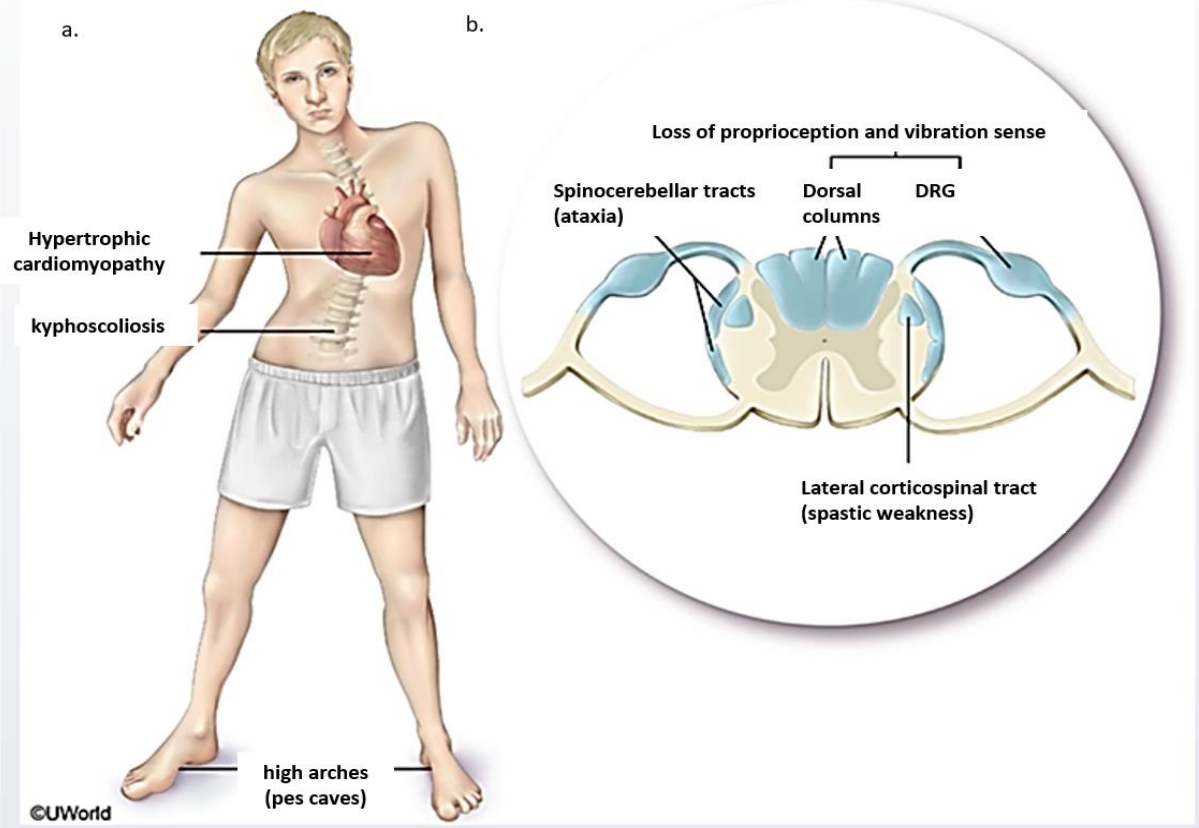

Figure 1-1. Overview of the main sites of neuronal loss and organ dysfunction in Friedreich ataxia.

Pathological features are shown in the a) hypertrophic cardiomyopathy, kyphoscoliosis, high arches (pes caves); b) spinal cord degeneration (UWorld).

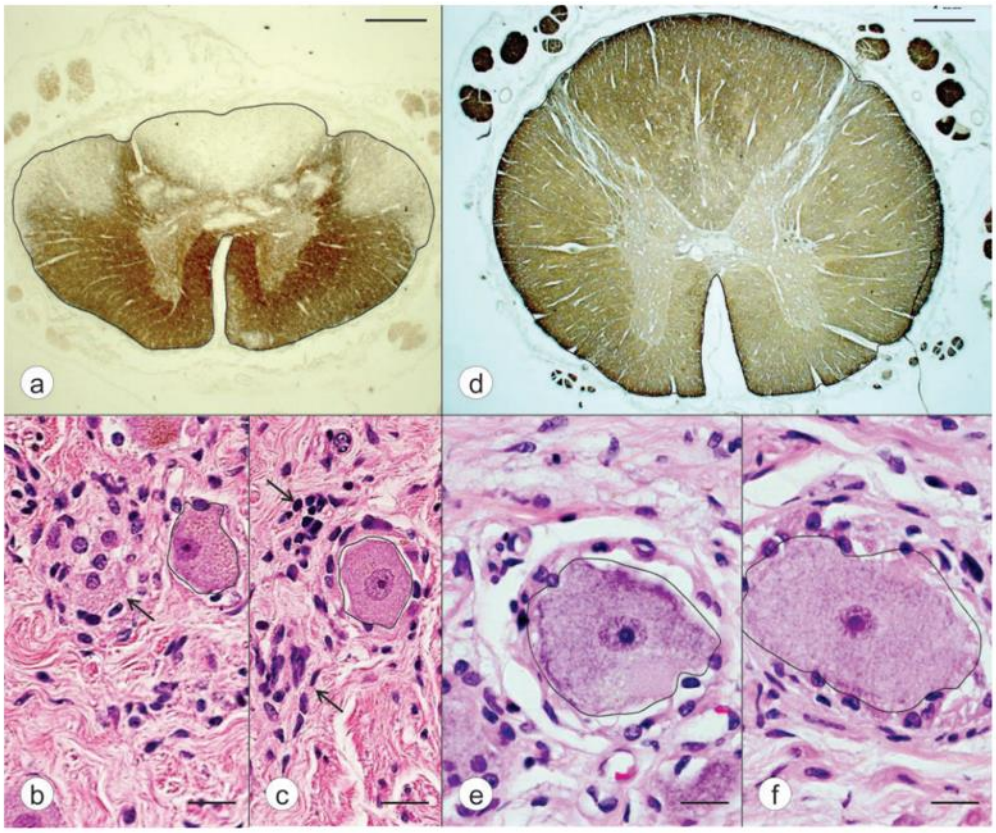

Figure 1-2. Thoracic spinal cord and DRG neurons in FRDA

(a–c) FRDA; (d–f) normal control. (a, d) Immunostain of MBP (major basic protein); (b, c, e, f) hematoxylin and eosin. The transverse section of the thoracic spinal cord in FRDA (a) shows the overall reduction in size and the characteristic symmetrical loss of myelinated fibers in dorsal columns, dorsal spinocerebellar, and lateral corticospinal tracts. In FRDA, neurons were generally smaller (b, c). The section shown in (c) reveals residual nodules (arrows). In (b), a neuron is undergoing active invasion by satellite cells or monocytes (arrow). Scale bars: a, d, 1 mm; b, c, e, f, 20 mm (Koeppen, 2011).

The cerebellar cortex is not affected, but there is damage to neurons in the dentate nuclei (Koeppen *et al.*, 2007), which is the primary site of cerebellar output, and degeneration of the superior cerebellar peduncles (Koeppen *et al.*, 2007). There is also damage to the upper motor neurons (Betz cells) and degeneration of the lateral corticospinal tracts (Koeppen *et al.*, 2007). Macroscopically, the diameter of the spinal cord is diminished at all levels; however, the thinning is more evident in the thoracic region (Koeppen, 2011) (Figure 1-3).

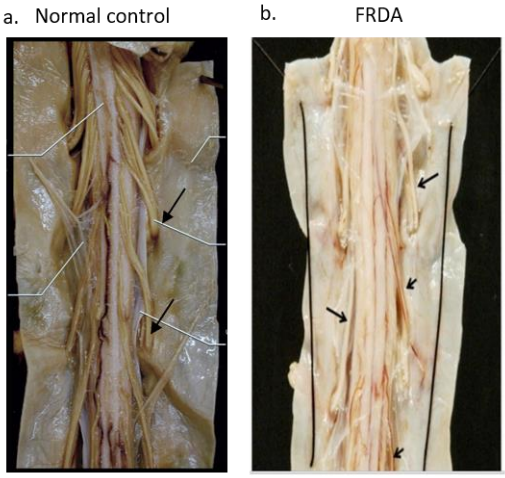

Figure 1-3. The spinal cord in FRDA.

a) normal control, b) FRDA. This view of the dorsal surface of the spinal cord shows normal thick white anterior roots (long arrows) in both spinal cords from normal control (a) and from FRDA (b) that stand out in contrast to thin dorsal roots (short arrows) in FRDA (b) (Koeppen, 2011).

1.3 Molecular genetics

FRDA is the only inherited trinucleotide expansion repeat (GAA) that is autosomally recessive (Figure 1-4) (Schulz *et al.*, 2009). Trinucleotide expansions repeat in the gene and consequently cause an abnormal conformation in the DNA which leads to decreased transcription of the frataxin gene and therefore reduced expression of the frataxin protein (Bidichandani, Ashizawa and Patel, 1998). Ninety-five per cent of affected individuals are homozygous for the GAA repeat expansion in the first intron of the frataxin gene (FXN) on chromosome 9q21.11 (Figure 1-5) (Bidichandani, Ashizawa and Patel, 1998). The other 5% are compound heterozygotes with an expansion on one allele and mutations on the other (Bidichandani, Ashizawa and Patel, 1998).

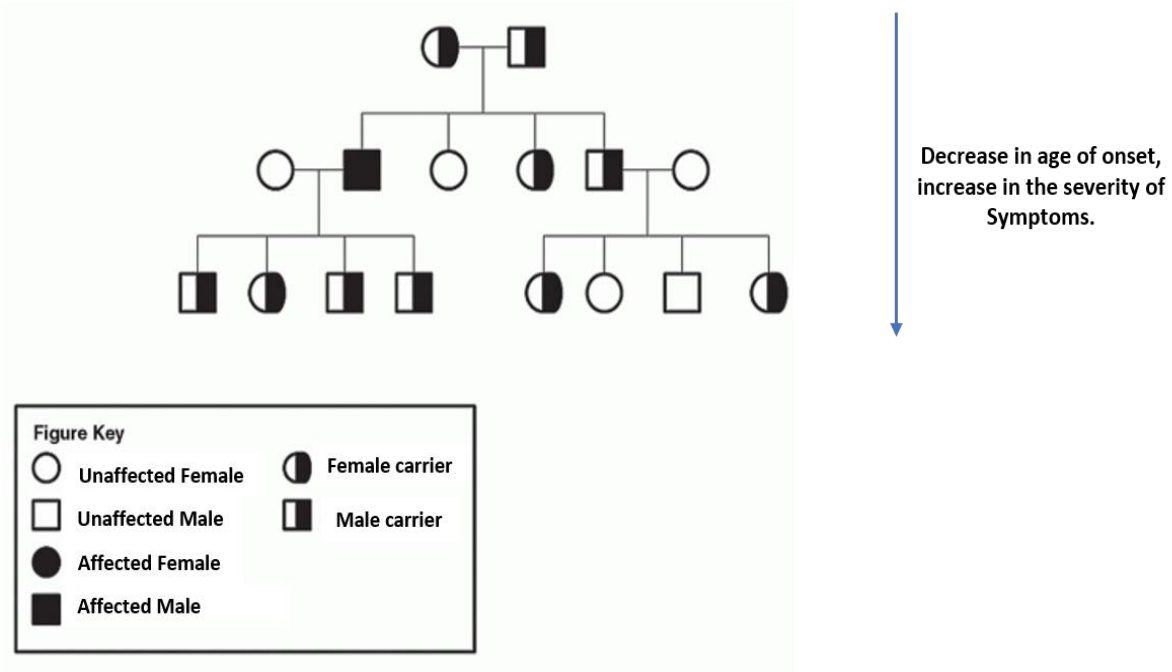

Figure 1-4. The pedigree of a family affected by Friedreich's Ataxia (fictional).

Due to the nature of the inheritance, the seriousness of symptoms rises while the age of onset reduces with each generation. Heterozygous individuals who have one allele along with the repeat expansion do not develop symptoms and are thus unaffected carriers. The expression of Friedreich's Ataxia happens only when a person carries two mutated frataxin alleles (UNSW Embryology).

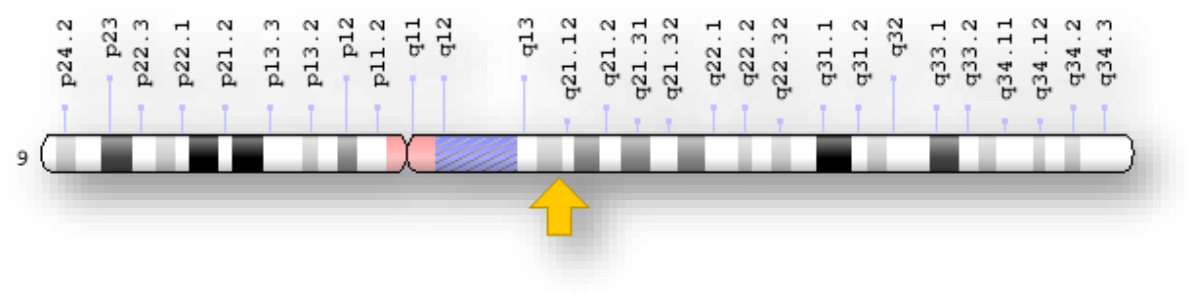

Figure 1-5. location of the frataxin gene on chromosome 9. (UNSW Embryology)

Until recently, there have been no reported cases of symptomatic carriers, although frataxin expression is significantly reduced (Tsou *et al.*, 2011). Less than ten trinucleotides repeat is known as short and more than 11 triplets are long normal alleles (Schöls *et al.*, 1997). Long normal more than 30 are more susceptible to pathogenic expansion (Schöls *et al.*, 1997). Expansion associated with FRDA varies from 44 to 1,700 repeats with most of the abnormal alleles ranging from 600 to 900 GAAs (Figure 1-6) (Schöls *et al.*, 1997). The GAA repeat in FRDA is considered to be unstable when transmitted from parent to offspring (Schöls *et al.*, 1997). Maternal transmission leads to either larger or smaller alleles in offspring, while paternal transmission always results in a decrease in the size of the triplet GAA repeat in the offspring (Schöls *et al.*, 1997). The instability of the GAA expansion repeat is influenced by the size, as smaller alleles are subjected to growth in size and larger alleles are more likely to decline in size (Schöls *et al.*, 1997). An atypical FRDA phenotype has been related to excessively long or short alleles and point mutation (Gellera *et al.*, 2007). The activity of the frataxin is impaired by nonsense, missense, deletion/insertion nucleotide change, and extensive deletion (Gellera *et al.*, 2007). The disease manifestation in mixed heterozygotes varies from classical FRDA in which the tendon reflexes are maintained, significant spasticity, mild or absent cerebellar symptoms, and a milder course of disease progression (Gellera *et al.*, 2007). An early manifestation of the illness is commonly seen in deletions, and rapid progression and severe phenotypes of the disease with the increasing

incidence of non-neurological symptoms (Bürk, 2017). Several studies have shown that FRDA has the highest level of expression in the heart and spinal cord, intermediate levels in the cerebellum, skeletal muscle, liver and pancreas, and limited expression in the cerebral cortex in which the mRNA levels were very low or undetectable (Delatycki, Williamson and Forrest, 2000). Protein levels were also low, but not absent (Delatycki, Williamson and Forrest, 2000). It has been found that the size of the GAA repeat correlates inversely with the level of residual frataxin (Bürk, 2017). The decreased levels of mRNA are the consequence of transcription inhibition and inversely correlated to the size of the GAA repeat (Bürk, 2017). The repeat forms an unusual DNA structure and this interrupts transcription (Bürk, 2017).

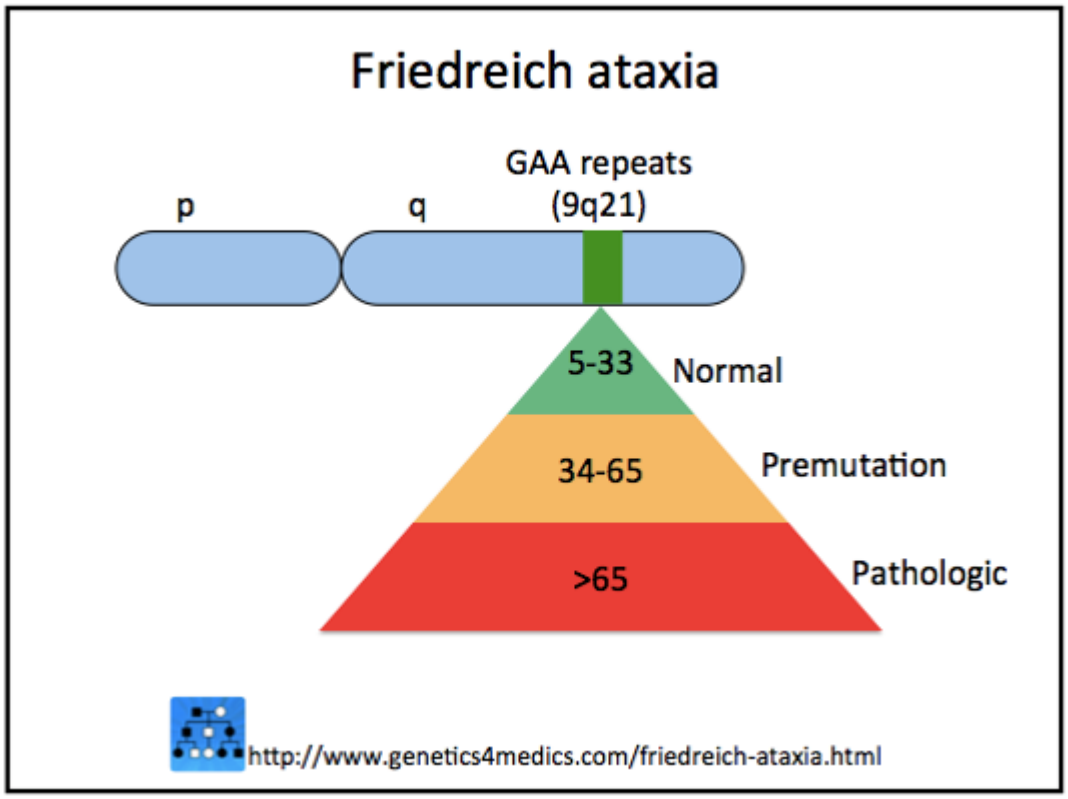

Figure 1-6. GAA repeats in Friedreich ataxia

1.3 Gene regulation and epigenetics in Friedreich's ataxia

1.3.1 Deficiency of FXN mRNA

The reduced level of frataxin mRNA could be the effect of the intronic repeats on transcription (Buratowski, 2011), or it could be a result of some post-transcriptional event (Buratowski, 2011). *In vitro* studies have shown that transcription of templates that have as few as 11 GAA expansion repeats could result in shorter RNA than templates with no repeats (Grabczyk and Usdin, 2000). The repeats result in a mixture of odd secondary structures under the same conditions (Grabczyk and Usdin, 2000), such as purine:purine: pyrimidine and pyrimidine:purine: pyrimidine triplexes (Figure 1-7) (Grabczyk and Usdin, 2000; Potaman *et al.*, 2004) and a related structure is known as sticky DNA (Sakamoto *et al.*, 1999). Studies have shown that triplex formation could affect the transcription by sequestering transcription factors or RNA polymerase (RNAP) (Kohwi and Kohwi-Shigematsu, 1991; Sakamoto *et al.*, 1999). It could be that a pre-existing triplex or sticky DNA pauses RNAP by making it harder for the transcription complex to unwind the template (LeProust *et al.*, 2000).

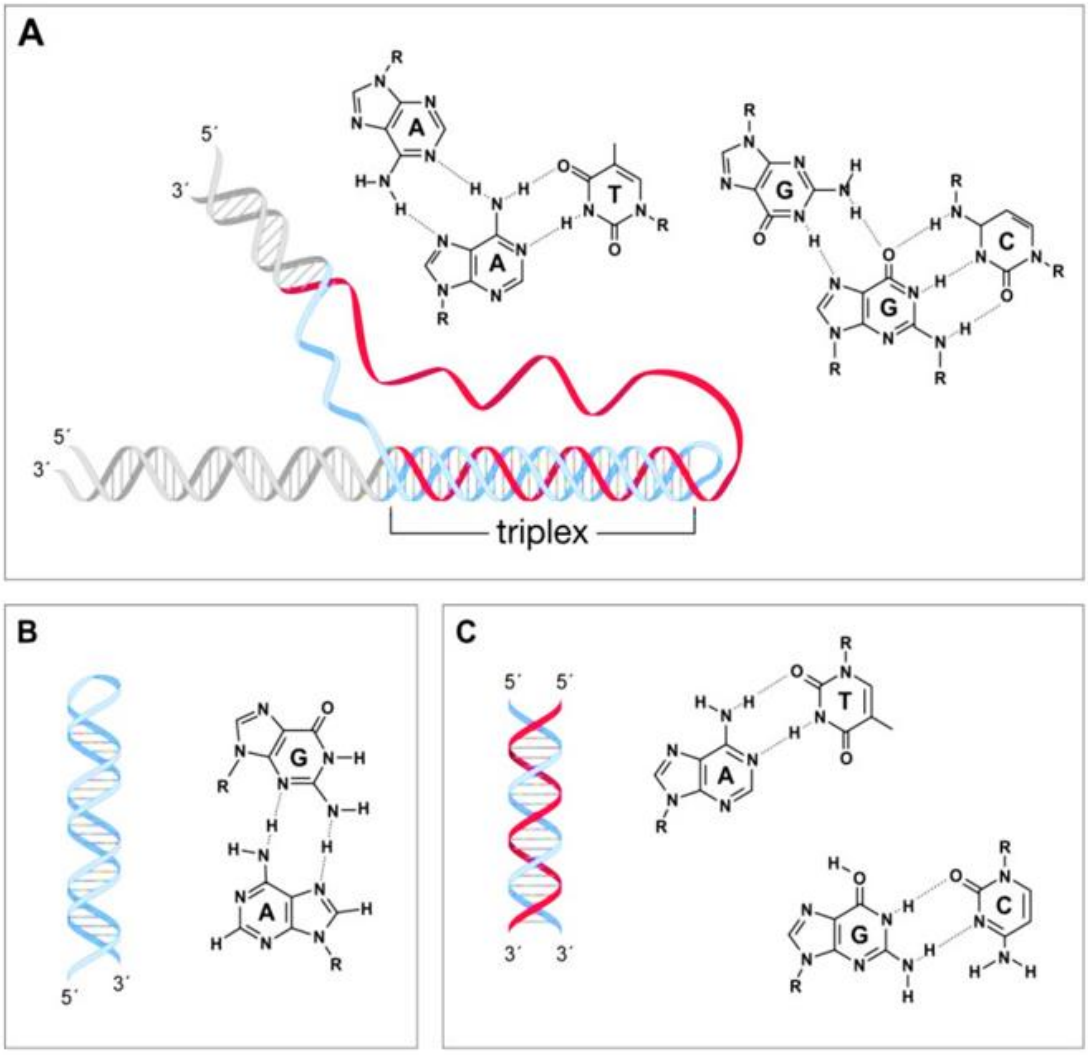

Figure 1-7. Structures created by GAA repeats demonstrating their constituent hydrogen bonding schemes.

a) A purine:purine: pyrimidine triplex (Grabczyk and Usdin, 2000; Potaman *et al.*, 2004) b) A GAA hairpin (Papers *et al.*, 2001). Several hydrogens bonding schemes (Chou, Chin and Wang, 2003) c) A parallel duplex (LeProust *et al.*, 2000).

In addition to the triplex formation, there is also evidence that triplexes formed during transcription *in vitro* could form an RNA: DNA hybrid (Figure 1-8) (Bentin *et al.*, 2005). This would cease transcription and trap RNAP on the template at the end of the repeat (Bentin *et al.*, 2005).

Other situations could cause the formation of R-loops may also affect transcription (Bentin *et al.*, 2005).

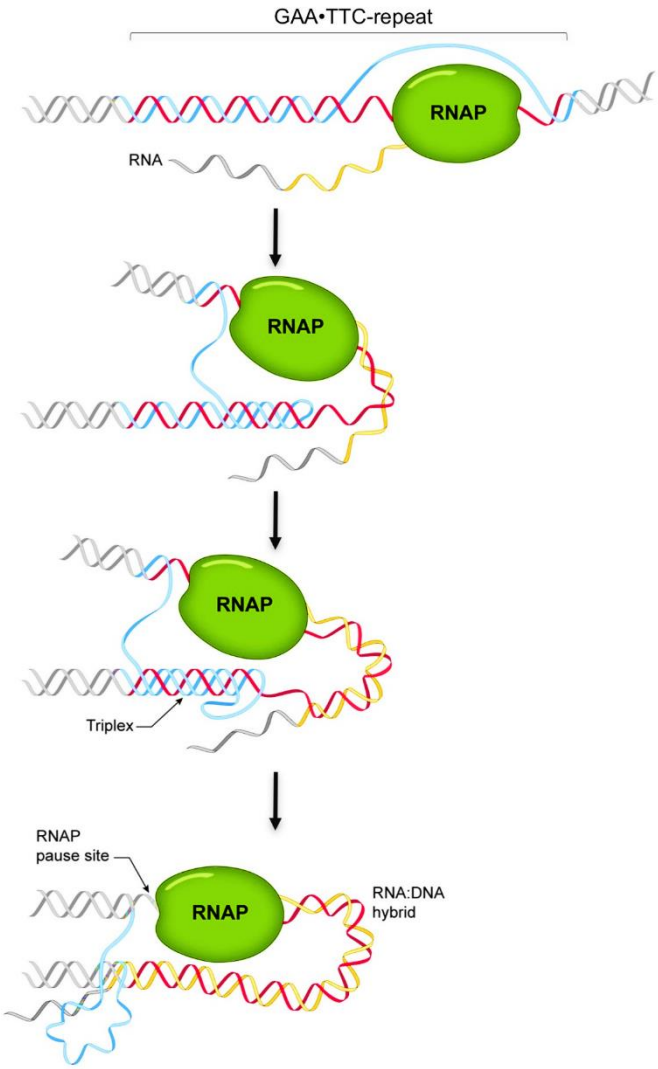

Figure 1-8. A triplex/RNA: DNA hybrid model for Friedreich ataxia (FRDA) (Grabczyk and Usdin, 2000; Potaman et al., 2004).

1.3.2 Epigenetics in Friedreich's ataxia

The process of packing DNA into a chromosome in a eukaryotic nucleus is started by folding the DNA around histone proteins to develop a nucleosome, which is the main subunit of chromatin

(Bannister *et al.*, 2001; Kouzarides, 2007). The chromatin can be packed less densely, which makes it easy to access for RNA polymerase (RNAPII) (euchromatin), or it could be packed tightly, which makes it more difficult (heterochromatin) (Bannister *et al.*, 2001; Kouzarides, 2007). The accessibility of chromatin is largely determined by the interaction of DNA with histone proteins (Bannister *et al.*, 2001; Kouzarides, 2007) (Figure 1-9).

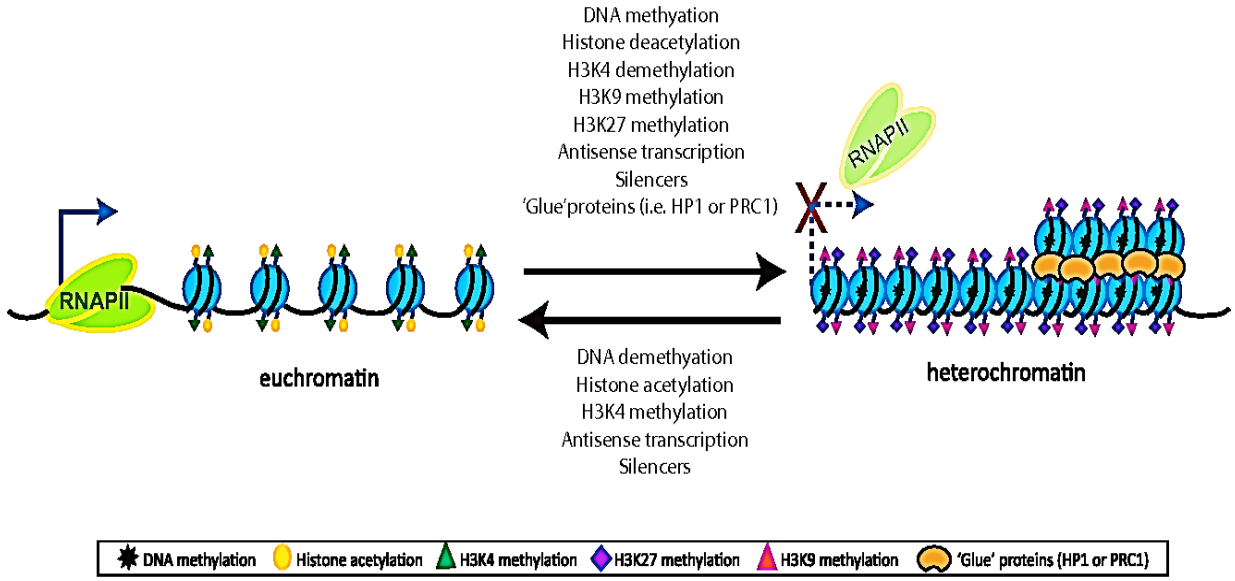

Figure 1-9. Competition among euchromatin and heterochromatin.

Effortlessly accessible euchromatin is linked with DNA demethylation, histone acetylation, and H3K4 methylation. On the other hand, inaccessible and tightly packed heterochromatin is correlated to DNA methylation, histone deacetylation, H3K4 demethylation, H3K9, and H3K27 methylation (Bannister *et al.*, 2001; Kouzarides, 2007).

Around 55% of the human genome is made of repetitive DNA sequences (Yoder, Walsh and Bestor, 1997); heterochromatin is believed to have developed as a defensive response to the disruptive effect of transcriptional errors (Yoder, Walsh and Bestor, 1997). Studies have shown that repetitive DNA DNA sequences are related to genomic instability in cancer and aging (Schulz, Steinhoff, and Florl, 2006; Belancio, Hedges and Deininger, 2008; Ting *et al.*, 2013). Heterochromatinisation of repetitive DNA is crucial for the preservation of nuclear architecture

that is required for the spatial organisation of centromeres and sister chromatid segregation during cell division (Fisher and Merkenschlager, 2002; Peters, Tedeschi and Schmitz, 2008).

There are three steps in the epigenetic mechanism (Beisel and Paro, 2011). It is started by the movement of specific silencing complexes towards the DNA sequences to be inactivated (Bannister *et al.*, 2001; Kouzarides, 2007), followed by the inhibition of RNA polymerase or other nuclear enzymes (Bannister *et al.*, 2001; Kouzarides, 2007). Finally comes the propagation of silent chromatin into the daughter cells (Beisel and Paro, 2011). These findings highlighted the potential role of epigenetic mechanisms in FRDA and indicate that long GAA expansion repeats could repress the expression of an adjacent heterochromatin-sensitive cell surface reporter gene (hCD2) by a phenomenon called position effect variegation (PEV) (Evans-galea *et al.*, 2012) (Figure 1-10).

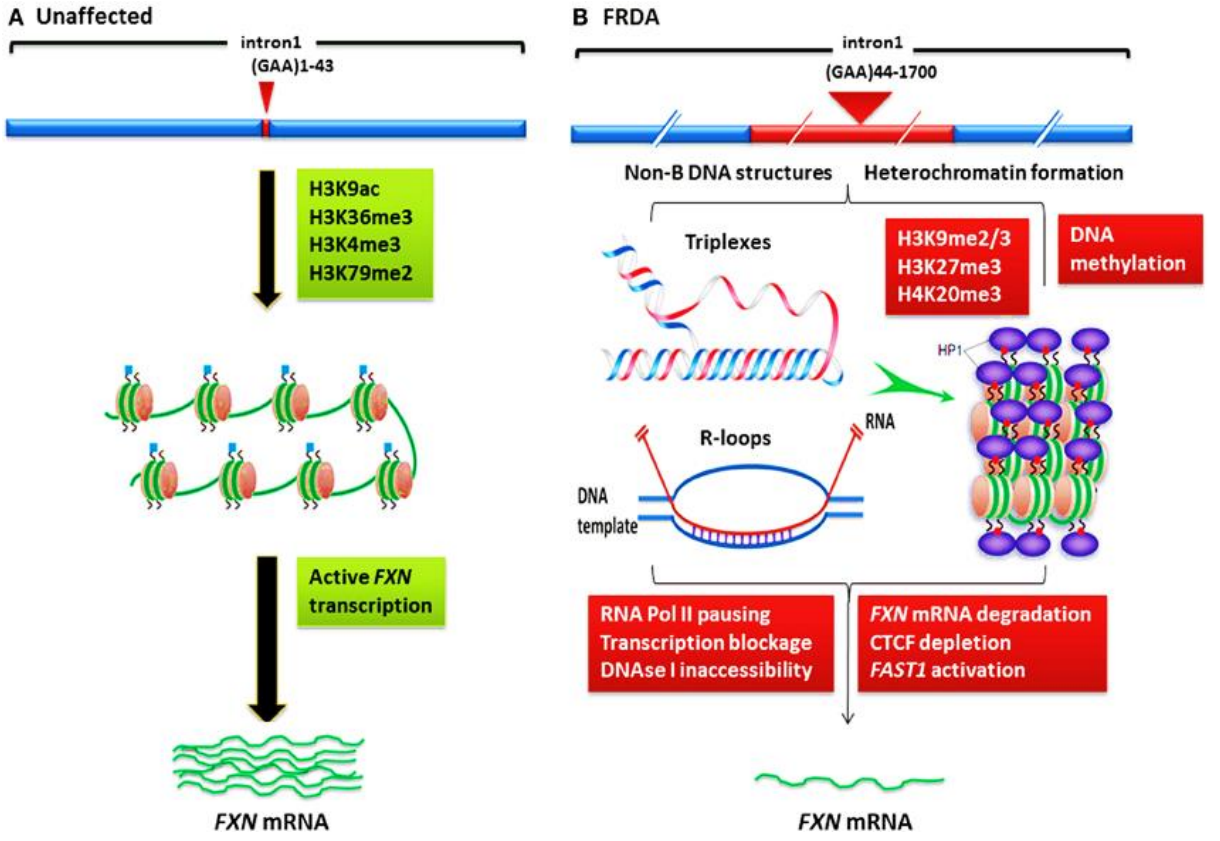

Figure 1-10. Models of Frataxin gene silencing in FRDA.

a) healthy people who carry up to 43 GAA repeats include active histone marks of gene transcription initiation and elongation at the *FXN* promoter and intron 1 regions. b) In Fredrich patients, the occurrence of a large GAA repeat expansion cause frataxin gene silencing by two possible mechanisms: (i) the GAA repeat could form an abnormal non-B DNA structures (triplexes) or DNA•RNA hybrid structures (R loops), which obstruct the process of RNA polymerase and hence decrease frataxin gene transcription. (ii) increased levels of DNA methylation and HP1 and significant enrichment of repressive histone marks at the frataxin gene cause heterochromatin formation that can lead to further obvious frataxin gene silencing (Chan *et al.*, 2013)

The following sections summarise the significant findings related to epigenetic gene silencing in FRDA.

1.3.3 DNA methylation

This is defined as the covalent modification of DNA by adding a methyl residue to cytosine bases (Robertson, 2001). It is one of the most highly investigated epigenetic mechanisms in many diseases, such as cancer (Robertson, 2001), where it maintains a stable gene silencing mechanism

that is crucial for regulating gene expression and chromatin architecture (Robertson, 2001). There have been two large-scale studies on peripheral blood mononuclear cells which indicated that the frataxin gene that is located upstream of the GAA expansion repeat demonstrates higher levels of DNA methylation on the pathologically-silenced frataxin gene locus (Castaldo *et al.*, 2008; Evans-galea *et al.*, 2012). In both studies, a negative correlation was found between age at the onset of symptoms and the level of DNA methylation on the frataxin gene.

The studies also indicated that there is a positive correlation between frataxin gene silencing, illness severity, and the level of DNA methylation.

1.3.4 Histone modifications

In eukaryotes, the essential building unit of the chromatin structure is the nucleosome (Kouzarides, 2007). It is of an octamer of two copies of each of the four histone proteins, H2A, H2B, H3, and H4 with 147 bp of DNA (Kouzarides, 2007). These histone proteins consist of a globular C-terminal domain and an unstructured N-terminal tail (Kouzarides, 2007). The histone tail is made of various modified residues (Kouzarides, 2007). Different histone modifications can control gene expression by making the genetic loci either more or less accessible to the transcriptional process (Kouzarides, 2007). Previous studies have shown that silenced a frataxin locus with GAA repeat expansion demonstrates histone modification changes and has an increased level of heterochromatin marks (Ohno, Fukagawa and Lee, 2002; Saveliev, Everett and Sharpe, 2003).

1.3.5 Antisense transcription

Antisense transcription is characterised by the transcription of the antisense strand to the protein-coding or sense strand (Khalil *et al.*, 2008). Recent research has indicated that antisense transcripts can be found in many genes, including non-pathogenic alleles; these are known as natural antisense transcripts (NATs) (Khalil *et al.*, 2008). Microsatellite repeat expansion diseases such as Friedreich's ataxia have been associated with NATs (Khalil *et al.*, 2008). Other studies have demonstrated a relationship between heterochromatin and antisense transcription (De Biase *et al.*, 2009), and it has been shown that there is a frataxin antisense transcript (*FXN*

antisense transcript 1', FAST1) (De Biase *et al.*, 2009) found at a higher level in fibroblasts from FRDA patients compared to healthy cells (De Biase *et al.*, 2009).

1.4 Frataxin

Frataxin is a small protein of only 23 KDa. The mature form consists of 81-210 amino acids (Cook, 2010; Schmucker *et al.*, 2008). Human frataxin is synthesised in the cytoplasm and then imported to the mitochondria through a signal peptide (Schmucker *et al.*, 2008). In the mitochondria, the N-terminal is removed in two sequential steps of proteolysis (Schmucker *et al.*, 2008) and the protein is processed to give the intermediate form, 169-amino acid with a MW of 18,826 KDa and then the mature form, 81-210 amino acids with a MW of 14,268 KDa (Schmucker *et al.*, 2008). The processed form of frataxin is a globular compact peptide that is comprised of an N terminal helix, a middle-sheet region composed of seven strands, a second helix, and a C-terminus in an extended conformation (Dhe-Paganon et al., 2000). These helices are folded around the sheet, with the C-terminal filling a groove between the helices. The outer surface has a ridge of negatively charged residues and a patch of highly conserved hydrophobic residues. The acidic region is crucial for frataxin's function (Figure 1-11) (Dhe-Paganon et al., 2000).

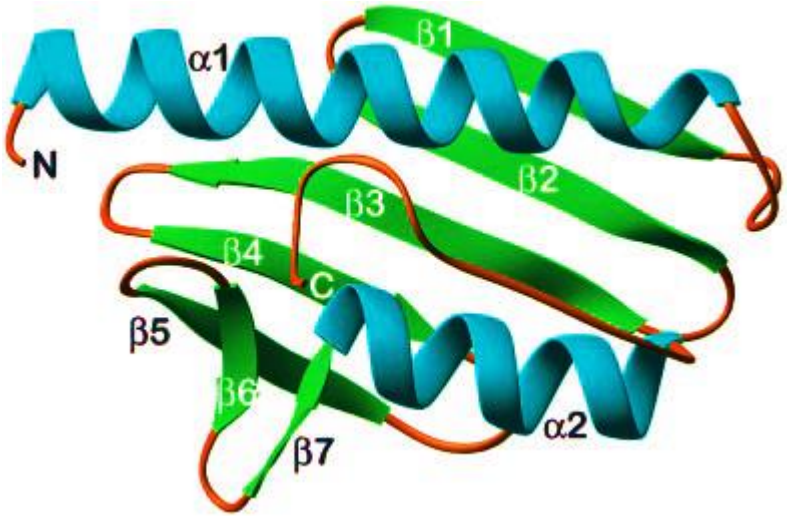

Figure 1-11. Structure of frataxin.

The graph is demonstrating the folds of frataxin, a compact αβ sandwich, along with a helices coloured turquoise and b strands in green. Strands β1– β5 create a flat antiparallel b sheet that interacts with the two helices, α1 and α2. The two helices are almost parallel to each other and to the plane of the large β sheet. A second smaller β sheet is created by the C terminus of β5 and strands β6 and β7 (Dhe-Paganon et al., 2000).

1.5 Frataxin function

Frataxin is a ubiquitous protein that is required for iron haemostasis (Cook, 2010). Although the exact role in regulating iron metabolism is still not yet well understood, frataxin has been hypothesised to be involved several functions: 1) as an iron chaperone or donor during cellular heam- and iron-sulphur (Fe-S) cluster synthesis; 2) as an iron-storage protein in cases of iron overload; 3) in restoring oxidatively damaged Fe-S groups; 4) in the repair of oxidatively damaged aconitase Fe-S groups; 5) in the control the concentration of reactive oxygen species (ROS) production; and 6) as an active participant in pathways involved in energy conversion and oxidative phosphorylation (Cook, 2010) (Figure 1-12).

1.5.1 Frataxin as iron-binding protein

Frataxin can bind iron (the iron-bound form of frataxin), form iron-loaded oligomers, and regulate the redox chemistry (Cook, 2010). *In vitro* studies have shown that yeast (*Saccharomyces*

cerevisiae) and bacterial (*Escherichia coli*) orthologues of frataxin homo-oligomerise in the presence of an increasing concentration of ferrous iron and that these aggregates have the ability to store iron in a mineralised ferric state and have ferroxidase activity (Lane et al., 2013). The overexpression of human frataxin in *E. coli* leads to the assembly of a homo-oligomer which is capable of binding approximately ten iron ions per frataxin molecule (Cavadini *et al.*, 2002). This helps to keep iron in its inactive state and prevent it from redox cycling and limits iron-dependent oxidative stress (Gakh *et al.*, 2006).

1.5.2 Frataxin as an iron chaperone

It has been found that holo-frataxin (the iron-bound form of frataxin) has a high binding affinity for ferrochelatase, the enzyme responsible for the insertion of ferrous into protoporphyrin IX in the final step of haem synthesis; therefore, frataxin may function as an iron chaperone during haem synthesis and deliver iron directly to ferrochelatase and limit the toxicity of free iron in the cell (Yoon and Cowan, 2004). There is evidence that frataxin may function as an iron chaperone in the assembly of the iron-sulphur cluster (ISC) (Yoon and Cowan, 2003). ISCs play an essential role in several biological processes, including the electron transport chain and other regulatory and enzymatic processes (Rouault and Tong, 2005). Friedreich cells are deficient in ISC, especially mitochondrial ISC-containing subunits of respiratory chain complexes I, II and III, and aconitase activities (Lane and Richardson, 2010).

1.5.3 Frataxin as a metabolic regulator

Frataxin may function as a negative regulator of ISC biogenesis, which prevents the synthesis of ISC in cases of high iron availability (Lane *et al.*, 2013). Some studies have shown that frataxin may also have a role in the metabolic switch, which results in an increased input of iron into the haem synthesis pathway through ferrochelatase and a decrease in ISC biogenesis in cells that are going haem biosynthesis (Richardson et al., 2010; Huang et al., 2011; Lane & Richardson, 2010).

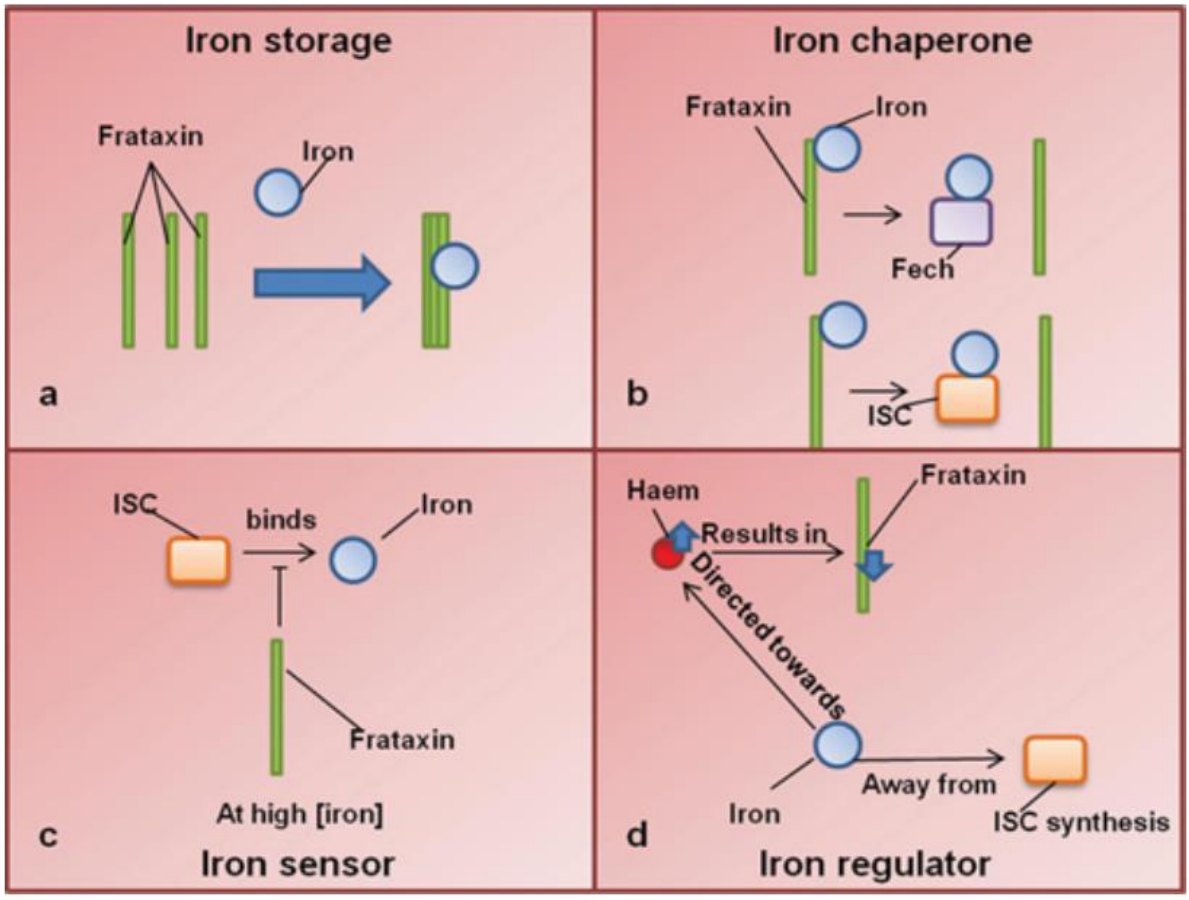

Figure 1-12. Projected functions of frataxin in iron metabolism.

Frataxin has been proposed to be engaged in several iron-related activities such as (a) iron storage, (b) acting as an iron chaperone, (c) iron sensing, and (d) iron regulation (Lane & Richardson, 2010).

The role of frataxin in iron-sulfur cluster synthesis

Iron-sulfur clusters are highly conserved and ubiquitous prosthetic groups of proteins (Rouault, 2012), made of iron and sulfide, that are present in almost all living organisms (Rouault, 2012). They play cardinal roles in various functions throughout the cell, including electron transport in the respiratory complexes, ATP production, and DNA repair or metabolism (Paul *et al.*, 2017). Therefore, decreased activity should significantly impair mitochondrial function(Paul *et al.*, 2017). Frataxin's role in iron–sulphur cluster biogenesis makes it essential for the enzymatic activity of iron-sulfur containing aconitase and respiratory chain complexes (Oliver and Lill, 2013).

Consequently, decreased frataxin levels result in decreased aconitase activity in cell culture models, *in vivo*, and heart tissues as shown in biopsies of FRDA patients (Clark *et al.*, 2018). These effects on key enzymes of energy production lead to a failure of ATP production in FRDA, as observed in humans in muscle spectroscopy (Clark *et al.*, 2018).

A growing number of genes involved in the synthesis of iron–sulphur clusters have been identified (Press and Doi, 2017). The process in the three systems can be divided into several steps: (i) release of sulfur from cysteine, catalyzed by a cysteine desulfurase; (ii) sulfur transfer, and cluster assembly by the scaffold proteins (Press and Doi, 2017). It has been suggested that frataxin participates in an additional step, specific of the ISC pathway, where the protein acts as an iron donor (Oliver and Lill, 2013). Finally, in the last step, the mature iron–sulphur cluster is transferred and inserted into the apoprotein (Oliver and Lill, 2013). Previous studies reported that frataxin deficiency results in decreased activity of iron–sulphur proteins such as succinate dehydrogenase and aconitase (Mouse *et al.*, 2013). Also, it was shown that frataxin deficiency causes impaired iron–sulphur proteins in other organisms such as conditional knockout mice, cultured human cells, and Arabidopsis knockdown plants (Mouse *et al.*, 2013).

Frataxin role as an iron chaperone protein to modulate mitochondrial aconitase activity

Aconitase is a Krebs-cycle enzyme that converts citrate to isocitrate, it belongs to the family of iron-sulfur–containing dehydratases whose activities depend on an intact $[4Fe\text{-}4S]^{2+}$ cluster (Lushchak *et al.*, 2014). The purified enzyme is highly susceptible to oxidant-induced inactivation (Lushchak *et al.*, 2014). Loss of mitochondrial aconitase activity is an intracellular indicator of superoxide generation and oxidative damage in a variety of degenerative diseases and aging (Cantu, Schaack and Patel, 2009). However, aconitase is rapidly inactivated when isolated rat cardiac mitochondria are treated with H_2O_2, suggesting that aconitase may be an intramitochondrial sensor of redox status (Cantu, Schaack and Patel, 2009). Frataxin can play a dynamic role in the regulation of aconitase activity during oxidative stress (Bulteau *et al.*, 2004). The roles for frataxin include (i) maintenance of iron in a bioavailable state; (ii) prevention of the production of potentially deleterious free radicals; (iii) protection of the $[4Fe\text{-}4S]^{2+}$ cluster from disassembly; and (iv) facilitation of Fe(II) transfer to the $[3Fe\text{-}4S]^{1+}$ cluster of aconitase (Bulteau

et al., 2004), resulting in reactivation of the enzyme. and converted inactive $[3Fe\text{-}4S]^{1+}$ enzyme to the active $[4Fe\text{-}4S]^{2+}$ form of the protein (Bulteau *et al.*, 2004).

1.6 Cellular effect of frataxin deficiency

1.6.1 Iron accumulation

In FRDA patients, iron accumulation has been detected in the heart, liver, and spleen, but not in the dorsal root ganglion, spinal cord, skeletal muscle, pancreas, cerebellum, or peripheral nerves (Lane *et al.*, 2013)**.** In frataxin-deficient cells, there is mitochondrial iron accumulation, which is the result of the up-regulation of cellular iron uptake, lower cytosolic iron storage, and increased uptake by the mitochondria with deficient incorporation into haem and ISCs (Huang *et al*., 2011; Richardson *et al*., 2010).

1.6.2 Oxidative stress

Iron accumulation within the mitochondria results in the production of profoundly damaging and reactive hydroxyl radicals through Fenton's reaction (Lane *et al.*, 2013):

$$Fe^{2+} + H_2O_2 \rightarrow Fe^{3+} + OH^- + {}^{\bullet}OH$$

The collection of mitochondrial iron results in oxidative stress and free radical-induced cytotoxicity (Lane *et al.*, 2013). It has been shown from FRDA animal and cell models that low frataxin levels cause autophagy, a phenomenon that occurs due to intracellular degradation of protein that provides amino acid supply during starvation. However, ROS can attenuate the lysosomal membrane, and this can affect the operation of autophagy (Bürk, 2017). Apoptosis is considered to be an alternative mechanism in autophagy failure (Bürk, 2017).

1.7 Clinical symptoms and diagnosis

Neurological manifestation of the disease usually appears around adolescence; however, early and late-onset variants have been recorded (Schulz *et al.*, 2009). The non-neurological manifestation, specifically pes cavus (Figure 1-14) and scoliosis (Figure 1-16) can appear many years before the neurological symptoms (Schulz *et al.*, 2009).

The clinical diagnostic criteria by Harding (1981) provides up to 90% specificity and 70% sensitivity and requires the presence of a slowly progressive, recessively inherited, ataxic disorder that

cannot be explained by any other primary cause, that the disease should start before the age of 25 years, that there should be areflexia of the lower limbs, and that dysarthria should become apparent within 5 years of disease onset (see Table 1-2). However, as the GAA repeat expansion in the first intron of the frataxin gene is the cause of Friedreich's ataxia, patients have frequently been diagnosed with the disease after the age of 25 (Schulz *et al.*, 2009a). In Friedreich's ataxia, there is absent or mild atrophy of the cerebellum. Contrary to the dominantly inherited ataxia, the ataxia in FRDA is the consequence of degeneration of the dorsal root ganglia neuron, which manifests as peripheral neuropathy and atrophy of the posterior column of the spinal cord and causes afferent ataxia. The patients present with hearing disability and vision impairment. Non-neurological manifestation includes hypertrophic cardiomyopathy and diabetes mellitus. The average life expectancy is usually between 40-50 years, although some patients may survive until their seventh or eight decades (Schulz *et al.*, 2009a).

Table 1-2. Diagnostic criteria for FRDA proposed by Geoffroy et al. (1976) and Harding (1981).

Criteria	Geoffroy *et a*l., 1976	Harding, 1981
Primary	(1) the onset of symptoms before the end of puberty (never after the age of 20 years), (2) progressive gait ataxia, (3) dysarthria, (4) absent of joint position or vibration sense, (5) loss of tendon reflexes in the legs, (6) muscle weakness	(1) the age of onset of symptoms before 25 years, (2) progressive ataxia of gait and limbs (3) loss of knee and ankle jerks
Secondary	(1) positive extensor plantar responses, (2) pes cavus, (3) scoliosis, (4) cardiomyopathy	(1) Dysarthria, (2) extensor plantar responses
Additional		If secondary criteria are absent, the following have to be present: (1) an affected sib fulfilling primary and secondary criteria, (2) median motor nerve conduction velocities of greater than 40 m/s thus excluding cases of type I hereditary motor and sensory neuropathy (HMSN)

1.8 Neurological manifestation

Although most sufferers have a loss of tendon reflexes in their lower limbs, patients can present with intact and even exaggerated reflexes, especially in late-onset disease (Schulz *et al.*, 2009a).

Oculomotor manifestation includes fixation instability with square waves, and gaze-evoked nystagmus can occur in up of one-third of patients (Fahey *et al.*, 2008). The absence of vibration and position sense is a consistent feature of the disease, but this may not be evident during the

early stages (Santos *et al.*, 2010) The pain and touch sensations may be normal during the early stages of the illness but decrease as the disease progresses (Bürk, 2017). Pyramidal manifestation includes a positive Babinski sign (extensor plantar response) (Figure 1-13) and progressive weakness, which become severe during the advanced stages of the disease (Koeppen and Mazurkiewicz, 2013). Muscle tone is often normal during the early stages, but as the condition progresses, there is a marked increase in tone (spasticity) and many patients start to complain of spasms, especially during the night (Schulz *et al.*, 2009a). Ataxia and poor coordination are the major causes that limit mobility, as muscle strength is relatively well preserved (Koeppen and Mazurkiewicz, 2013). Most patients become wheelchair-bound within 15 years of illness commencement (Bürk, 2017). The cranial nerves are frequently involved in FRDA patients and this usually manifests as impairment of ocular movements, visual field defects, hearing loss, dysarthria, and dysphagia (Schulz *et al.*, 2009a).

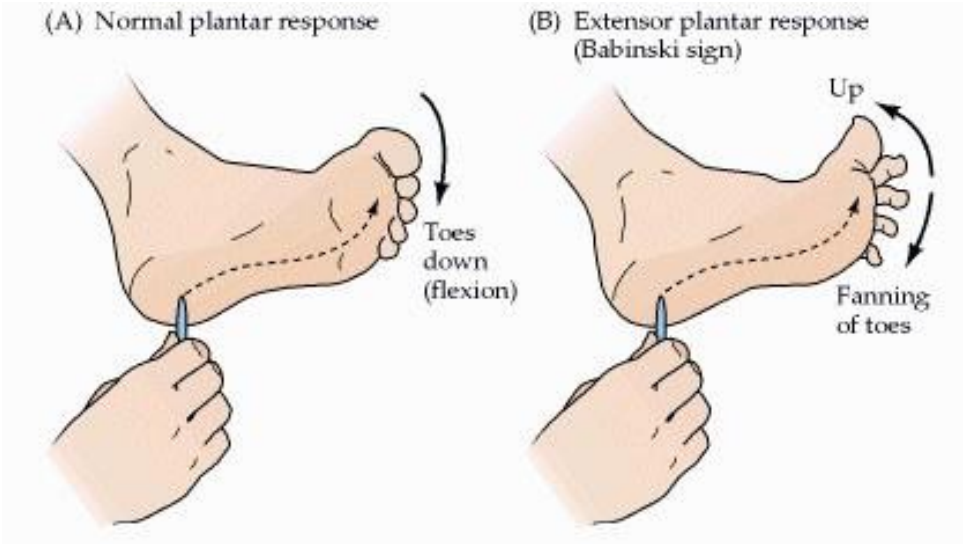

Figure 1-13. a) normal response which is plantar flexion. b) dorsiflexion of the big toe with fanning of the other toes.

1.8.1 Cardiac manifestation

Most patients with Friedreich's ataxia have cardiac involvement, which is considered to be the leading cause of disability and premature death, especially during the early stages of the disease (Pousset *et al.*, 2015; Hanson *et al*., 2019). This includes ventricular hypertrophy (Figure 1-14), conduction disturbance such as supraventricular ectopic beats, and atrial fibrillation (Hanson *et al*., 2019). Atrial fibrillations contribute to an increased risk of thromboembolic complications and heart failure (Payne and Wagner, 2012).

A minority of patients present with myocardial infarction and coronary heart disease, which could be related to diabetes (Report, 2007). A few patients may present with severe cardiomyopathy associated with a poor ejection fraction of the left ventricle and chronic heart failure (Report, 2007). Heart failure and supraventricular arrhythmias are the most reported causes of death in Friedreich patients (Störk, 2014).

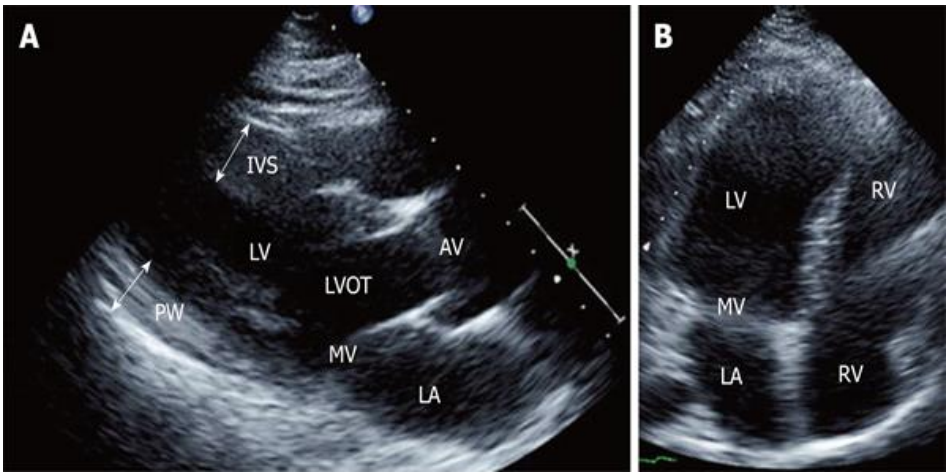

Figure 1-14. Two-dimensional echocardiography from a patient with Friedreich's ataxia.

a) Parasternal long-axis view showing thickening of the interventricular septum and posterior wall; b) Apical four-chamber view reveals dilatation of left ventricular cavity.

IVS: Interventricular septum; PW: Posterior wall; LV: Left ventricle; LA: Left atrium; MV: Mitral valve; AV: Aortic valve; LVOT: Left ventricular outflow tract (Hanson *et al*., 2019).

1.8.2 Skeletal system

Skeletal involvement, especially foot and spine deformities, is very common in Friedreich's ataxia (Nachbauer *et al.*, 2012) and up to 66% of cases can have hyperkyphosis (Koeppen, 2011) (Figure 1-15) which can be either a severe progressive type with the curve >60° or non-progressive with the curve >40° (Tsirikos and Smith, 2008). Progressive hyperkyphosis curve tends to occur before the age of 10 years, whereas the non-progressive hyperkyphosis curve usually occurs at or around puberty (Nachbauer *et al.*, 2012).

Pes cavus (high arched foot) occurs in up to 96% of cases (Milbrandt, Kunes and Karol, 2008) (Figure 1-16). Other joint involvement does not usually happen during the early course of the disease, but the limitation of range of motion in other joints may occur later as the disease progresses due to spasticity and immobility (Milbrandt, Kunes and Karol, 2008).

Figure 1-15. A) Posteroanterior and B) lateral radiograph of 13 year-old-male presenting with a severe left thoracolumbar scoliosis (Tsirikos and Smith, 2008).

Figure 1-16. Pes cavus foot deformity as a consequence of Friedreich's ataxia (Grice, Willmott and Taylor, 2016).

1.8.3 Metabolic manifestation in patients with Friedreich's ataxia

Patients with Friedreich's ataxia have an increased risk of developing diabetes mellitus (Delatycki *et al.*, 1999). This is usually the result of both insulin deficiency and insulin resistance, and according to some studies is correlated to the size of the GAA trinucleotide repeat (Coppola *et al.*, 2009; Cnop, Mulder and Igoillo-esteve, 2013). Hyperglycaemia usually develops at around 15 years after the onset of neurological manifestation and most of the patients typically present acutely with ketoacidosis as the first sign of diabetes (Cnop, Mulder and Igoillo-Esteve, 2013)(Grice, Willmott and Taylor, 2016).

Table 1-3. Percentage of the study population showing specific signs and complications of FRDA in three series.

	Harding	Dürr et al	Delatycki et al
Limb ataxia	99	99	100
Lower limb muscle weakness	88	67	-

Diminished vibration sense	73	78	88
Pes cavus	55	55	74
Dysarthria	97	91	95
Extensor plantar responses	89	79	74
Cardiomyopathy	66*	63	65
Diabetes	10	32	8
Scoliosis	79	60	78
Reflexes LL	0.9	12	2
Sphincter disturbance	_	23	41
Decreased visual acuity	18	13	_
Hearing loss	8	13	_

LL=lower limbs. —=not reported. *=dependent on abnormal ECG excluding 9.6% where ECG changes were described as insignificant (Delatycki, Williamson and Forrest, 2000).

1.9 Differential diagnosis

Various diseases can have presenting symptoms that are similar to FRDA; therefore, a careful clinical history with appropriate tests should be done to differentiate whether the cause of ataxia is a toxic, metabolic or paraneoplastic syndrome (see Table 1-4) (Schulz *et al.*, 2009a) The diagnosis of Friedreich's ataxia cannot be based on clinical manifestations alone, even when the patients presenting with atypical symptoms that make the possibilities of FRDA very unlikely such as late onset of the disease, spasticity or retained reflexes. It has been found that among patients with atypical presentation, around 15% tested positive for FRDA when genetically tested (Entezam *et al.*, 2017).

Table 1-4. Main clinical and genetic features of Friedreich's ataxia and recessive ataxias with similar clinical characteristics.

Feature	Friedreich's ataxia	Ataxia with vitamin E deficiency	Ataxia with oculomotor apraxia type 1	Ataxia with oculomotor apraxia type 2	Autosomal-recessive spastic ataxia of Charlevoix–Saguenay
The usual age of onset	<20 years (range Two years to >50 years)	<20 years (range 2–52 years)	<7 years (range Two years to young adult)	10–22 years	12–18 months
Cerebellar atrophy	Present only in advanced cases	sometimes	present	present	present
Pyramidal signs	Frequent	Absent	Absent	sometimes present	present
Peripheral neuropathy	Present (sensory axonal)	Present (sensory axonal)	Present (motor and sensory axonal)	Present (motor and sensory axonal)	Present
Other signs and symptoms	Kyphoscoliosis; pes cavus; optic atrophy; deafness; diabetes.	Head titubation; dystonia; retinopathy	Oculomotor apraxia; chorea; dystonia; low albumin and high cholesterol levels	Oculomotor apraxia; dystonia; chorea; tremor; cognitive impairment; high α-fetoprotein, creatine kinase, IgG, IgA and cholesterol levels	Myelinated optic nerve fibres in the retina; scoliosis; pes cavus
Cardiomyopathy	Present	Absent	Absent	Absent	(but mitral valve prolapse common)
Gene and nature of the mutation	FXN; GAA repeat expansion, rare point mutations (always in	TTPA; missense, nonsense, frameshift and splice-site	APTX; missense, nonsense, frameshift and splice-	SETX; loss-of-function missense, nonsense and truncating mutations;	SACS; missense mutations, deletions and insertions

	heterozygosity with GAA repeat expansion)	mutations, insertions and deletions	site mutations	large-scale rearrangements	
Postulated pathogenic mechanisms	Mitochondrial dysfunction	vitamin E deficiency (oxidative stress?)	Defective single-strand DNA break repair	Defective double-strand DNA break repair	impaired response to misfolded proteins
Abbreviation	APTX, aprataxin; FXN, frataxin; SACS, sacsin; SETX, senataxin; TTPA, α-tocopherol transfer protein (Schulz *et al.*, 2009)				

1.10 Treatment

Treatment approaches that target mitochondrial pathogenesis include the use of enhancers of mitochondrial function, free radical scavengers, iron chelator, and increased frataxin level (Villa *et al.*, 1988; Sturm *et al.*, 2005; Aranca *et al.*, 2016) (Figure 1-19).

1.10.1 Decrease oxidative stress and increased mitochondrial function

FRDA is characterised by impaired mitochondrial respiratory chain function and oxidative stress damage (Lane *et al.*, 2013). Therefore, patients could benefit from therapies that inhibit free radical formation (Aranca *et al.*, 2016).

Treatments that have been tested or are currently under investigation in Friedreich's patients include: L-acetylcarnitine idebenone (Raxone®/Catena0, Vincerinone® (EPI-743); Santhera Pharmaceuticals, Switzerland), coenzyme Q10, vitamin E, RTA-408 OX1®, resveratrol, and dPufas (Aranca *et al.*, 2016)

Idebenone

Idebenone (Raxone/Catena), an analogue of coenzyme Q10, is an antioxidant and a potent free-radical scavenger (Chan *et al.*, 2013), but research results for treatment of FRDA with idebenone have been inconclusive (Khalil *et al.*, 2008; Lynch, Perlman and Meier, 2010). A 6-month randomised, double-blind trial did not find a significant decrease in left ventricular (LV)

hypertrophy or improvement of cardiac function (Khalil *et al.*, 2008). It has also been found that Idebenone has no significant effect on the neurologic status of patients (Lynch, Perlman and Meier, 2010). Two other studies have reported a significant reduction of interventricular septal (IVS) thickness and LV mass, and a reduction of cardiac hypertrophy in subjects taking idebenone (Lynch, Perlman and Meier, 2010).

Vitamin E

Several researchers have studied the effect of coenzyme Q10 and vitamin E in Friedreich's patients (Lodi *et al.*, 2001), but the results were inconclusive. Some failed to find any consistent benefits in neurological and echocardiographic testing (Lodi *et al.*, 2001), although another found significant improvements in cardiac and skeletal muscle bioenergetics (Lodi *et al.*, 2001).

A0001 (α-tocopheryl quinone, Edison Pharmaceuticals)

A0001 is a potent antioxidant that has been evaluated in several studies; however, the results are inconclusive (Lynch *et al.*, 2012).

Resveratrol

Resveratrol is a natural phenol and an antioxidant that has been found to increase frataxin gene expression in FRDA animal models (Li *et al.*, 2013).

Acetylcarnitine

L-acetylcarnitine is a derivative of L-carnitine, a substance involved in fatty acid transport into the mitochondria (Zange *et al.*, 2005). Preclinical studies suggest L-acetylcarnitine can alter the levels of membrane proteins in the cerebellar mitochondria and thus may reduce oxidative stress (Villa *et al.*, 1988). Several studies investigated its effectiveness in Friedreich's patients; however, the results are considered to be controversial as it has shown a significant improvement in patient coordination, muscle tone in one study (Sorbi *et al.*, 2000), but no evidence of significant improvement in neurological deficit in another (Zange *et al.*, 2005).

Deuterated polyunsaturated fatty acids (D-PUFAs)

Studies of both animal and human FRDA fibroblasts have revealed the potential benefits of D-PUFAs in the reduction of oxidative stress (Lodi *et al.*, 2001). One agent, RT001, is currently in

Phase I/II study as a potential treatment for FRDA. RT001 is deuterated linoleic acid that has been chemically altered to enable its entry into the cell, where it has the potential to reduce oxidative stress in the mitochondria and increase ATP production (Ramberson *et al*., 2015).

1.10.2 Iron chelators

FRDA is characterised by frataxin deficiency, which is an essential component in the assembly of iron-sulphur clusters (Cook, 2010). Frataxin deficiency results in mitochondrial iron accumulation (Pandolfo and Hausmann, 2013). Therefore, iron chelation has been considered as a potential treatment for FRDA; however, iron chelators have poor permeability across biological membranes (Pandolfo and Hausmann, 2013).

Deferiprone

Deferiprone is an orally-administered iron chelator with good permeability, which has been tested treatment of FRDA (Pandolfo and Hausmann, 2013).

1.10.3 Modulators of frataxin-controlled metabolic pathways

Apoptosis occurs in FRDA due to reactive oxygen species (ROS) in the mitochondria of the neuronal, cardiac and beta cells (Lane *et al.*, 2013). This oxidative stress is caused by a lack of frataxin and decreased production of iron-sulphur (Fe-S) clusters leading to reduced activation of Fe-S enzymes and increased iron levels (Pandolfo and Hausmann, 2013). The excessive iron in the mitochondria reacts with the ROS resulting in cellular destruction (Pandolfo and Hausmann, 2013).

Incretin analogues

Incretin analogues act by decreasing oxidative stress and increasing cAMP production in beta cells lacking frataxin (Igoillo-Esteve *et al.*, 2015). This has been found to decrease cell death, normalise free radical production, and increase frataxin levels and partially protect frataxin-deficient islet cells from apoptosis (Igoillo-Esteve *et al.*, 2015).

Pioglitazone

Peroxisome proliferator-activated receptor (PPAR)-γ agonists, such as rosiglitazone and pioglitazone are used to treat diabetes but may be effective in treating FRDA (Marmolino *et al.*,

2009). One PPAR-γ agonist, Azelaoyl PAF, has been found to increase frataxin mRNA expression and frataxin protein in primary fibroblasts from FRDA patients and healthy controls (Marmolino *et al.*, 2009).

Nuclear factor erythroid-derived 2-related factor 2 (Nrf2) activators

Previous studies on FRDA fibroblasts have shown that the GAA repeats in the *FXN* gene inhibitor Nrf2 in patients with FRDA, allowing oxidative mechanisms to dominate (Paupe *et al.*, 2009). Therefore, the development of pharmaceuticals to activate Nrf2 could reduce intracellular oxidative stress and damage to the mitochondria in FRDA patients.

1.10.4 Frataxin stabilisers, enhancers, and replacements

Erythropoietin

Erythropoietin (EPO) is a hormone that controls erythropoiesis. Recombinant human erythropoietin has been shown to raise frataxin levels in cellular models (Sturm *et al.*, 2005). An open-label study in 12 FRDA patients who received 5,000 units of recombinant human erythropoietin administered subcutaneously three times weekly reported a significant increase in frataxin levels in isolated lymphocytes after eight weeks ($p < 0.01$) (Boesch *et al.*, 2007). However, several additional clinical trials have failed to report improvement in clinical outcomes with EPO testing (Boesch *et al.*, 2014).

Ubiquitin competitors

The ubiquitin-proteasome system controls frataxin degradation. By blocking the ubiquitination of frataxin, intracellular frataxin levels increase. A ubiquitin competing molecule, NSC620299, has been found to decrease frataxin degradation within the cell (Rufini *et al.*, 2011).

Cell-penetrating frataxin fusion peptide

Cell-penetrating peptides (CPP) or (protein transduction domains) are small peptides, typically 5 -30 amino acids, which can not only cross the cell membrane rapidly but also reach the nucleus of mammalian cells (Derakhshankhah and Jafari, 2018). CPPs have been used as a vector for various macromolecular cargoes such as DNA, drugs, proteins, nucleotides, fluorophores, peptides and even particles such as liposomes and magnetic nanoparticles (Papademetriou,

2015). Cargos can be linked to CPPS either by covalent or non-covalent bond formation. The agents can be covalently linked to CPPs by chemical linkages such as thioester or disulphide bonds or by cloning (Guidotti, Brambilla and Rossi, 2017). Non-covalent complex formation depends on electrostatic or hydrophobic interaction between large, negatively charged cargoes such as oligonucleotides and positively charged CPPs (Guidotti, Brambilla and Rossi, 2017). The transactivator of transcription (TAT) protein of human immunodeficiency virus-1 (HIV1) provides a powerful tool for biologically active molecule delivery (Guidotti, Brambilla and Rossi, 2017). The HIV1 TAT peptide corresponds to amino acids 48-57 of the TAT protein, and it can translocate in bulk quantities across the cell membrane of living cells within a very short time (3-5 minutes) (Derakhshankhah and Jafari, 2018). The TAT-PTD consists of two lysines and six arginines which make the peptide strongly cationic (Papademetriou, 2015). The amount and rate of cellular uptake are related mainly to the number of basic residues present, specifically the number of arginines. Proteins with more than 100 KDa, 40 nm nanoparticles, and even 200 nm liposomes have been successfully delivered to the cellular interior by TAT peptides (Papademetriou, 2015).

TAT has the ability to directly deliver human frataxin into the mitochondria (Vyas *et al.*, 2012). By using a mouse model in which Frataxin was depleted in the brain, intraperitoneal (IP) TAT-frataxin injections showed evidence of mitochondrial localisation and rescued the lethal phenotype (Vyas *et al.*, 2012). Although the mechanism of cellular internalisation of CPPs has been heavily investigated, the pathway involved is still not fully understood (De Figueiredo *et al.*, 2014). This could be related to the differences in the physiochemical properties, size ,and concentration of diverse CPP or CPP- cargo conjugates (De Figueiredo *et al.*, 2014). The mechanism of entry is generally divided into two mechanisms: energy-dependent endocytosis and energy-independent direct penetration of the plasma membrane (De Figueiredo *et al.*, 2014). Although direct translocation across the cell membrane happens in cases of high concentration, generally most CPPs and CPP- cargo conjugates enter cells by endocytosis (De Figueiredo *et al.*, 2014). The process of membrane transduction has two important features: not only is it energy independent, but it still can happen even in the presence of endocytic inhibitors (Gräslund *et al.*, 2011). It also involves several routes of entry that are based on the interaction between positively charged CCPs and negatively charged membrane components and the phospholipid bilayer

(Gräslund *et al.*, 2011). This is followed by peptide entrance by various mechanisms such as transient pore formation and membrane destabilisation (Thennarasu *et al.*, 2010). In the transient pore formation models, the CPPs were reported to shape either toroidal pores or barrel-stave pores within the plasma membrane. The CPPs accumulate on the outer leaf of the phospholipid bilayer, which leads to distortion of the membrane and causes the formation of a transient pore (Thennarasu *et al.*, 2010). Several direct translocation mechanisms are thought to occur in the mechanism by membrane destabilisation through: 1) the carpet-like model, which occurs by a transient increase in membrane fluidity as a result of the interaction between positively charged amino acids of CCPs with the negative charges on the membrane surface (Thennarasu *et al.*, 2010); and 2) the inverted-micelle mechanism, which is characterised by invagination of the phospholipid bilayer with the formation of inverted micelle that encapsulate the peptide. (Alves *et al.*, 2008) The translocation of CPPs across the cell membrane occurs within the micelle, which releases the peptide into the cytosol by inversion once they have entered the cell (Alves *et al.*, 2008). Endocytosis is a natural and energy-dependent process which occurs in all cells. It can be classified as micropinocytosis, clathrin- or caveolin-mediated endocytosis and clathrin- or caveolin-independent endocytosis (Guidotti, Brambilla and Rossi, 2017) (Figure 1-17).

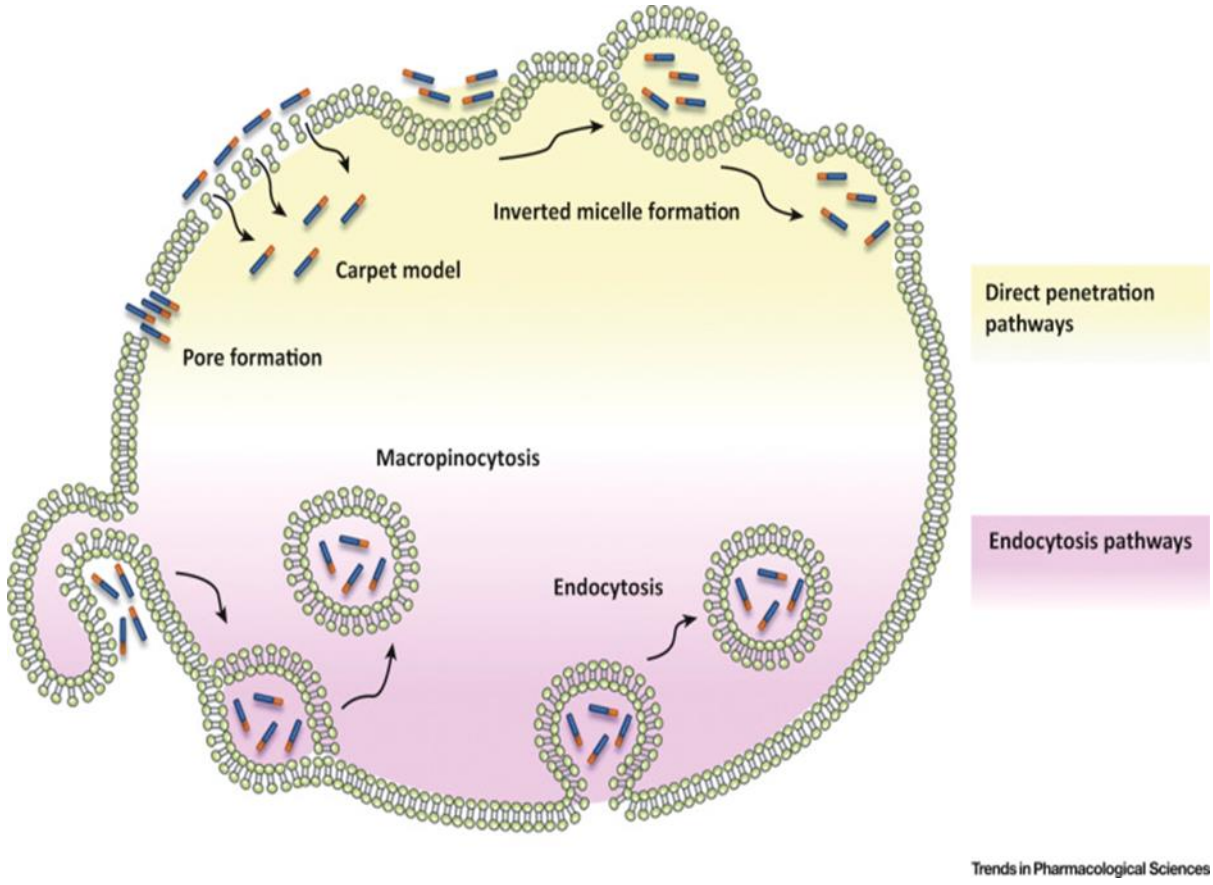

Figure 1-17. Mechanisms for Cell-Penetrating Peptide (CPP) Internalisation.

The diagram shows that the involved pathways can be divided into two groups: direct penetration of plasma membrane (yellow) and endocytic pathways (purple). The first involves several energy-independent models including membrane insertion of CPPs through pore formation and membrane destabilisation through the carpet-like model or inverted micelle formation. Endocytic internalisation of CPPs is an energy-dependent process that comprises micropinocytosis and endocytosis (Guidotti, Brambilla and Rossi, 2017).

Studies have been conducted to test the role of CPPs as therapeutic agents, and many have provided promising results (Harada *et al.*, 2002; Borsello *et al.*, 2003; Huang *et al.*, 2011; Hosseini *et al.*, 2012). In cerebral ischemia which results from impairment of cerebral blood flow because of obstruction of the artery that supplies that area, leading to oxygen deprivation and consequently a neuronal death, studies have shown that a rise of the level of the anti-apoptotic proteins Bcl-2/Bcl-XL in rodent brains was associated with enhanced resistance to ischemic injury

by generating a PTD-hemagglutinin (HA)-Bcl-XL fusion protein in which Bcl-XL was conjugated to the protein transduction domain (PTD) TAT (Hu *et al.*, 2017). Intraperitoneal administration of the TAT fusion protein to the mouse has been associated with a decrease in the size of the infarct (Guidotti, Brambilla and Rossi, 2017).

Neuronal death in cerebral ischemia is largely due to excitotoxic mechanisms, which are known to activate the c-Jun N-terminal kinase (JNK) pathway (Borsello *et al.*, 2003). And the administration of an inhibitor of JNK (D-JNKI-1) and TAT (D-JNKI-1) fusion protein, either systematically or intraventricular to the mouse has been found to provide a potent neuroprotective effect *in vivo* (Borsello *et al.*, 2003).

Studies have shown that direct delivery of human frataxin to mitochondria could be an effective approach in Friedreich's ataxia (Vyas *et al*., 2012), the fusion protein of frataxin and the TAT protein transduction domain has been able to penetrate cells and to prolong life in an animal model of FA (Bürk, 2017). Therefore, TAT-frataxin fusion proteins seem to be a good candidate for frataxin delivery in FRDA (Vyas *et al*., 2012).

The use of CPPs as a carrier for molecular delivery has shown encouraging results (Harada *et al.*, 2002; Borsello *et al.*, 2003; Huang *et al.*, 2011; Hosseini *et al.*, 2012); however, it still has many limitations such as low serum stability and considerable cytotoxicity (Vivès, Schmidt and Pèlegrin, 2008). Cationic peptide CPPs recruited from a peptide library or derived from microorganisms such as viruses and bacteria could have a high risk of immunogenicity and toxicity (Vivès, Schmidt and Pèlegrin, 2008). The problems arising from CPP sequences of non-human origin could be overcome by using CPP from human sequences (Gerke, Creutz and Moss, 2005).

Table 1-5. Therapeutic Applications for CPP–Cargo in Animal Models of different diseases (Guidotti, Brambilla and Rossi, 2017).

	Animal model	Therapeutic use	References
PTD-HA–Bcl-XL	MCAO in mice	Cerebral ischemia	(Guidotti, Brambilla and Rossi, 2017)
PTD–FNK	Cerebral ischemia in gerbils	Cerebral ischemia	(Harada *et al.*, 2002)
TAT–JBD(D-JNKI-1)	MCAO in mice	Cerebral ischemia	(Borsello *et al.*, 2003)
TAT–dPKC	MCAO in rats	Cerebral injury	(Bright, 2004)
TAT–NBD	Infection sensitised midbrain infection	Perinatal infection in HI brain injury	(Yang *et al.*, 2013)
TAT-BH4	hSOD1G93A mice	ALS	(Boisguerin *et al.*, 2011)
TAT–JBD(D-JNKI-1)	TgCNRD8mice	AD	(Sclip *et al.*, 2014)
Antp-NBD	mdx mice	DMD	(Guidotti, Brambilla and Rossi, 2017)
PEP-1–SOD1 **PEP-1–CAT**	Myocardial IR injury In rats	Myocardial IR injury	(Huang *et al.*, 2011)
RI-TAT–p53C0	Terminal peritoneal carcinomatosis/ lymphoma in mice	Cancer	(Snyder *et al.*, 2004)
(R-Ahx-R)4–PMO (AVI-5126)	Corneal transplantation In rats	Corneal transplant rejection	(Hosseini *et al.*, 2012)

Middle cerebral artery occlusion (MCAO), ischemia-reperfusion (IR), Hypoxic-ischemic (HI), Alzheimer's disease (AD), Duchenne muscular dystrophy (DMD).

One study has found that human membrane-interacting peptide could be the right candidate for the discovery of a novel CPP, since membrane interaction is the first step in entering the cell (Gerke, Creutz and Moss, 2005). Calcium ion-regulated annexin protein has been chosen as the CPP. It is membrane-associated and regulates actin dynamics through membrane interaction

(Gerke, Creutz and Moss, 2005). It can bind to the negatively-charged head groups of phospholipids in the membrane (Benz and Hofmann, 1997). Annexin can manage the intracellular calcium ion level in eukaryotic cells by responding to extracellular stimulation, which shows that the protein has different interactions inside and outside the membrane (Kim *et al.*, 2015a). This CPP has demonstrated an excellent cell-penetrating ability and cellular uptake of the peptide, which was mediated by various endocytosis mechanisms (Kim *et al.*, 2015a).

1.10.5 Gene therapy

Gene therapy seeks to cure a disease by transferring one or more therapeutic nucleic acids to a patient's cells or by correcting a defective gene, such as by gene editing (Kumar *et al.*, 2016a). Hence, this technology has the potential to cure diseases that are treatable but not curable with conventional medications and to provide treatments for diseases previously classified as untreatable. Gene and cell therapies are being developed as promising treatments for several genetic diseases (Gonçalves and Paiva, 2017) (Table 1-6; Table 1-7). The therapy could be either by direct delivery, in which the therapeutic gene is packed into a delivery vehicle such as retro- or lentivirus and directly injected back into the patient (Mali, 2013), or cell-based delivery (ex *vivo* cell therapies) in which stem-, progenitor- or differentiated cells are taken from patients are grown ex vivo by genetic modification and administered back into the patient (Burnight et al., 2015) (Figure 1-18).

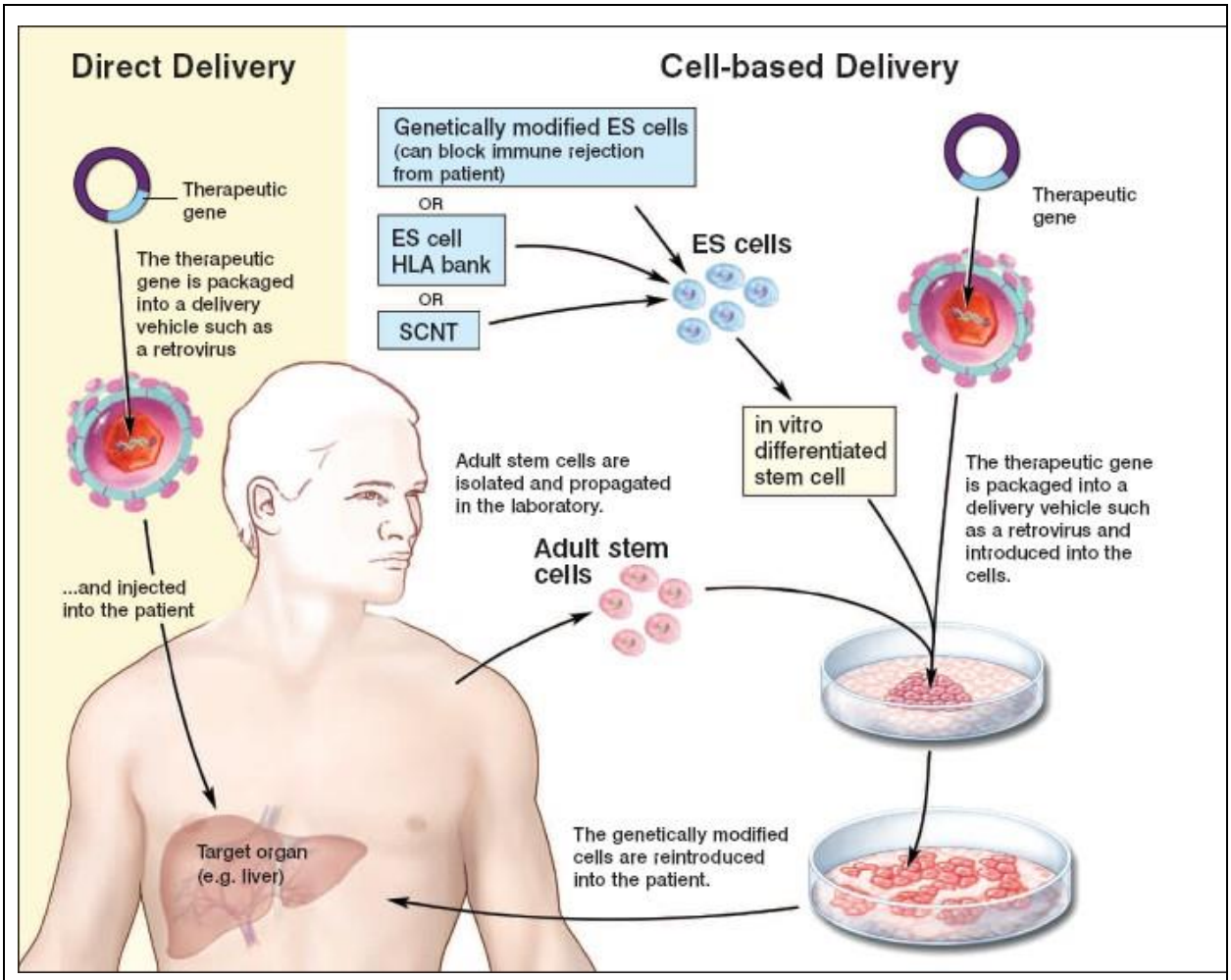

Figure 1-18. Direct vs cell-based delivery.

a) direct gene therapy, in which the therapeutic gene is packed into a delivery vehicle and injected back to the patient. b) cell-based delivery (*ex vivo* gene therapy), in which the patient's cells are taken out of the body and then transduced by a vector in culture to incorporate the therapeutic gene. Finally, the gene-modified cells are transplanted back to the patient (Winslow, 2006).

Since the discovery of haematopoietic stem cells (HSCs) in the 1960s (Mahla, 2016), HSC transplantation has increasingly been used, primarily in oncology and regenerative medicine, because of its unique self-renewal potential and of differentiation into mature cells of different lineages (Mahla, 2016). Transfecting or transducing the true HSCs, therefore, will facilitate the generation of genetically modified peripheral blood (PB) T and B-lymphocytes, natural killer cells, monocytes, granulocytes, eosinophils, basophils, megakaryocytes, and macrophages, including hepatic and alveolar macrophages, dermal Langerhans cells, microglial cells of the brain and

osteoclasts (Wang and Rivière, 2017). All these cell types could also participate as secreting pumps for the delivery of therapeutic products that may facilitate the correction of non-haematological disorders (Yeagy *et al.*, 2011; Rocca *et al.*, 2015; Chevronnay *et al.*, 2016; Syres *et al.*, 2016) Genetically modified HSC is considered an excellent therapeutic option for patients with a monogenetic disorder (Wang and Rivière, 2017), where it has been shown to be an effective approach to primary immunodeficient syndromes (PIDs) such as severe combined immunodeficiency due to adenosine deaminase deficiency (ADA-SCID), X-linked severe combined immunodeficiency (X-SCID) (Aiuti *et al*., 2009) and Wiskott-Aldrich syndrome (WAS) (Aiuti *et al.*, 2015) X-linked adrenoleukodystrophy (Cartier et *al.*, 2009), chronic granulomatous disease (CGD) (Ott *et al*., 2006), Leber congenital amaurosis (Cideciyan *et al.*, 2009), haemophilia (May *et al.*, 2000) and, more recently, and metachromatic leukodystrophy (Biffi *et al.*, 2013).

The primary sources for haematopoietic progenitor and stem cells (HPSCs) are either bone marrow (BM) or mobilised peripheral blood (MPB)(Wang and Rivière, 2017). There are several gene delivery vectors such as adenoviral, adenovirus-associated virus-derived vectors (AAV), herpes simplex viral vectors, retroviral vectors, and lentiviral vectors which can either provide non-integrating transient gene correction or integrating stable gene transfer (Vannucci *et al.*, 2013).

It has been shown that human haematopoietic stem and progenitor cells (HSPCs) are perfect candidates for use in regenerative medicine and cell replacement treatment, and this is attributed to their ease of isolation, self-renewal capacity and safety (Mahla, 2016). It has also been shown that a sole systemic transplant of wild-type mouse haematopoietic stem cells had long-term thyroid, eye, and kidney preservation in a mouse model of the multisystemic lysosomal storage disorder cystinosis (Yeagy *et al.*, 2011; Rocca *et al.*, 2015; Chevronnay *et al.*, 2016; Syres *et al.*, 2016). In this mouse model, the disease phenotype was rescued by the differentiation of wild-type HSPCs into macrophages that distributed lysosomes bearing functional cystinosin into diseased host cells, possibly through long tubular extensions known as tunnelling nanotubes (Naphade *et al.*, 2016). Tunnelling nanotubes have been called an intercellular transfer route for chemical mediators, proteins, and organelles such as lysosomes and mitochondria (Domhan *et*

al., 2011; Nanotubes *et al.*, 2012; Sisakhtnezhad and Khosravi, 2015). Another study showed that the development of FRDA pathology such as degeneration of DRG sensory neurons, neurobehavioral deficits, muscle weakness had been prevented by a sole transplant of wild-type mouse HSPCs into young adult YG8R mice (Celine J. Rocca *et al.*, 2017) The critical advantage of exogenous haematopoietic stem cells transplantation is their capacity to permanently repopulate the bone marrow and migrate from their niche to differentiate into phagocytic cell types within multiple tissues (Naphade *et al.*, 2016). Haematopoietic stem cells are capable of transmigrating across the blood-brain barrier and engraft within the CNS as differentiated microglia (Priller *et al.*, 2001). In this study, they showed that the transplanted wild-type mouse haematopoietic stem cells were able to differentiate into microglial cells in the central nervous system of the YG8R recipient mice and into macrophages in the dorsal root ganglions, peripheral nerves, skeletal muscle, and heart, the primary sites of FRDA pathology (Celine J. Rocca *et al.*, 2017).

Table 1-6. Key examples of current ongoing gene therapy and stem-cell-based clinical trials (Clément *et al*., 2017).

Injected cells/GT	Diseases	Clinical trial
	—	
CD34+ HSPC+ cells/SIN GT	X-linked chronic granulomatous disease	I, II
CD34+ HSPC+ cells/SIN GT	X-linked severe combined immunodeficiency	I, II
Bone marrow cells/SIN GT	Severe combined immunodeficiency	I, II
Gene editing	Hemophilia B	I
Gene editing	Mucopolysaccharidosis II	I
PD-1 knockout CRISPR-Cas9 engineered T cells	Metastatic non-small cell lung cancer	I
MSCs	Spinal cord injury	II, III
ESCs	Macular degeneration diseases	I

ESCs	Dry age-related macular degeneration	Early phase I
Placental and umbilical cord blood SCs.	Malignant and non-malignant disorders	I
Umbilical cord MSCs	Nerve and spinal cord injury	I, II
Neural SCs	Nerve and spinal cord injury	I, II
MSC and stromal vascular fraction	Osteoarthritis	II
Endothelial progenitor CD133+ cells	Coronary artery disease, refractory angina	II
GT, gene therapy; SIN, self-inactivating; MSC, mesenchymal stem cell; ESC, embryonic stem cell.		

Viral Vectors in Gene Therapy

The spectrum of viral vectors is very wide involving both delivery vehicles developed for transient short-term and permanent long-term expression (Lundstrom, 2018). Furthermore, the types of vectors are represented by both RNA and DNA viruses with either single-stranded (ss) or double-stranded (ds) genomes (Lundstrom, 2018).

There are several types of viral vectors such as adenoviruses (AAV) genomes (Lundstrom, 2018). Naked dsDNA adenoviruses possess a packaging capacity of 7.5 kb of foreign DNA giving a short-term episomal expression of the gene of interest in a relatively broad range of host cells. The original adenovirus vectors generated strong immune responses, whereas the so-called gutted second and third-generation vectors containing deletions have proven to elicit substantially reduced immunogenicity genomes (Lundstrom, 2018). Mostly, AAV is considered to generate low pathogenicity and toxicity and provides long-term transgene expression through chromosomal integration (Wang *et al.*, 2012). One limitation of using AAV relates to the immune response triggered by repeated administration (Mingozzi and High, 2016). Another issue relates to the limited packaging capacity of foreign DNA into recombinant AAV particles (Mingozzi and High, 2016). Another drawback of AAV vectors is their small packaging capacity within the vector genome (Mingozzi and High, 2016). AAV can also integrate at chromosome breakage sites (Miller, Petek and Russell, 2004) and a specific site in chromosome 19 (McCarty, 2008). AAV (serotype 2) has also been demonstrated to preferentially integrate with low-efficiency inactive genes in mice

(Nakai *et al*., 2003). An important advance has been the development of self-complementary AAV (scAAV) vectors that generate a single-stranded genome with both the coding and complementary sequences packaged (McCarty, 2008). The scAAV vector removes the lag time for second-strand synthesis (a required step with AAV), facilitates more rapid expression once in the nucleus, and increases transduction efficiency. A major disadvantage, however, is that scAAV vectors have only half of the already small packaging capacity of AAV (McCarty, 2008).

An early study evaluated AAV correction in human FRDA fibroblasts and showed that cells experienced reduced sensitivity to oxidative stress upon AAV-dependent expression of human FXN (Fleming *et al*., 2005). A very recent study demonstrated not only correction but also reversal, of a severe cardiomyopathy phenotype in a conditional FRDA mouse model, where frataxin is deleted in cardiac and skeletal muscle; the muscle creatine kinase-Cre or MCK mouse (Puccio *et al*., 2001), following a single intravenous injection of AAV constitutively expressing human FXN (Perdomini *et al*., 2014). This study reports for the first time that MCK mouse cardiomyocytes that have already undergone severe energy failure, iron-sulfur cluster deficiency, and mitochondria and sarcomere ultrastructural changes can be fully rescued with vector-dependent FXN expression. Importantly, FXN expression also restored compromised ventricular function to wild-type levels (Perdomini *et al*., 2014).

Herpes simplex viruses (HSV) are large enveloped dsDNA viruses characteristic of their lytic and latent nature of the infection (Evans-galea *et al.*, 2014), which results in life-long latent infection of neurons and allows for long-term transgene expression (Evans-galea *et al.*, 2014). The deletion of HSV genes has generated expression vectors with low toxicity and excellent packaging capacity of >30 kb foreign DNA (Evans-galea *et al.*, 2014).

In 2007, Lim and colleagues developed a localized frataxin knock-out mouse lacking frataxin in the olivary neurons of the brain stem (Lim *et al*., 2007). Using a rotarod assay, the authors showed this FRDA model developed motor incoordination, within 4 weeks of frataxin deletion. Crucially, this neurological phenotype was reversed upon stereotaxic injection of an HSV1 amplicon expressing human frataxin into the brain stem (Lim *et al*., 2007). This demonstrates that vector-

dependent frataxin expression can rescue neurological deficits to restore motor coordination in FRDA mice.

Retroviruses possess an ssRNA genome with an envelope structure (Lundstrom, 2018). Typically, retroviruses are randomly integrated into the host genome, which has been problematic, such as in the treatment of children with severe combined immunodeficiency (SCID) (Lundstrom, 2018), although the treatment was successful, the integration of the retrovirus-delivered therapeutic gene into the LMO2 proto-oncogene region triggered the development of leukemia in some cases (Lundstrom, 2018). However, this drawback has triggered the development of safer vectors showing targeted integration (Escors and Breckpot, 2011). Retroviruses can accommodate up to 8 kb of foreign inserts and have represented the gold standard vectors for long-term gene therapy applications (Escors and Breckpot, 2011). Another downside, of retroviruses, is their incapability to infect nondividing cells, which has enhanced the interest in the application of lentivirus vectors for gene therapy (Lundstrom, 2018). Even though lentiviruses are considered to be a family of retroviruses, they have the capability of infecting both dividing and nondividing cells providing low cytotoxicity (Lundstrom, 2018). Possessing the same packaging capacity and chromosomal integration as conventional retroviruses (Escors and Breckpot, 2011), lentiviruses have become attractive for therapeutic applications requiring long-term expression (Escors and Breckpot, 2011), lentiviral vectors showed a significantly lower tendency of proto-oncogene activation (Escors and Breckpot, 2011). The third generation lentiviruses have also contributed to improved delivery and safety (Lundstrom, 2018). For instance, the deletion of the viral tat gene makes the vector replication-incompetent (Lundstrom, 2018). Moreover, lentiviral vector packaging functions have been placed on three plasmids instead of two to reduce the risk of recombination (Escors and Breckpot, 2011). Modifications of the 30 LTR prevents integrated genes from being repackaged providing a self-inactivating system (Escors and Breckpot, 2011). Additionally, VSV-G pseudotyped lentiviral vectors allow transduction of a much wider range of cell types and the enhanced vector stability, which facilitates high titer vector concentration by ultracentrifugation (Evans-galea *et al.*, 2014). Retroviruses present the classic approach for long-term gene therapy applications and the first human gene therapy trial involved implantation of autologous bone marrow cells transduced ex vivo with gamma retrovirus vectors (Evans-galea *et*

al., 2014). Latest-generation lentiviral vectors represent an appropriate system to potentially treat FRDA, and one study showed that lentiviral vector-dependent expression of human FXN in fibroblasts isolated from FRDA patients increases their resistance to oxidative stress (Fleming *et al*., 2005).

Table 1-7. Examples of clinical trials using viral vectors (Lundstrom, 2018).

Disease	Viral Vector	Response
Hemophilia A Hemophilia B	AAV-FVIII/FIX Lenti-FVIII Lenti-FIX	Cure of hemophilia Potential cure Life-long production of FVIII
HGG	Toca 511 Toca 511/FC	Improved survival Phase II/III trial in progress
Glioblastoma	HSV G207	Antitumor activity in Phase I
CGD	Gamma RV	Resolution of infections, but malignant transformation
ATC	MV-NIS	Targeting iodine-resistant ATC
Colorectal cancer	Oncolytic VV	Induction of immune response
Kidney cancer	LipoSFV-IL12	Transient IL-12, repeated injections
Pancreatic cancer	PANVAC-VF	Failure in phase III, encouraging results in new phase I trial
Prostate cancer	NDV-TAA	Improved survival in phase II
Melanoma	NDV CVA21	Phase II/III failed to show superiority to control Anti-tumor activity in melanoma patients
Solid tumors	NDV PV701	Progression-free survival

AAV, adeno-associated virus; ATC, anaplastic thyroid cancer; CF, cystic fibrosis; CGD, chronic granulomatous disease; CVA21, Coxsackievirus CVA21 strain; FIX, Factor IX; FVIII, Factor VIII; Gamma RV, gammaretrovirus; HGG, high-grade glioma; HIV; HSV, herpes simplex virus; LipoSFV-IL12, liposome-encapsulated Semliki Forest virus-interleukin-12; MV-NIS, measles virus-sodium iodide symporter; NDV-TAA, Newcastle disease virus-tumor associated antigen; PANVAC-VF, vaccinia-fowlpox virus; VEE; VV, vaccinia virus.

1.10.6 Insulin/insulin-like growth factor 1 (IGF-1)

IGF-1 is a polypeptide hormone that is important to central nervous system cell proliferation and death, metabolism, and homeostasis (Sanz-gallego, Torres-aleman and Arpa, 2014). Neurodegenerative diseases, such as Alzheimer's disease, Huntington's disease, and spinocerebellar ataxia, were thought to be related to a defect in the insulin-like system and, therefore, IGF-1 has been studied in these disease states (Sanz-gallego, Torres-aleman and Arpa, 2014). Currently, IGF-1 is being evaluated as a potential treatment in FRDA due to its neuroprotective qualities in Purkinje cells (Sanz-gallego, Torres-aleman and Arpa, 2014).

1.10.7 Agents that increase FRDA gene expression

The expanded GAA repeats in FRDA lead to heterochromatin formation, which causes gene silencing and decreases transcription of frataxin mRNA (Gottesfeld, Rusche and Pandolfo, 2013).

HDAC Inhibitors

Histone deacetylase (HDAC) inhibitors could potentially restore affected genes to normal function by increasing histone acetylation on the frataxin gene (Libri *et al.*, 2014). Studies have shown that HDAC inhibitors could increase frataxin in cellular and animal models (Libri *et al.*, 2014) and raise the level of frataxin mRNA in FRDA lymphocytes (Herman *et al.*, 2006).

Zinc finger nucleases (ZFNs)

The excision of the GAA repeats using zinc-finger nucleases (ZFNs) leads to an increase in frataxin mRNA and consequently to raise in frataxin expression (Li *et al.*, 2015).

1.10.8 Interferon-gamma

Interferon-gamma is a medication that is used in chronic granulomatous disease (CGD) and malignant osteopetrosis. Its action mimics interferon-gamma that is naturally occurring in the body by regulating nearly all phases of the immune and inflammatory response. Its effects mediate the activation and differentiation of T-cells, B-cells, macrophages, and NK cells. It is a cytokine that is involved in iron metabolism and immune response. Interferon-gamma has been shown to stimulate frataxin production by increasing transcription of the gene frataxin in both cell and animal models of FRDA (Marmolino *et al.*, 2009).

1.10.9 Miscellaneous medications

Physostigmine

Physostigmine is used for the treatment of anticholinergic toxicity and has been used as a treatment in Alzheimer's disease and cerebellar ataxia (Libri *et al.*, 2014)

Riluzole

Riluzole is used as a treatment for amyotrophic lateral sclerosis (ALS) and had positive effects on ataxia patients in one clinical trial (Ristori, Romano and Visconti, 2010). It is thought that the mechanism of action may relate to the small conductance calcium-activated potassium channels that appear to regulate excitability in neurons found within deep cerebellar nuclei (Alviña and Khodakhah, 2008). Abnormal, rapid firing of these neurons may contribute to ataxia, and it may be that riluzole reduces this hyper-excitability (Cao *et al.*, 2002).

1.10.10 Rehabilitation therapy

Rehabilitation therapy is still considered to be the mainstream treatment for Friedreich's ataxia (Ilg *et al.*, 2009). Furthermore, there is increasing evidence that physical therapy could improve the symptoms of cerebellar degeneration in short and in the long-term (Ilg *et al.*, 2009).

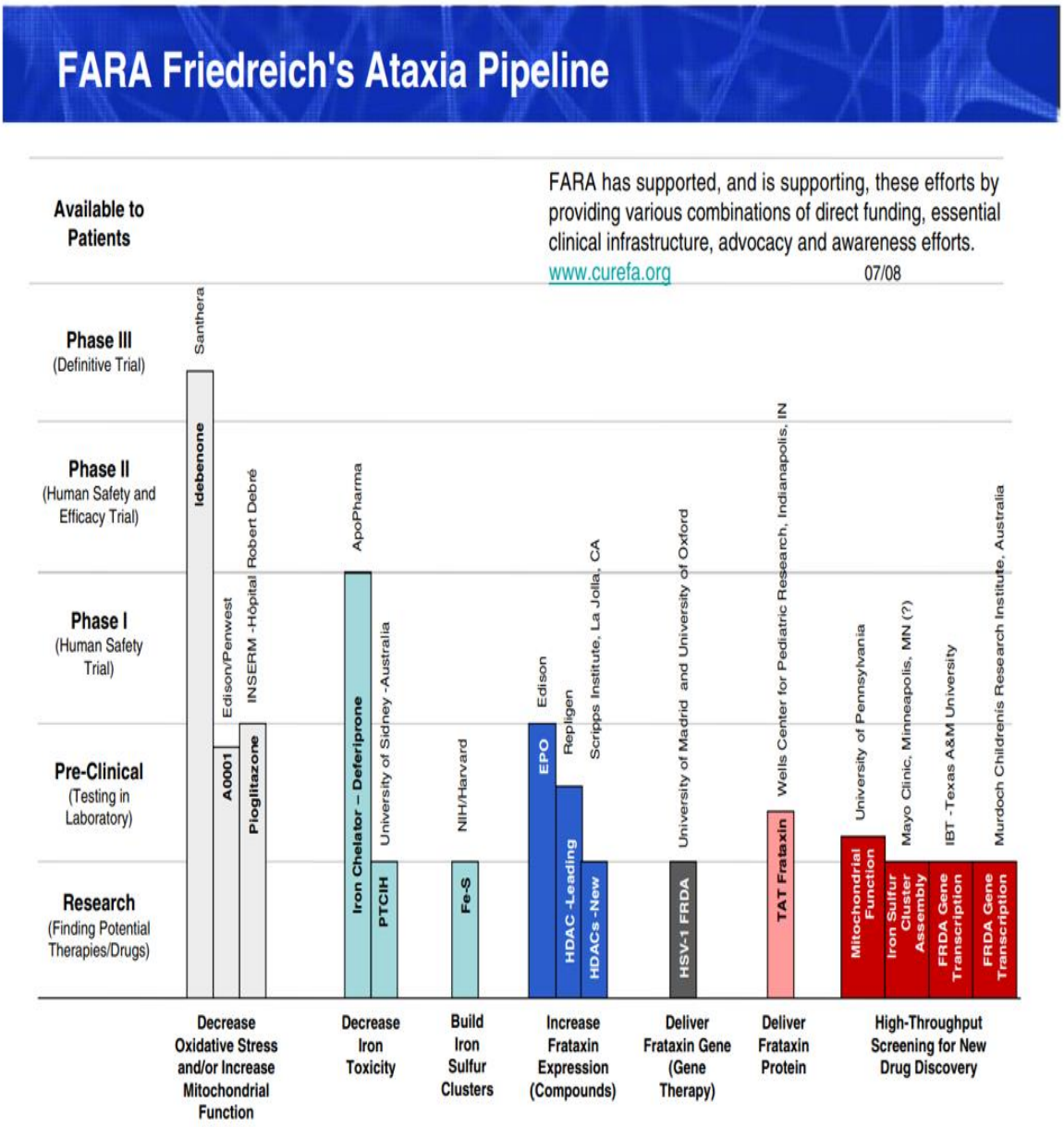

Figure 1-19. Schematic representation of the research status of several promising drugs for the treatment of FRDA.

The FARA pipeline is an illustration of the various therapies being developed by FRDA scientists. On the horizontal axis, each leading drug candidate is represented by its own bar and is grouped by its mechanism of action. Each mechanism of action targets one of the known causes of FRDA. The milestones for drug development are listed on the vertical axis. (http://www.curefa.org/pipeline.html)

1.11 Hypothesis and aims of the project

The main hypothesis of this research is that a tissue-penetrating version of frataxin could be delivered to diseased tissues by genetically modified patient-derived haematopoietic stem cells. In comparison to a recent approach that used systemically-injected frataxin peptide fused to TAT, our gene and cell therapy method presents two significant advantages. First, the delivery of Frataxin will be continuous and long term as the therapeutic stem cells should be able to survive in the bone marrow for many years. Second, there is no need for multiple injections of frataxin, which would be both inconvenient and expensive.

1.12 Specific objectives

1) The study aimed to transfect HEK 293T cells and transduce human haematopoietic stem cells with frataxin fusion peptide constructs and use the supernatant to deliver the cell-penetrating peptide constructs to fibroblasts isolated from FRDA patients. Functional studies were conducted to test the ability of the construct to rescue frataxin-deficient cells.
2) The study also aimed to investigate the expression and normal differentiation of human haematopoietic stem cells and confirm that different frataxin peptides are secreted by progenitor and differentiated haematopoietic cells.

Chapter 2.

Material and methods

2.1 Solutions and reagents

General

- 1x DMEM medium, 10% foetal bovine serum (FBS), 1% Pen-Strep (5000 U/ml penicillin, and 5000 mg/ml of streptomycin, Fisher Scientific).
- Opti-MEM™ (Fisher Scientific).
- StemSpan (Stem cell Technologies) (Stem cell Technologies) 1x culture medium (Stem Span), with full cytokine cocktail; hSCF 100 ng/ml, hFlt3L 100 ng/ml, hTPO 20 ng/ml, hIL3 20 ng/ml (Peprotech), 1% PenStrep.
- IMDM medium, 10% FBS, 1% Pen-Strep (Gibco), and GCSF 100 ng/ml.
- Methocult H4434 StemSpan (Stem Cell Tech).
- RPMI, RPMI medium, 10% FBS, 2% Pen-Strep (5000 U/ml penicillin, and 5000 mg/ml of streptomycin, Fisher Scientific).

Western blot analysis

- Running buffer: 25 mM Tris, 190 mM glycine, 3.5 mM SDS.
- Sample buffer: 80 mM Tris-HCl (pH 6.8), 12.5% glycerol, 10% SDS, 0.5% BPB, 1% BME.
- Transfer buffer: 25 mM Tris, 190 mM glycine, 10% methanol.
- PBS/T: 0.2% Tween-20 in PBS.
- 5% milk PBS/T: 5% w/v milk, 0.2% Tween-20 in PBS.
- Immunofluorescence analysis.
- Fixing solution: 4% paraformaldehyde in PBS pH7.4.
- Block buffer: PBS 0.5% Triton-X 100 10% FBS.
- Permeabilisation buffer (PB): PBS, 0.5% Triton-X 100.

Flow cytometry analysis

- Wash buffer: PBS.

General buffers and solutions

- Tris/EDTA (TE) buffer: 10 mM Tris-HCl (pH 7.5), 1 mM EDTA.
- TAE buffer: 40 mM Tris, 20 mM Acetic acid, 1 mM EDTA.
- PBS buffer: For 1 L: 8.0 g NaCl, 1.15 g Na2HPO4, 0.2 g KH2PO4, 0.2 g KCl.
- Luria-Bertani (LB) medium for 1L: 10 g NaCl, 5 g Yeast extract, 10 g tryptone peptone. Autoclave. LB (Luria-Bertani) Agar For 1 L: 10 g NaCl, 5 g Yeast extract, 10 g tryptone peptone, 15 g bacto agar. Autoclave.
- Digestion buffer: 100 mM Tris-HCl (pH 8), 5 mM EDTA, 200 mM NaCl, 0.2% SDS.

Table 2-1. Details of the human primary fibroblasts ID Gender Age (Years).

ID	Gender	Age (Years)	Ethnicity	Number of GAA repeats
GMO7492	Male	17	Caucasian	Normal
C4	ND	ND	Caucasian	Normal
FA1	ND	ND	Caucasian	460/700
FA4	ND	ND	Caucasian	790/970

ND=not determined

Table 2-2. Details of general cell lines.

ID Gender	Ethnicity	Organism	Tissue	Cell type	Age
HEK 293T	ND	Homo sapiens	ND	ND	Foetus
K-562	ND	Homo sapiens	ND	Myelogenous leukaemia	ND
CD34+ HSPC	ND	Homo sapiens	ND	Stem cell	Foetus

ND=not determined

2.2 General guidelines

The experiments were carried out in HNZW 138, 139, and 140 laboratories of the College of Health and Life Sciences, Brunel University, London. The industrial methylated spirit, IMS (70% alcohol) was used to clean all working areas and materials before and after every experiment. The solutions were prepared under fully controlled conditions and autoclaved before use, except when sterility was guaranteed by the manufacturer. Cell culture was performed under sterile conditions.

Dilutions

All dilutions and stock solutions were prepared in deionised water (18.2 MΩ) unless otherwise specified. However, for DNA cloning and dilutions, DNase-RNase-free DEPC-treated sterile water was used.

Centrifugations

For sample spin down, different centrifugation instruments were used depending on the sample size and required temperature. A room temperature standard benchtop microcentrifuge (16 K,

BioRad) and a 4°C refrigerated microcentrifuge (max speed 14 K x g, 5415R – Eppendorf) was used for small samples (≤ 1.5 ml). Whereas large volume samples (50 ml) and plate centrifugation were carried out using a Centaur 2 centrifuge (Sanyo/MSE) and Legend T centrifuge (max speed 1000 x g, Sorvall), respectively.

Incubations and pH regulation

Generally, water baths (Grant) were used for lower temperature incubation (37-60°C), and for higher temperatures (60-100°C), a heating block (DB-2A, Techne) was used.

Complementary DNA (cDNA) samples were stored at -20°C. Reagent kits were stored according to the manufacturer's recommendations at room temperature, 4°C or -20°C and, if needed, in the dark. Antibodies were also stored according to the manufacturer's recommendations at either 4°C or -20°C. Frozen cells were stored overnight in a container with isopropanol at -80°C, after which they were transferred to the liquid nitrogen tank. The pH of solutions was tested using a pH meter (Delta 340, Mettler), and pH adjustments were made by adding either concentrated HCl or NaOH.

Sterilisation

All materials and reagents used in tissue culture and molecular analysis were sterilised in an autoclave at 121°C, 100 kPa for 20 minutes.

Agarose gel electrophoresis

Agarose gel electrophoresis was used to detect and separate gDNA and cDNA fragments depending on their size. The gels were usually prepared in the range of 1-2% with agarose (Ultrapure electrophoresis grade; Invitrogen) in 1x TBE/TAE buffer. Initially, the agarose mixture would be boiled in 1x TBE using a standard microwave, and then left to cool down. 1 µl SYBR safe gel stain (ThermoFisher, UK) added to the gel for visualisation, and the gel mixture then poured immediately into the casting tray and the fitting comb. After that, the gel was left for about 20 minutes at room temperature to set. The gels were visualised and recorded using a UV transilluminator imaging system (Alpha Innotech).

General cell culture maintenance

Both HEK 293T and fibroblast cell lines were cultured in Dulbecco's Modified Eagle Medium (DMEM) (Invitrogen) 10% FBS, 1% Pen-Strep. K-562 cell lines were cultured in RPMI (Invitrogen) 10% FBS, 1% Pen-Strep. CD34+ HSPC were cultured in StemSpan (Stemcell Technologies) 1x culture medium (Stem Span, with full cytokine cocktail; hSCF 100 ng/ml, hFlt 3L 100 ng/ml, hTPO 20 ng/ml, hIL3 20 ng/ml, Peprotech), 1% PenStrep and differentiated in either IMDM medium, 10% FBS, 1% Pen-Strep (Gibco), and GCSF 100 ng/ml or Methocult H4434 StemSpan (Stem Cell Tech). They were filter sterilised through a 0.22 µM pore filter unit (Nalgene) with 10% FBS, 1% penicillin and streptomycin (Invitrogen). This was carried out in tissue culture biological safety cabinet, and the medium mixture was stored at 4°C until use. Generally, cells were cultured in a T-25 flask (Fisher Scientific) or T-75 at 37°C in a 95% humidified atmosphere of 5% $C0_2$. All cell culture procedures were carried out in a temperature-controlled laboratory.

Regeneration of cell lines

To prevent the possibility of cell damage by ice crystal formation, frozen cells were rapidly thawed in a 37°C water bath when taken from liquid nitrogen storage. To regenerate, the cells were then immediately moved into a 15 ml conical tube with 10 ml pre-warmed culture medium. The cells were then gently mixed by pipetting up and down. After that, the cells would be collected by centrifugation at 161x g for five minutes, then transferred to a T-25 flask or T-75 flask containing a new culture medium. The cells were incubated at 37°C in a $C0_2$ incubator reach a confluent level.

Sub-culturing and passaging of cell lines

Sub-culturing was carried out when cells reached log phase growth and were about 80% confluent. The culture medium, 1x phosphate-buffered saline (PBS; Invitrogen), and 0.25% trypsin-EDTA (Invitrogen) solutions were pre-warmed at 37°C in a water bath. The cell medium was removed by vacuum suction in a disinfected biological safety cabinet and washed gently with sterile PBS. 2 ml 0.25% trypsin-EDTA was used to detach the bound fibroblast cells for 5 minutes at 37°C, followed by gentle tapping to bring them into complete suspension. 10 ml DMEM culture medium was then added to the detached fibroblast cells to neutralise the trypsin/EDTA solution.

The cells were collected by centrifugation at 252x g for five minutes. Depending on when the cells were required for use, they were sub-cultured in 10 ml DMEM culture medium at a 1:2, 1:4 or 1:6 ratios in a T-25 or T-75 flask. The cells were then incubated at 37°C, 5% $C0_2$ and 95% humidity and growth were observed daily.

Cryopreservation of cell lines

To avoid microbial contamination and to conserve a stock of cell lines for any prospective experiments, 1-2 vials of each cell line were cryopreserved in liquid nitrogen. The adherent cells were detached with 0.25% trypsin-EDTA, followed by cell counting and viability assessment by trypan blue exclusion assay, after which the cells were pelleted by centrifugation at 161x g for 5 minutes. The supernatant was discarded, and the cells were resuspended in 1 ml DMEM culture medium containing 10% (v/v) DMSO and transferred to the cryo-vials (Sarstedt). Around 0.5-$1x10^6$ cells/ml of cells were frozen. To prevent ice crystallisation damage to the cells, they were initially slowly frozen to -80°C for up to 24 hrs in a cooling box containing isopropanol (Sigma-Aldrich). After this, they were moved to liquid nitrogen for extended storage.

Cell quantification and viability (trypan blue exclusion assay)

Knowing the cell number in the culture at a given stage is critical as it indicates whether there are enough viable cells for an experimental procedure. The Trypan Blue dye exclusion assay is based on the fact that viable live cells that have an intact membrane do not take up the dye, whereas dead non-viable cells do. In this analysis, cells were first trypsinised with 0.25% trypsin, followed by centrifugation at 161 x g for 5 minutes and suspension in 1 ml 1x PBS buffer. 10 µl of the cell suspension was gently mixed with an equal volume of 0.4% (w/v) trypan blue (Sigma). Subsequently, a Countess® automated cell counter (Invitrogen) was used to count the cells, and the following formula determined their viability:

%viable cells= (number of viable cells x100)/ number of total cells

2.3 Cloning

DNA cloning is creating identical copies of a piece of DNA. The gene or other DNA fragment of interest is inserted into a circular piece of DNA (a plasmid). This is performed using a restriction

enzyme and DNA ligase followed by the introduction into bacteria by the transformation. The bacteria carrying the plasmid are selected using antibiotics and used to form further plasmid DNA or induced to express the gene and make protein.

2.3.1 Frataxin- cell-penetrating peptide cDNA construction

The cDNA for human precursor frataxin was obtained from Invitrogen TAT-Frataxin fusion peptide (clone ID 17ABUDPP), APP-Frataxin fusion peptide (clone ID 17ADYQ2P) and APP-truncated frataxin fusion peptide (clone ID 18ADXK2P). The synthetic gene FRAT was assembled from synthetic oligonucleotide or PCR products. The fragments were inserted into pMA. The plasmid DNA was purified from transformed bacteria.

Restriction enzyme digestion is an essential part of molecular biology and gene cloning. Special enzymes were used to cut DNA (dsDNA or ssDNA) at distinct sites. *Bam* HI and *ECO* RI (Promega) were used. The enzyme digestion was performed in a volume of 20 µl. In a sterile tube, the following components were assembled in the following order: sterile, deionised water 11.67 µl, followed by a restriction enzyme 10x Buffer 2, followed by acetylated BSA 10 mg/µl (0.2 µl) followed by DNA, 1 mg/µl (2 µl). The mixture was mixed gently by pipetting, and the following restriction enzymes were added: *ECO* RI (1 µl) and *Bam* HI (1 µl). The mixture was gently mixed by pipetting followed by centrifugation for a few seconds; after that, it was incubated at 37°C for 4 hours.

2.3.2 Digest of vectors for cloning

The enzyme digestion was performed in a total volume of 20 µl. In a sterile tube, the following components were assembled in the following order: sterile, deionised water (11.67 µl), followed by the restriction enzyme 10x Buffer (2 µl), followed by acetylated BSA 10 mg/µl 0.2 µl followed by DNA, 1 mg/µl 2 µl. The mixture was mixed gently by pipetting, and the following restriction enzymes were added: *ECO* RI 1 µl and *Bam* HI 1 µl. The reaction mixture was gently mixed by pipetting followed by centrifugation for a few seconds; after that, it was incubated at 37°C for 4 hours. Agarose gel electrophoresis was used to visualise the size of the product, and DNA was cut off the gel and purified (Figures 2-1).

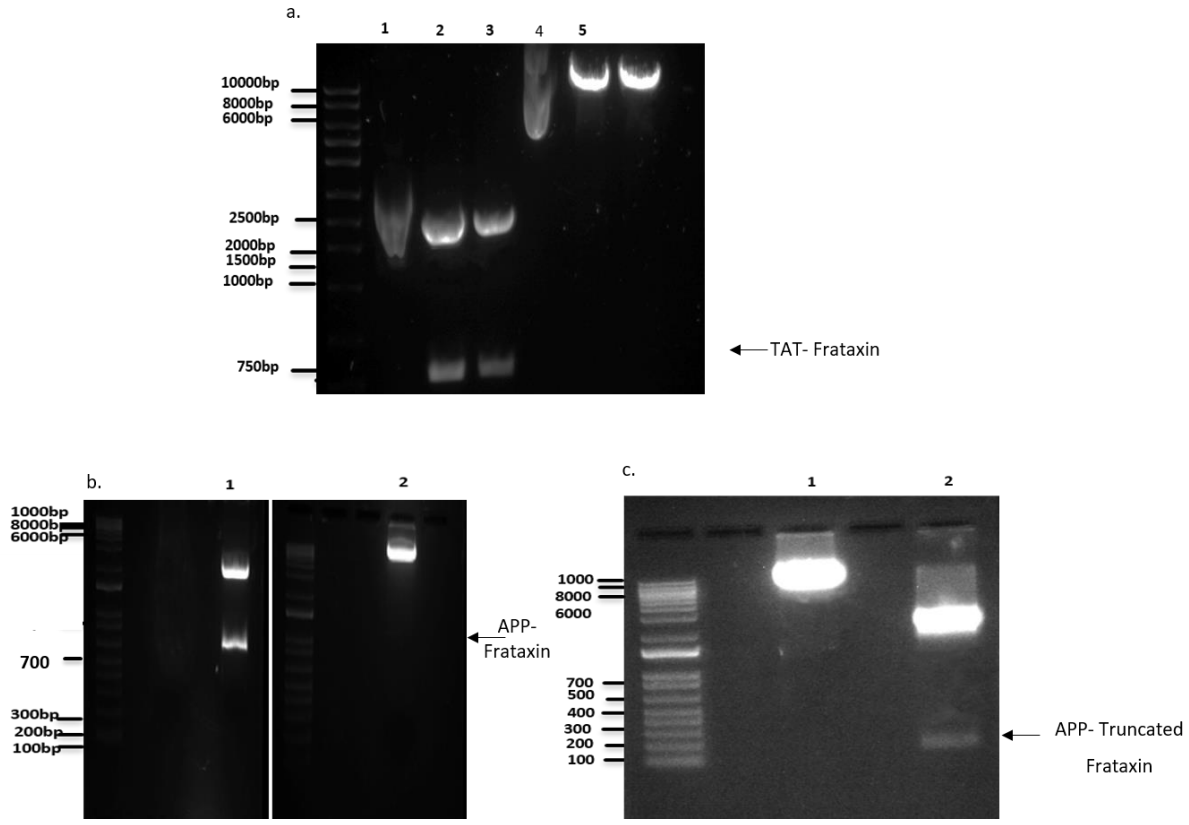

Figure 2-1. Vector digestion.

a) Digestion of plasmid vector containing TAT-Frataxin fragment by *Eco* RI and *Bam* HI restriction enzymes. Lane 1: undigested vector. Lane 2 and 3: digested plasmid. Lane 4: undigested PLIG vector. Lane 5 and 6: digested PLIG vector. b) Digestion of vector containing APP-Frataxin fragment by *Eco* RI and *Bam* HI restriction enzymes. Lane 1: digested pMA-T. Lane 2: digested PLIG vector. c) Digestion of plasmid vector containing truncated Frataxin fragment by *Eco* RI and *Bam* HI restriction enzymes. Lane 1: digested PLIG vector. Lane 2: digested pMA.

2.3.3 Agarose gel DNA extraction

Agarose Gel DNA Extraction Kit from Roche was used for isolation of the DNA fragments from agarose gels; the isolated DNA fragment could then be ligated into a plasmid cloning vector. After sufficient DNA separation by a 1% agarose gel, the DNA fragments were cut out, after which agarose solubilisation buffer was added in the concentration 960 µl, followed by 10 µl silica suspension to the samples. The mixture was then incubated for 10 minutes at 56°C with vortexing every 2-3 min, after which the mixture was centrifuged for 30 seconds. The supernatant was

discarded and the matrix containing the DNA resuspended with 500 µl of nucleic acid binding buffer, followed by centrifugation. The supernatant was discarded as before, and the pellet was washed with washing buffer followed by centrifugation and discarding of the supernatant. This step was repeated once more then the tube was inverted on an absorbent tissue and left for 15 minutes at room temperature to dry. The DNA was eluted with 100 µl of distal water.

Visualisation and checking of the size of the sample mixture were done using agarose gel electrophoresis. This was done in 1% agarose: TAE (Tris-Acetate-EDTA) buffer (1 g of agarose in 100 ml of 1x TAE buffer). The mixture was carefully heated in a microwave and gently stirred and then moved to an electrophoretic tank, 1 µl SYBR safe gel stain added to the gel (ThermoFisher, UK) for visualisation.

The gel comb was placed in the gel to create equal dimension loading wells for sample loading. 2 µl of DNA loading dye was mixed with 4 µl of the vector sample mixture, and 2 µl of DNA loading dye was mixed with 2 µl of insert sample mixture and 20 µl of DNA ladder.

2.3.4 Ligation

Ligation of the insert

DNA ligation is usually used in molecular cloning experiments to physically join DNA fragments to the plasmid vector. The ends of the DNA fragments can be either blunt or cohesive and should contain monophosphate groups on the 5' ends. DNA ligases catalyse the formation of a bond between the 3' hydroxyl and 5' phosphate of adjacent DNA residues to form a closed circular molecule that can transform a host bacterial strain. To achieve this, T4 ligase from Promega was used and the following reagents were added in a sterile microcentrifuge tube: 1.87 µl of insert DNA, 2.44 µl of vector DNA, 10x buffer 1 µl, T4 DNA ligase buffer 0.5, and nuclease-free water to a final volume of 10µl. frataxin fusion peptide constructs were digested by restriction enzymes and loaded on 1% agarose gel to visualise the insert.

2.3.5 Ligation of control

A control ligation was done after the transformation of plasmid DNA in a competent bacterium to test whether the DNA or gene of interest has been successfully transformed in the competent cells during the transformation. To achieve this reaction, the following were added in a sterile microcentrifuge tube:

2.44 µl of vector DNA, 1.87 µl of nuclease-free water, ligase 10x buffer 1 µl, T4 DNA ligase buffer o.5, and nuclease-free water to a final volume of 10 µl.

2.4 Transformation

Bacterial transformation is the process whereby bacteria can take up foreign DNA either chemically or by electroporation.

One Shot™ Stbl3™ chemically competent *E. coli* from Thermofisher Scientific was used. 3 µL of the DNA (10 pg to 100 ng) was added to a thawed-on-ice vial of One Shot™ cells and mixed gently, after which the vial was incubated on ice for 30 minutes and then the cells were heat-shocked for 45 seconds at 42°C without shaking.

The vials are then removed from the 42°C bath and placed on ice for 2 minutes.

250 µl of liquid broth (LB) was added to the vial and placed in a shaking incubator at 37°C for 1 hour at 225 x g, then 50 and 100 µl from each transformation were spread on pre-warmed ampicillin selective plates and incubated overnight at 37°C.

2.4.1 Transformation of control

1 µL of the DNA (10 pg to 100 ng) was added to a thawed-on-ice vial of One Shot™ bacteria and mixed carefully, after which the vial was incubated on ice for 30 minutes, and then heat-shocked for 45 seconds at 42°C without shaking. The vial was then removed from the 42°C bath and placed on ice for 2 minutes. 250 µl of LB was added to the vial and placed in a shaking incubator at 37°C for 1 hour at 225x g, and then the transformation mix was diluted 1:10 into LB (100 µl of the transformation mix added to 900µl of LB) then 50 and 100 µl of the transformation mix was spread on a pre-warmed ampicillin selective plates and incubated inverted overnight at 37°C.

2.4.2 Isolation of plasmid from *E. Coli*

Several colonies of transformed *E. coli* were isolated from the agar plate and inoculated in 5 ml LB + ampicillin. Then they were incubated at 37°C overnight in a shaker incubator at 200 x g with 2 ml of inoculant for plasmids to be harvested. 1.5 ml of inoculant was pipetted into labelled Eppendorf tubes and centrifuged for 30 seconds at 11,000 g, and the supernatant discarded. Isolation and purification of plasmids were done using the Ultraclean Mini Plasmid Prep Kit (QIAGEN, UK). The DNA was then digested by restriction enzymes and loaded on 1% agarose gel to visualise the insert as previously described. Afterward, 1 ml of the selected inoculant was pipetted in 100 ml of LB + ampicillin and incubated overnight at 37°C in a shaker incubator at 200 x g, and plasmid Isolation and purification of the plasmid was carried out following the manufacturer's instructions (NucleoBond® Xtra Midi, Macherey Nagel, USA).

2.5 Lipofectamine transfection of HEK 293T cells with a GFP-expressing plasmid

Transfection is defined as the process of introducing nucleic acids into cells either by physical (electroporation) or chemical (cationic lipid or calcium phosphate) methods. The insertion of DNA enables the expression of proteins using the cells' own machinery.

HEK 293T was plated in Dulbecco's Modified Eagle Medium (DMEM) (ThermoFisher Scientific), 10% FBS, and 1% penicillin/streptomycin and transfected by Lipofectamine 3000 (ThermoFisher Scientific). On the first day, the HEK 293T cells were seeded at 0.5×10^6 per well in 6 wells plate to be 70- 90% confluent at the time of transfection. 6µl of Lipofectamine 3000 Reagent was diluted in 125 µl Opti-MEM (ThermoFisher Scientific) per well and vortexed for 3 seconds. The DNA master mix was prepared by adding 2.5 µg of DNA to 250 µl Opti-MEM and mixed well by pipetting, after which P3000 Reagent (2 µL/µg DNA) was added to the mixture. Diluted DNA was added to Lipofectamine 3000 Reagent (1:1 ratio). The mixture had been incubated for 15 minutes at room temperature and then added to the cells. The next day, the media were replaced by reduced serum media. Opti-MEM transfection efficiency was determined by GFP signal and after 48 hours the cells and the supernatant were collected for analysis.

2.5.1 Transfection with control

In another six-well plate, the same number of cells were seeded at 0.5× 10^6 to be 70-90% confluent at the time of transfection and 6 µl Lipofectamine 3000 Reagent was diluted in 125 µl Opti-MEM per well and vortexed for 3 seconds. The DNA master mix was prepared by adding 5 µg of DNA with empty vector to 250 µl Opti-MEM and mixed well by pipetting, after which P3000 Reagent (2 µL/µg DNA) was added to the mixture. Diluted DNA was added to Lipofectamine 3000 Reagent (1:1 ratio). The mixture was incubated for 15 minutes at room temperature and then added to the cells. The next day the media were replaced by reduced serum media Opti-MEM. Transfection efficiency was determined by GFP signal. After 48 hours, the cells and the supernatant were collected for analysis.

2.6 Western blot

Western blot is used to separate and identify proteins according to their molecular weight. The proteins are separated by gel electrophoresis, then the protein is transferred to a membrane. The membrane is incubated with labelled antibodies that are specific to the protein of interest. The unbound antibody will be washed off, which leaves only the antibody bound to the protein of interest. This can be detected by developing the film.

The cells were washed with 2 ml of PBS, then trypsinised with 500 µl of trypsin for 2 minutes at 37°C, after which 2 ml of DMEM 10% FBS was added to stop the effect of trypsin. The cells were collected in a 15 ml falcon tube and centrifuged for 5 minutes at 161 x g. The media was discarded, and the pellets resuspended in 2 ml ice-cold PBS and centrifuged for 5 minutes at 161 x g. The decant was removed and Laemmle buffer was added, volume dependent on cell count (1 µl for every 10,000 cells), followed by a short spin in the centrifuge for 10 seconds, and then the cells sonicated for 6 seconds to lyse the cells and release the protein. After that, 8 µl of protein were loaded in the gel wells, as described below.

2.6.1 Polyacrylamide gel electrophoresis (PAGE)

In a glass flask, a 12% resolving polyacrylamide gel (37:5:1 acrylamide (Bio-Rad), 0.5 mM Tris (pH 8.8), 0.1% SDS) was prepared followed by the addition of 0.05% TEMED (Fisher Scientific) to initiate polymerisation. The resolving gel was then poured between the gel plates set up on the

Bio-Rad mini gel casting stand up to 1 cm below the comb. Water-saturated butanol was instantly added on top of the gel mix to prevent air contact, after which the gel was left to polymerise for 30-40 minutes. The butanol was then washed off with dH_2O and 4% stacking polyacrylamide gel (37:5:1 acrylamide, 0.125 mM Tris (pH 6.8), (0.1% SDS) was then prepared, followed by the addition of 0.1% TEMED.

The stacking gel was then poured on the top of the resolving gel and the well comb fitted. The gel was set aside at room temperature for 45 minutes to polymerise. The casting gel was then placed inside the PAGE tank (Mini-PROTEAN® Tetra Cell (Bio-Rad) and approximately 1 L of 1x running buffer were drained into the two compartments to establish an electric current through the gel. Followed by the removal of the comb, the wells were flushed with running buffer. Before loading the samples, they were heated at 95°C for 5 minutes to denature and reduce the proteins entirely, and then 10 µl final volume was loaded into wells. Subsequently, the protein samples and a 10 µl Low molecular weight (LMW) protein marker (Precision Plus ProteinTM standard – Bio-Rad) were loaded into the wells, and the SDS-PAGE gels were run at 110 V for 2-3 hours. After electrophoresis, protein transfer was carried out by the wet-system (Mini TransBlot®; Bio-Rad).

After the SDS-PAGE was completed, the stacking gel was removed from the resolving gel and was equilibrated in a 1x transfer buffer for 5 minutes. One piece of nitrocellulose membrane (Amersham Biosciences) and four pieces of filter paper (3 MM Whatman; Fisher scientific) were cut to the gel size. The top corner of the nitrocellulose membrane was marked with a pencil to distinguish the right side of the membrane. The filter papers and the blotting sponges were soaked in 1x transfer buffer for 5 minutes. The blotting system was assembled in 1x transfer buffer. At every step of layering, a roller was used to remove any air bubbles. The blotting cassette was placed in the transfer tank in a vertical orientation, and the tank filled with ice-cold 1x transfer buffer and an additional ice-block so that the negatively-charged molecules would migrate towards the grey anode efficiently, transferring the protein from the gel into the nitrocellulose membrane. The transfer was carried out at a constant 350 mA for 1 hr 15 minutes. To assess the effectiveness of the protein transfer, the membranes were stained for 1 minute with 1x ponceau stain and washed with distal water to remove the excess of the stain.

The membrane was blocked for 1 hour with 5% milk powder in TBS-Tween 0.1% (5 g milk powder in 10 ml TBS-Tween) at room temperature with gentle agitation then the blot was incubated overnight at 4°C with gentle agitation with the 1st antibody (1:200), ab 110328 (Abcam, UK) in 10ml of 5% milk powder in TBS-Tween 0.1%, then washed with 5% milk TBS-Tween 0.1%, 3 times each for 5 minutes. The blot was incubated for 1hr with a secondary antibody in 10ml of 5% milk powder (1:10,000 α-mouse, horseradish peroxidase coupled which specifically bound the primary antibody and washed in 5% milk powder in TBS-Tween 0.1% for five minutes, x3).

To check whether or not the same amount of protein had been loaded into each well for the SDS PAGE, housekeeping genes/proteins (genes/proteins that are always expressed in cells) were measured from the same blot to which our proteins of interest were transferred. To achieve this, blots were washed with TBS-Tween 0.1% for 5 minutes (x3). After, which they were incubated for 1 hour with actin antibody (C-2) from Cruze (1: 1000) then washed in TBS-Tween 0.1% for 5 minutes (x3). The blot was incubated for 1 hour with a secondary antibody in 10ml of 5% milk powder (1:10,000 α-mouse, horseradish peroxidase coupled which binds the primary antibody specifically and washed in 5% milk powder in TBS-Tween 0.1% for 5 minutes, x3).

Chemiluminescent (ECL) substrate was used for the detection of high and low abundance proteins. Initially, the membrane was transferred onto a saran wrap with the protein side upwards. The chemiluminescent reagent mix was prepared according to the manufacturer's instructions (1:1 ratio of substrate components) in a total volume of 2 ml. This was then pipetted onto each membrane covering its entire surface and incubated for 5 minutes at RT. The reagent was drained and the membrane tightly covered with saran wrap. To detect the luminescence, the membrane was exposed to Amersham Hyperfilm ECL films (GE Healthcare) for various lengths of time up to 1 hour in x-ray cassettes. The films were developed in the dark using an automatic firm processing unit (Xograph).

2.6.2 Western Blot quantifications

Western blot signals were quantified using the LI-COR software program. The developed films were scanned and were saved as jpg files. The files were then imported to LI-COR where the single protein bands were measured, resulting in one profile blot for each captured signal. Profile

blots showed the relative density of the respective lanes, with darker signals giving higher peaks and broader signals resulting in lower peaks.

2.7 Frataxin protein quantification

For the quantification of frataxin in the supernatant of transfected HEK 293T, a SimpleStep ELISA kit was used. The ELISA (ab176112) (Abcam) kit has an affinity tag that was labelled capture antibody, in addition to a reporter conjugated detector antibody for immunocapture of the sample analyte in solution. The entire complex (capture antibody/analyte/detector antibody) is immobilised via the immunoaffinity of an anti-tag antibody coating the well.

To quantify the protein, the supernatant of HEK 293T transfected with frataxin fusion peptides was collected 72 hours post-transfection for analysis (24 hours post-transfection the media was changed to FBS-free media). The samples and standards were added to the wells, followed by the antibody mix. After incubation, the wells were rinsed to remove any unbound material, after which TMB Development Solution was added which, during incubation, is catalysed by HRP, turning blue. The addition of Stop Solution then stops the reaction. The signal generated was proportional to the quantity of bound analyte, and the strength of the signal was assessed at 450 nm.

2.8 Acetone protein precipitation from the supernatant

Using the acetone protein precipitation method, the protein was precipitated from the supernatant for further analysis. The supernatant was collected 72 hours post-transfection from the cells. The supernatant was centrifuged at 160 x g for 5 minutes, then four times the sample volume of cold (-20°C) acetone was added. The tube was vortexed and incubated for 60 minutes at -20°C than centrifuged for 10 minutes at 1792 x g. The supernatant was discarded and the kept uncapped at room temperature for 30 minutes to allow the acetone to evaporate. Then the Laemmli buffer was added and sample sonicated for six seconds, after which 10 µL of protein was loaded into the gel wells as described above.

2.9 Immunofluorescence

Immunofluorescence (IF) microscopy is used to evaluate the localisation and the expression level of endogenous protein. Immunofluorescence microscopy uses fluorophores to visualise the site of bound antibodies. The immunofluorescence can be categorised into two forms: primary (direct) and secondary (indirect). The primary form uses a solo antibody that is directly conjugated to a fluorescent dye that can be visualised by a microscope. Secondary immunofluorescence uses double antibodies; a primary antibody that recognises the target biomolecule and binds to it and a secondary antibody that is conjugated to a fluorescent dye, which recognises and binds to the primary antibody and indirectly localises the target for visualisation.

HEK 293T cells were plated in DMEM 10% FBS and 1% penicillin/streptomycin and transfected by Lipofectamine reagents following the same protocols described previously and the supernatant collected 48 hours post-infection. Three out of 6 wells were seeded with fibroblast (FA) from FRADA patients on coverslips. The coverslips were immersed in 70% ethanol washed with PBS and left to dry for 4 hours under ultraviolet light. Two wells were seeded with C4 on coverslips from healthy individuals at 0.5×10^{6} cells the day before the supernatant was collected. The next day the media was changed for two of the FA wells and replaced with supernatant collected from HEK 293T cells and incubated for 2 and 4 hours before immunofluorescence staining. The third FA well did not have its media changed. Healthy fibroblast cells did not receive supernatant from HEK 293T cells, with one of the normal fibroblast coverslips stained with primary and secondary antibodies and the other stained with only secondary antibodies.

The cell was then fixed using 4% paraformaldehyde in PBS pH 7.4 for 10 minutes at room temperature and then rinsed with PBS for 3 minutes (x3). The cells were permeabilised by incubating the samples for 10 minutes with PBS containing 0.5% Triton X-100 on ice and then washed for 3 minutes (x3). The samples were then incubated with a blocking solution of 10% FBS in BPS for 1 hour. After this, 5 µl in 1 ml PBS (concentration of 0.5 µg/ml) of the primary antibody (ab110328, Abcam) was added and incubated overnight at 4°C, then washed with PBS for 5 minutes (x3). Then the cells were incubated with secondary antibodies (5 µl in 1 ml PBS Alexa

Fluor® 594 (2 µg/ml), Abcam) at room temperature for an hour and washed with PBS (5 minutes x4) and covered with slow antifade with DAPI (Thermofisher), left to dry overnight and analysed by the Leica DM 4000 fluorescence microscopy.

The FRDA and normal fibroblast cells were also double-stained with fluorophore-conjugated primary frataxin (ab110328, Abcam) at 0.5 µg/ml dilution and antimitochondrial ab92824 (Abcam) at dilution 1/800 and analysed using Leica DM 4000 fluorescence microscopy as described above.

ImageJ is useful for getting information from images, including pixel intensity, where the image is imported as a jpg. The region of interest (ROI) is selected and measured and subtracted from the background reading.

2.10 Silver staining of the polyacrylamide gel

The SilverXpress Silver Staining Kit is considered to be a highly sensitive silver staining kit that can provide nanogram-level sensitivity with a little background. The mechanism behind silver staining is the ability to reduce silver nitrate to metallic silver in a protein band, after which the bands can be visualised via the silver grain deposits.

The supernatant of the transfected HEK 293T was collected 48 hours post-transfection with HEK 293T, APP-truncated frataxin fusion peptide, and from cells transfected with APP-frataxin fusion peptide construct (used as a positive control) and empty vector (used as a negative control). The protein was acetone precipitated, and the samples separated on 4-20% PROTEAN TGX precast polyacrylamide gel from Bio-Rad and stained with SilverXpress Silver Staining kit from Thermo Fisher. After the electrophoresis was finished, the membrane was fixed in 200 mL methanol, acetic acid and Ultrapure water for 10 minutes, then sensitised in in 200 mL methanol, Ultrapure water and sensitiser for 20 minutes, followed by washing with ultrapure water for 40 minutes and stained in 100 mL stainer solution (A 5 mL Stainer B 5 mL Ultrapure Water 90 mL) for 15 minutes, followed by washing with Ultrapure Water 400 mL for 10 minutes. The membrane then was then developed in a 100 mL developer solution (5 mL Ultrapure Water 95 mL) for 15 minutes. Stopper (5 mL) was directly added to the developing solution. Finally, the membrane was washed

again with Ultrapure water for 30 minutes. Frataxin bands were detected at 20 KDa in supernatant collected from HEK 293T transfected with APP-frataxin fusion peptides, and at 14 KDa in supernatant collected from cells transfected with APP-truncated frataxin. There was no protein band detected from supernatant collected from HEK 293T transfected with the empty vector.

2.11 Cell proliferation assay MTS

The CellTiter 96 AQueous Non-Radioactive Cell Proliferation (Promega) is a colourimetric assay that is used for detecting the sum of viable cells in cytotoxicity, chemosensitivity, and proliferation assays. The CellTiter 96 AQueous One Solution Reagent has a tetrazolium and an electron coupling reagent (phenazine methosulfate) PMS. MTS is bio-reduced by dehydrogenase enzymes that are found only in viable cells to form a formazan product that is soluble in the tissue culture medium. The formazan product can be detected at 490 nm and is directly proportional to the number of living cells in culture.

To perform the assay, HEK 293T was seeded in 6-wells at 0.5×10^6 for 24 hours to reach 70-90% confluency at the time of transfection. The following day it was transfected with Lipofectamine 3000 with DNA that has the insert and DNA with an empty vector following the same protocol before transfecting it with the plasmid containing frataxin fusion peptide constructs. The media was changed 24 hours post-transfection, and the cells were washed with PBS following the steps described above. FA and normal fibroblast cells were seeded in a 96-well plate containing 100 µl of DMEM, 10% FBS, and 1% penicillin/streptomycin at 20,000 cells per well of FA1 and C4. Four plates were used in total. On the day of the assay, the media was changed and replaced with 100 µl of supernatant from transfected HEK 293T cells one hour before adding the H_2O_2 35 wt.% solution from ACROS Organics™.

The first three wells of each plate were just media (MDEM) with no cells to be used as a blank. The first plate of FA was incubated with supernatant that had Frataxin fusion peptide constructs. The second was incubated with the supernatant that had an empty vector. One of the 96-well plates was incubated with supernatant that had the Frataxin fusion peptide constructs and the other with supernatant that had the empty vector. After 1 hour, hydrogen superoxide (H_2O_2) at

concentrations of 50 µM and 200 µM was added to all the plates in triplicate. In each plate, the first three rows had the blank cells, then cells with MDEM media containing 10% FBS and 1% penicillin/streptomycin, then cells with either empty vector or frataxin fusion peptide constructs. These were treated with 50 µM of H_2O_2. The last triplicate were cells with supernatant from either frataxin fusion peptide constructs or empty vector with 200 µM of H_2O_2. They were incubated for 6 hours. The MTS and PMS were thawed 10 minutes before use in a 37°C water bath. 200 µl of PMS was added to 4 ml of MTS just before adding to the assay plates. 20 µl of mixed MTS and PMS was added to the assay plates and incubated for 3 hours at 37°C in a humidified, 5% $C0_2$ atmosphere, after which the plate reader determined the formazan formation at 490 nm. The cell viability was calculated according to the formula:

> %viable cells= ((absorbance sample-absorbance blank) x 100 / Absorbance control-absorbance blank)

2.12 Aconitase assay

An aconitase activity assay was performed on the cell lysates using Aconitase Assay Kit ab83459. In the protocol, aconitase is converted from citrate into isocitrate. The isocitrate is further processed, which results in a product that converts a near-colourless probe into an intensely coloured form with maximum absorbance at 450 nm.

Fibroblasts from FA and healthy individuals were incubated for 1 hour with supernatant collected from HEK 293T cells that had been transfected with frataxin fusions peptide constructs and empty vector as a control. Around $1x10^6$ human fibroblasts were harvested for the assay. The cells were washed with cold PBS and suspended in 100 µL of cold assay buffer and homogenised quickly by pipetting up and down a few times. This was followed by centrifuging the samples for 10 minutes at 4°C at 800 g using a microcentrifuge to eliminate any insoluble material. The supernatant was collected and moved to a clean tube.

All the material was equilibrated at room temperature. Aconitase activation solution was prepared by adding 100 µL of cysteine HCl to 100µL of $(NH_4)_2Fe\ (SO_4)_2$, mixed to prepare a new activation solution. 10 µL of activation solution was added to a 100 µL sample and incubated on

ice for 1 hour to activate aconitase in the sample. A substrate reaction premix was prepared as shown in Table 2-3

Table 2-3. Aconitase assay substrate reaction premix.

Component	Colourimetric Reaction mix (µL)	Background reaction mix
Assay Buffer	42	44
Enzyme Mix	6	6
Substrate	2	0

50 µL of the reaction mixture was added to each well of 96-well plates except sample background wells. In the sample background wells, 50 µL of background reaction mix was added in triplicate and incubated at 25°C for 30-60 minutes. 10 µL of the developer was added to each well. The output was measured at OD (Optical density) of 450 nm. The isocitrate standard curve was plotted, and ΔOD was applied to get the amount of isocitrate in nmol from the standard curve.

2.12.1 Virus titration using K-562 cells

The cells were resuspended at $2x10^5$ per ml, and around 500 µL cells were seeded per 12 wells. The virus was diluted at 1:50 (20 µL virus + 980 µL media), and 500 µL was put in the first well (1:100 dilution). Another three 1:10 serial dilutions from the 1 to 50 were performed (900 µL media and 100 µL previous dilution) and 500 µL of each dilution was added to 500 µL of cells to give dilutions of 10^{-3}, 10^{-4} and 10^{-5}. The cells were harvested for titration 72 hours later using flow cytometry for GFP expression. The titre was calculated from the dilution of a virus that gave about 3-10% GFP +ve.

2.13 Transduction of CD34+ HSPC cells

CD34+ $HSPC^+$ cells were thawed, counted, evaluated for viability, and seeded at $1x10^6$/ml in 1x culture StemSpan (Stem Cell Technologies) medium with full cytokine cocktail. hSCF 100 ng/ml, hFlt 3 L 100ng/ml, hTPO 20 ng/ml (Peprotech) + 1% PenStrep (Thermo fisher) were prepared. Following cytokine pre-stimulation for 24 hours, cells were seeded in 2x medium (Stem Span 1% PenStrep, 10 µl SCF, 10 µl Flt3, 2 µl TPO, 1 µl IL3 (Peprotech)) at a concentration of $2x10^6$ /ml in 24-well plates. The virus (MOI= 20) and protamine sulphate were then added to the cells (see Table 2-4; 2-5).

Twenty-four hours post-transduction, the cells were counted, and differentiation had started in both liquid and methylcellulose cultures.

Table 2-4. CD34+ HSPC transduction at MOI 20.

	Un-transduced (control)	**Transduced MOI 20**
Cells in 2x medium	125 µl	125 µl
Virus	-	X µl
Protamine Sulphate	2.5 µl	2.5 µl
Medium with no cytokines	122.5 µl	X µl
total	250 µl	250 µl

Twenty-four hours post-transduction, the cells were counted and seeded at 300,000/ml into IMDM (Gibco), 20% FBS, 1% PenStrep (Thermofiser), and GCSF (Peprotech) 100 ng/ml. The medium was added on Monday, Wednesday, and Friday. On Friday, the cells were spun down and resuspended at 300,000/ml. The differentiating analysis was carried out by FACS for 22 days.

Table 2-5. Media and cytokines used for CD34+ HSPC

Media	**Cytokines**
StemSpan (Stem cell Technologies)	hSCF 100ng/ml (Peprotech)
IMDM medium (Gibco)	hFlt3L 100ng/ml (Peprotech)
Methocult H4434 StemSpan (Stem Cell Tech).	hTPO 20ng/ml (Peprotech)
	hIL3 20ng/ml (Peprotech)

2.13.1 Cell differentiation analysis by flow cytometry

The cells were harvested after 22 days in liquid culture, washed and suspended to a concentration of 1-5 x 10^6 cells/mL in ice-cold PBS, 10% FBS. The cells were stained in polystyrene round bottom 12x75 mm^2 Falcon tubes. 0.2 mg/mL of 0.1-10 µg/mL of FACS CD11b Monoclonal Antibody (M1/70), APC, ™Bioscience (Thermofisher) was added, and the samples were incubated for 1 hour at 4°C. The cells were washed (x3) by centrifugation at 1792 x g for 5 min and resuspended in 500 µL of ice-cold PBS, 10% FBS, and then analysed by FACS.

Methocult ™ H4434 (StemSpan) is a complete methylcellulose-based medium which supports the expansion of haematopoietic progenitor cells in colony-forming unit (CFU) assays. Different colonies can be formed and detected, such as erythroid progenitor cells (BFU-E and CFU-E), granulocyte-macrophage progenitor cells (CFU-GM, CFU-G, and CFU-M), and multipotential granulocyte, erythroid, macrophage and megakaryocyte progenitor cells (CFU-GEMM). The cells were plated at a concentration of $1x10^6$/ml and 20 µl was taken and added to 180 µl of RPMI, from which 10 µl (1,000 cells) was added to 290 µl of RPMI on a new 15 ml tube. Then 3 ml of Methocult was added to the cells and mixed up carefully to avoid bubble formation. The cells were plated onto two six-well plates (1.5 ml each). The two middle wells were filled with 1.5 ml of PBS. The colonies were scored after 10-14 days.

2.14 Statistical analysis

Statistical analysis, such as detailed measurements and graphical visualisation, was done using Microsoft Excel 2016 software and GraphPad Prism7. All other measurements comparing sample groups were analysed using the Student's T-test. In all cases, a p-value lower than 0.05($*$), 0.01($**$), or 0.001 ($***$) were considered significant.

Chapter 3.

Cloning and *in vitro* expression and secretion of frataxin fusion peptides

3.1 Introduction

Gene therapy carries the potential to cure a variety of inherited and acquired diseases, as shown by the achievements in the treatment of X-linked severe combined immunodeficiency (SCID-X1), adenosine deaminase (ADA) deficiency and chronic granulomatous disease (CGD) (Kumar *et al.*, 2016b). In gene therapy, the defective gene is replaced by a functional copy made of three main components: 1) the therapeutic gene, 2) the vector that will deliver it, 3) the mode of administration (Sung, 2019).

Cell-penetrating peptides (CPPs) can be used to transport molecules into cells owing to their intrinsic capacity to penetrate into the cells and facilitate the uptake of an extensive range of macromolecular cargos (Stewart, Horton and Kelley, 2008; Tripathi *et al.*, 2018). This ability was exploited in our laboratory to develop a cell-penetrating version of frataxin, which could be delivered to diseased tissues in Friedreich's ataxia patients.

The aims of the experiments described in this chapter were:

- To clone different frataxin fusion peptides into a lentivirus vector.
- To transfect HEK 293T with the frataxin fusion peptide constructs.
- To observe the secretion of frataxin peptides into the supernatant of transfected HEK 293T.
- To prove the ability of the cell-penetrating peptide to deliver the frataxin into the fibroblast.

3.2 Cloning of frataxin fusion peptides into a lentivirus vector

To construct the delivery vector, frataxin fusion peptide constructs were cloned into an 8,801bp lentiviral vector (pLIG). The lentivirus vector pLIG (lentivirus-IRES-eGFP) has an *Xba*I site upstream of the IRES element, which permits cloning of any cDNA into the vector. It is expression-linked to GFP expression (Figure 3-1).

The cDNA for human precursor frataxin was fused to a signal peptide, signal peptides are short peptides directing newly synthesized proteins toward the secretory pathway (Peng *et al.*, 2019). After directing proteins to their specific locations they are removed by signal peptidases (Peng *et al.*, 2019). The constructs were custom synthesised using Gene Art services (Invitrogen) into pMA

(Figure 3-2). It was designed in the following order: 1) signal peptide for the secretion of the fusion protein; 2) cell-penetrating peptide; and 3) frataxin. The rationale for this design was that the frataxin fusion protein will be processed in the mitochondria, and the signal peptide and cell-penetrating peptides will be proteolytically removed leaving the mature frataxin isoform.

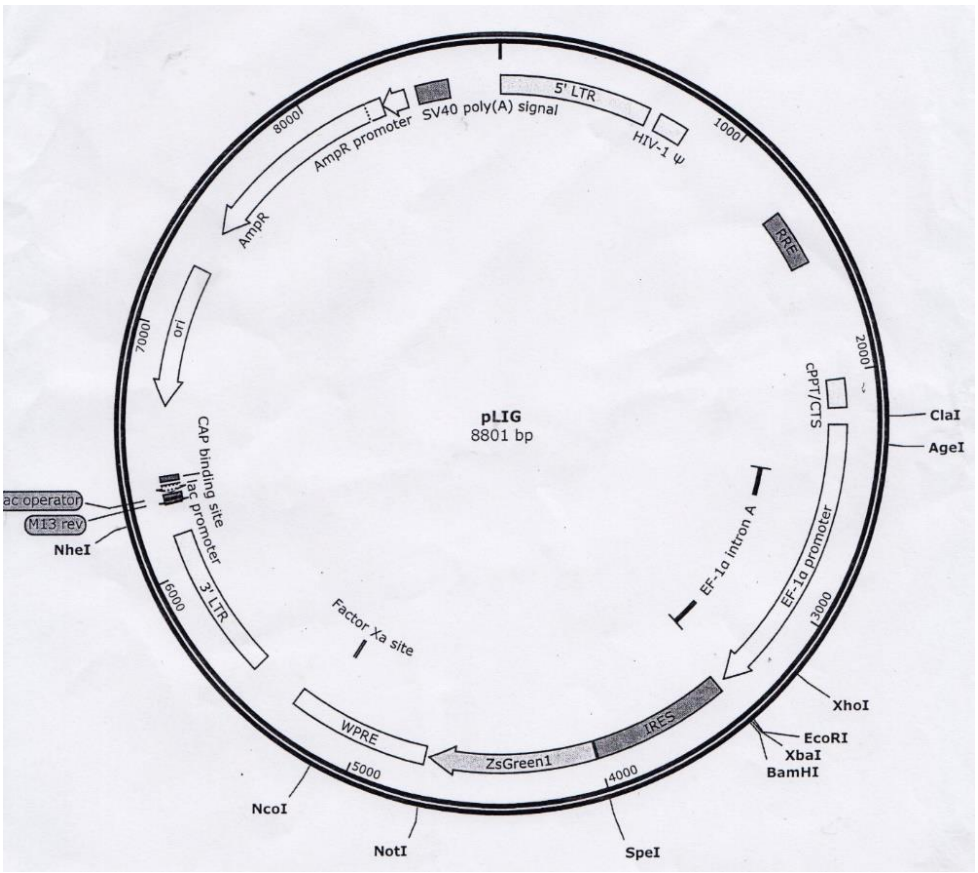

Figure 3-1. Schematic map of the pLIG vector 8,801bp displaying unique cloning sites.
LTR: Log terminal repeats. RRE: rev response element. cPPT central polypurine tract. WPRE: Woodchuck hepatitis virus post-transcription regulatory element. EF-1a promoter

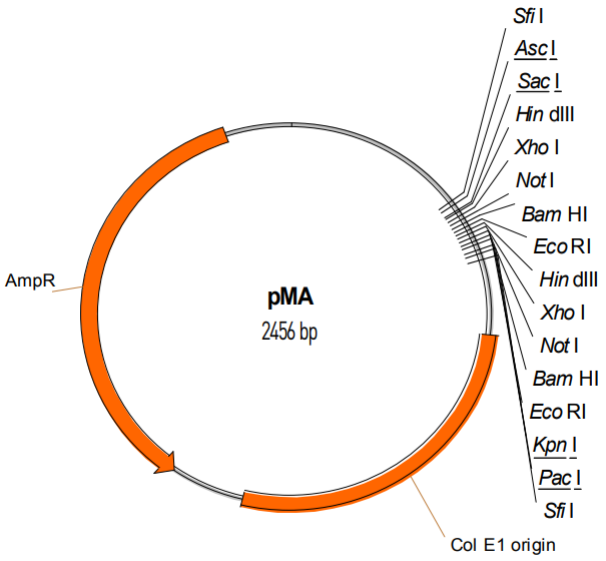

Figure 3-2. Schematic map of the pMA vector 2456 bp.

3.2.1 TAT-frataxin fusion peptides construct

Previous research has shown that a TAT-frataxin fusion protein could deliver frataxin to mitochondria and increase the lifespan of animal models of the disease (Vyas *et al.*, 2012; Britti, Tamarit and Ros, 2018). TAT is a short, cationic peptide that can effectively deliver a protein into various tissues and organelles, including the mitochondria and nucleus (Del Gaizo, MacKenzie and Payne, 2003), and that a TAT–FXN fusion protein can save FRDA patient fibroblast cells and the severe short-lived phenotype of the conditional frataxin knockout mouse model with deletion of the frataxin gene in cardiac and neural crest-derived tissues (Vyas *et al.*, 2012). Therefore, TAT was selected as a cell-penetrating peptide in our study. The 759 bp TAT-frataxin fusion peptide construct consists of the following part: MDFQVQIFSFLLISASVIISRG-YGRKKRRQRRR-frataxin (Figure 3-3a)

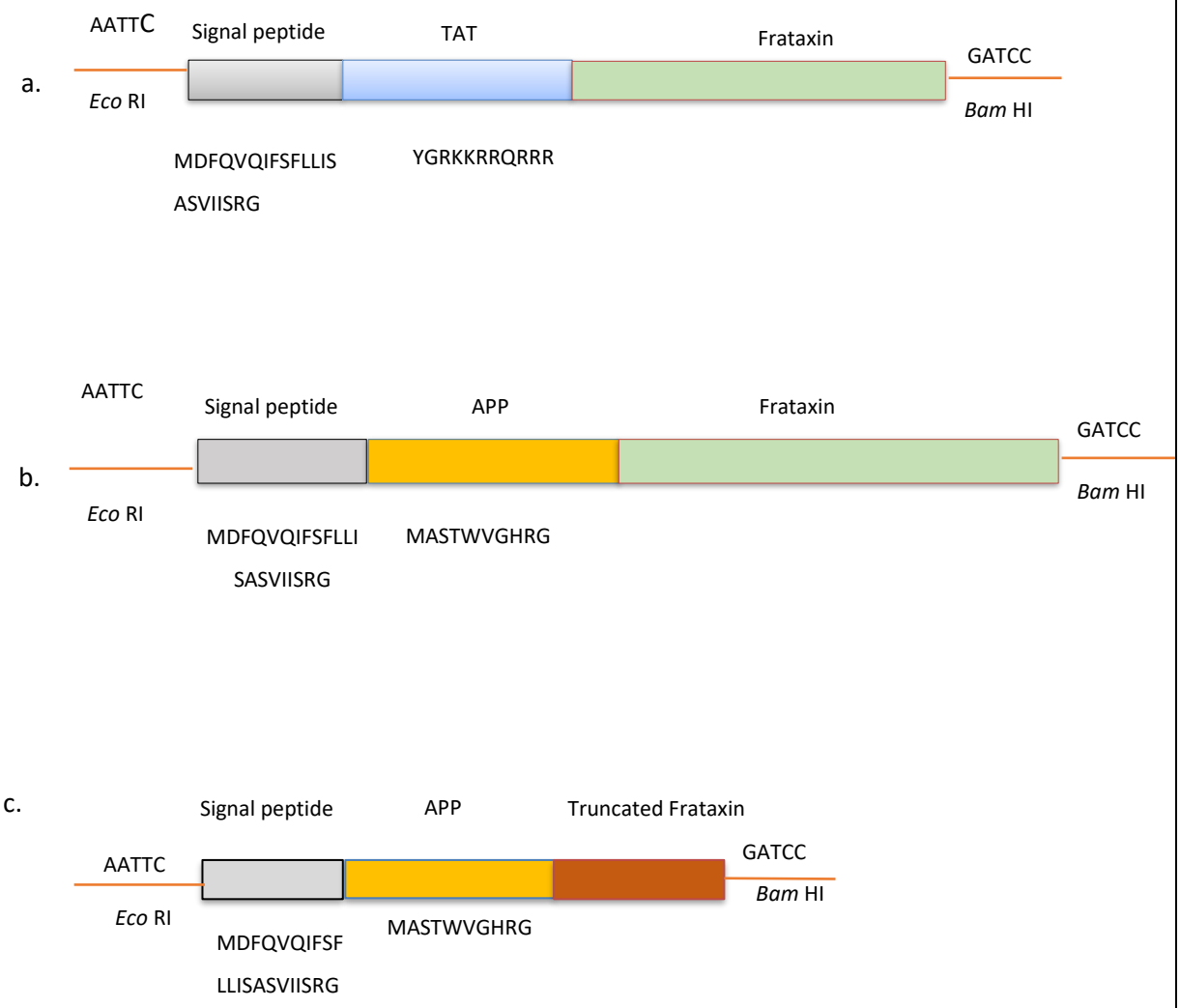

Figure 3-3. Frataxin fusion peptide constructs.

a) 759 bp TAT- frataxin fusion peptide construct. b) 764 bp APP- frataxin fusion peptide construct cloned into the pLIG vector. c) 173 bp truncated frataxin fusion peptide construct.

3.2.2 APP-frataxin fusion peptides construct

The disadvantages of using a TAT-derived peptide are its positive charge, potential cytotoxicity, and immunogenicity. Therefore, after analysis of the literature, we identified another tissue-penetrating peptide derived from human annexin, annexin penetrating peptide (APP) (Kim *et al.*, 2015a). APP is a non-cationic, membrane-interacting peptide that is less immunogenic than conventional CPPs and has a higher serum availability. Since it is of human origin, it is less likely than viral-derived peptides such as TAT to be immunogenic and thus is potentially more suitable for clinical use (Kim *et al.*, 2015a). The construct of frataxin fusion peptide 764 bp, consists of the following parts: MDFQVQIFSFLLISASVIISRG- MASTWVGHRG-frataxin (Figure 3-3b)

3.2.3 APP-truncated frataxin fusion peptides construct

There was a need to determine if any effect observed in our studies is related to the effect of the frataxin and not by any chance related to CPP action. TAT has been used in many other studies (Vyas *et al.*, 2012; Britti *et al.*, 2017; Britti, Tamarit and Ros, 2018), and therefore we designed a 173 bp construct made up of MDFQVQIFSFLLISASVIISRG-MASTWVGHRG-truncated frataxin. This construct has been used as a control to compare its effect against APP-Frataxin fusion peptide constructs in several functional studies (Figure 3-3c).

3.2.4 Subcloning the frataxin fusion peptides into pLIG

After the cDNA (1-50ng) of frataxin, fusion peptides were propagated by transforming Shot™ Stbl3™ E. coli (Invitrogen). The plasmids containing the inserts of frataxin fusion peptides have been purified and released from pMA vector by restriction enzyme digestion with *Bam* HI and *Eco* RI (Promega). Agarose gel electrophoresis was used to visualize the size of the product, and DNA was cut off the gel and purified described chapter 2.3.

Ligation of DNA products has been done by using T4 DNA ligase (Promega). A molar ratio of 1:3 vector to insert DNA ratio has been calculated using NEBio Calculator online software (New England Biolabs). Frataxin fusion peptides were expressed and purified from Shot™ Stbl3™ E. coli. TAT-Frataxin construction's DNA was digested by restriction enzymes and loaded on 1% agarose gel to visualize the insert.

The result was a new lentiviral vector containing TAT- frataxin fusion peptide gene 759 bp (Figure 3-4a), APP-frataxin fusion peptide 764 gene bp (Figure 3-4b) and APP-truncated frataxin fusion peptide gene (Figure 3-4c).

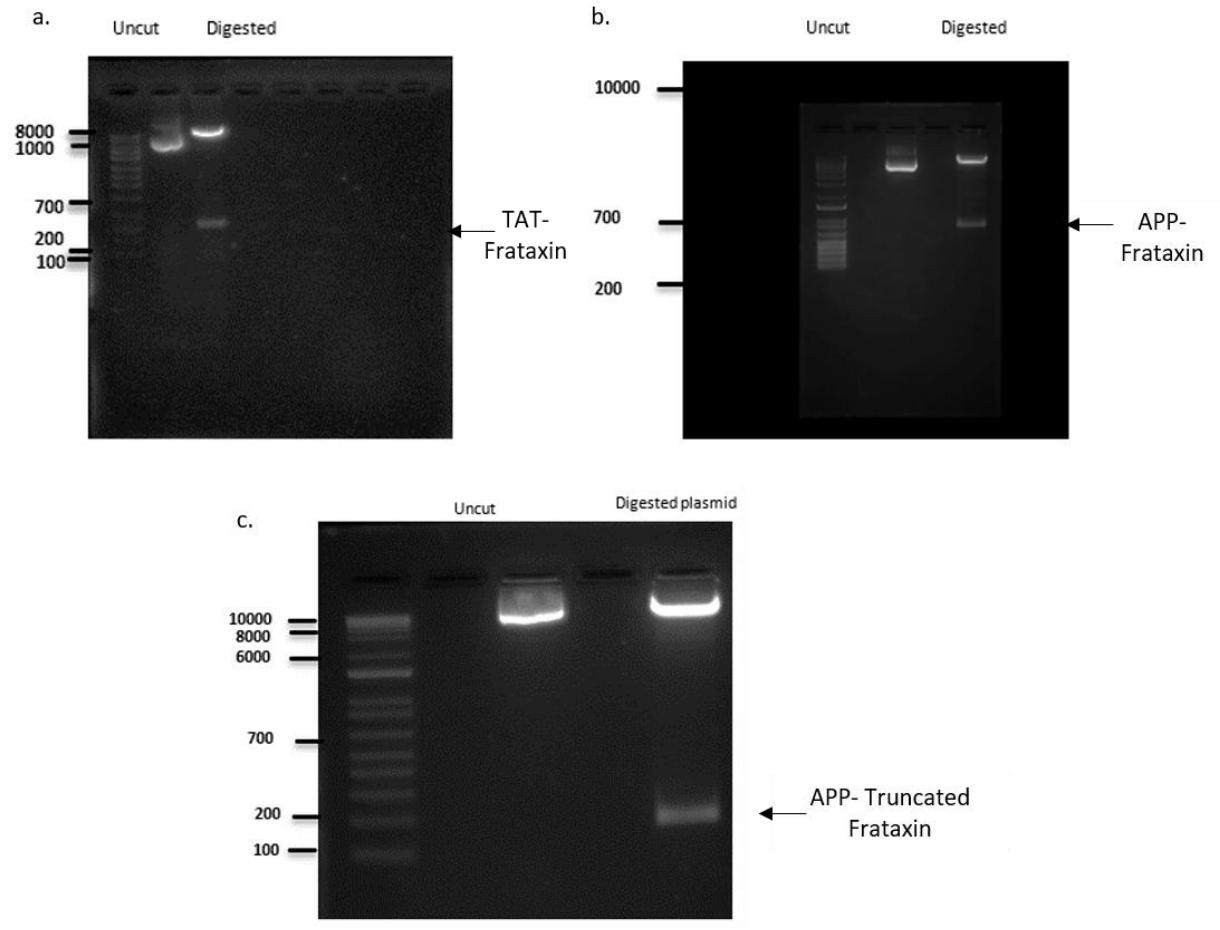

Figure 3-4. Subcloning the frataxin fusion peptides

a) TAT- Frataxin construction; DNA was digested by restriction enzymes and loaded on 1% agarose gel to visualise the insert. DNA was loaded on 1% agarose gel and run at 70 mV. b) APP- Frataxin construction; DNA was digested by restriction enzymes and loaded on 1% agarose gel to visualise the insert. DNA was loaded on 1% agarose gel and run at 70 mV. c) APP- truncated frataxin; DNA was digested by restriction enzymes and loaded on 1% agarose gel to visualise the insert. DNA was loaded on 1% agarose gel and run at 70 mV.

3.3 Transfection of pLIG-frataxin fusion peptides into HEK 293T cells

To determine the functionality of our plasmid constructs, they first needed to be evaluated in a cell line that allows highly efficient transfection and high protein expression. HEK 293T cells were selected for the transfection studies.

3.3.1 Preliminary studies

Before starting to work with our constructs, preliminary studies were performed using only the TAT-frataxin fusion peptide to set and validate the system for transfection, western blot, and protein precipitation from the supernatant.

The results showed successful transfection of HEK 293T, as demonstrated by cells expressing GFP 24- and 48-hours post-transfection using a JULITM Smart fluorescent cell analyser (Figure 3-5a). Western blot analysis confirmed that the transfection had been successful and the frataxin was being expressed inside the cells. The presence of the mature 14 kDa, and of the intermediate form of frataxin showed that the frataxin had been delivered to the mitochondria, where it has been processed by MPP to give the mature and intermediate forms (Figure 3-5b). Frataxin fusion peptide has been secreted successfully in the supernatant as indicated by the western blot and ponceau stain, where a frataxin band has been detected at 23 KDa (Figure 3-5c).

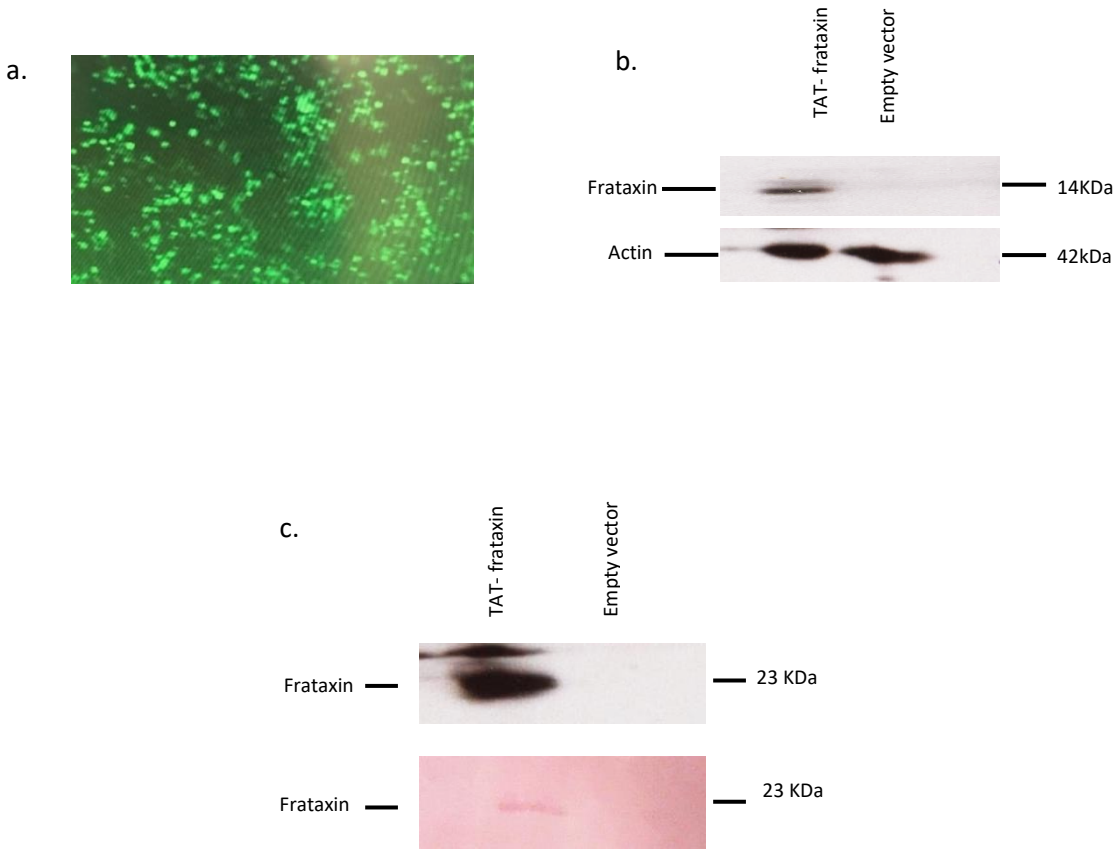

Figure 3-5. Transfection of HEK 293T transfected by TAT-frataxin fusion peptide.

a) HEK 293T transfected by TAT-frataxin fusion peptide, GFP signal using a JULITM Smart fluorescent cell analyser 24 hours post-transfection. b) Western blot of transfected HEK293T with empty vector as a negative control and TAT-frataxin fusion peptide which shows bands of mature frataxin at 18 and 14KDa from HEK 293Ttransfected with TAT-frataxin fusion peptide B. Shows the band of control actin at 42KDa for both HEK 293Ttransfected with empty vector and TAT-frataxin fusion peptide. c) Western blot analysis for protein precipitated from the supernatant collected from HEK 293T transfected with TAT-frataxin fusion peptide or with an empty vector as a negative control. Band of unprocessed frataxin is detected at 23 KDa in the protein precipitated from HEK 293T transfected with TAT-frataxin fusion peptide. Ponceau stain also shows frataxin.

HEK 293T were transfected with the control pLIG plasmid and a plasmid carrying various frataxin fusion peptides constructs. Lipofectamine 3000 (Invitrogen) was used as a transfection reagent. For each transfection reaction, a master mix of the DNA of frataxin fusion peptide and control was prepared and added to diluted Lipofectamine 3000 Reagent (1:1 ratio).

Estimation of HEK 293T expressing GFP was done by FACS analysis, and showed: 71.63% of cells expressing GFP signals in cells transfected by the TAT-frataxin fusion peptide; 72.18% of cells expressing GFP signals transfected by APP-frataxin fusion peptide; 70.83% of cells expressing GFP signals transfected by empty vector as a control, and 74.54% of cells expressing GFP signals transfected by the APP truncated frataxin fusion peptide (Figure 3-6).

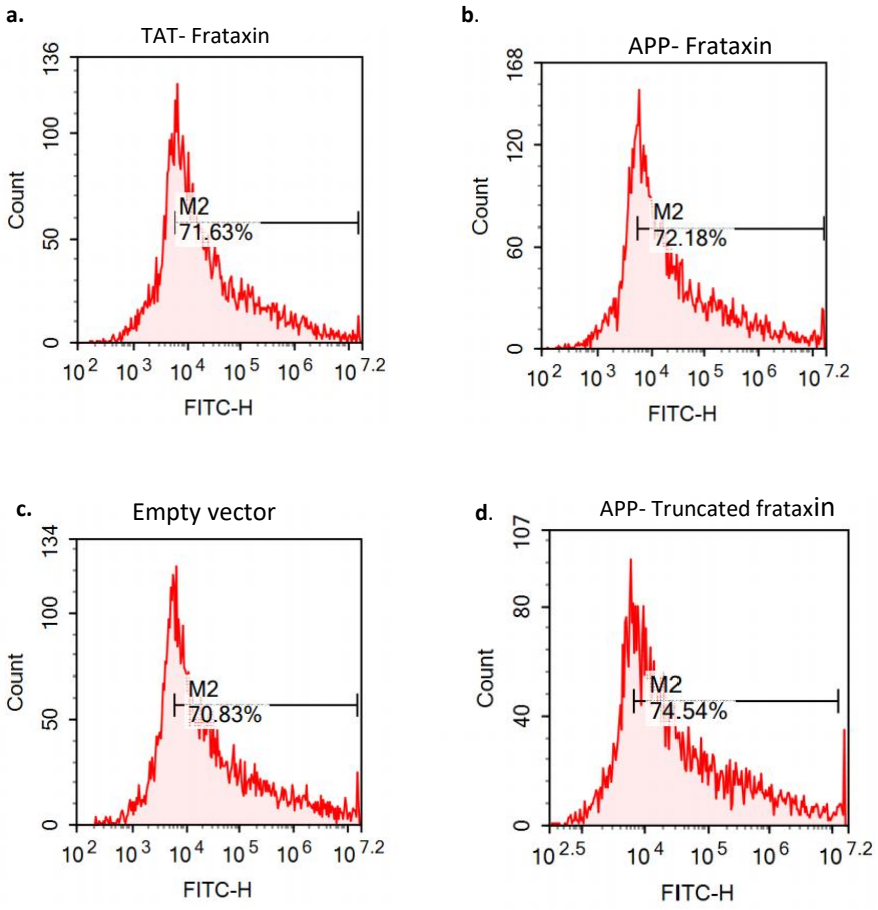

Figure 3-6. Flow cytometry estimation of transfected HEK-293t expressing GFP.

a). transfected by TAT- Frataxin fusion peptide. b) Transfected by APP- Frataxin fusion peptide. c) Transfected by empty vector as control. d). Transfected by APP- truncated Frataxin fusion peptide.

3.4 Frataxin band was detected by western blot in HEK 293T transfected with a penetrating version of the frataxin fusion peptide

To investigate whether the transfected HEK 293T cells express frataxin, the cells were harvested for analysis 48 hours post-transfection. The proteins were then separated on 12% SDS-polyacrylamide gel and transferred onto a nitrocellulose transfer membrane.

Frataxin was strongly overexpressed in cells transfected with TAT and APP frataxin fusion peptides. Strong frataxin bands were detected at 23 KDa in cells transfected with frataxin fusion penetrating peptide constructs, where a faint band was detected in HEK 293T transfected with empty vector at 23 KDa. This indicates that transfected cells were able to express the frataxin successfully (Figure 3-7).

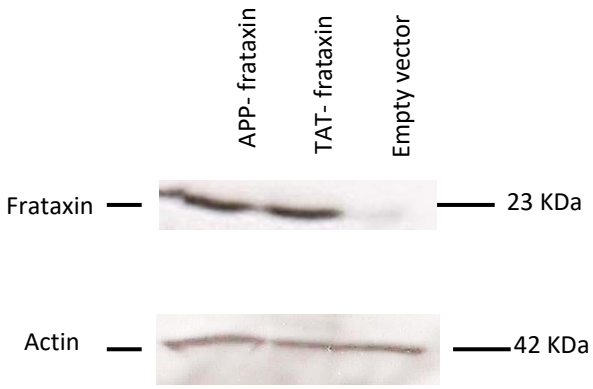

Figure 3-7. Western blot for transfected HEK 293T with APP- Frataxin fusion peptides, TAT- Frataxin fusion peptide, and empty vector.

TAT-Frataxin fusion peptide and APP-Frataxin fusion peptide both show bands of mature frataxin at 23 KDa from HEK 293T transfected with Frataxin fusion peptide construct, actin used as control protein with band detected at 42 KDa.

3.5 Frataxin fusion peptide had been secreted into the supernatant

3.5.1 Western blot analysis for TAT, APP-frataxin fusion peptide constructs

To determine whether the frataxin fusion penetrating peptides constructs were successfully secreted into the supernatant, the supernatant of transfected HEK 293T cells was collected 48 hours post-transfection and centrifuged. The protein was acetone precipitated, and samples were loaded onto 12% SDS-polyacrylamide gel.

The result showed that Frataxin was strongly over-expressed in the supernatant collected from cells transfected with TAT and APP frataxin fusion peptides, and there were strong bands detected at 23 KDa, in comparison to empty vector (control), where no bands were detected.

ELISA frataxin quantification for protein precipitated from the supernatant showed the following values: cells transfected with empty vector 35 ng/mL; cells transfected with TAT 400 ng/mL; and cells transfected with APP-frataxin APP- frataxin 360 ng/mL. This indicates that the frataxin fusion peptide constructs were successfully secreted into the supernatant at significantly higher levels than in the control (Figure 3-8).

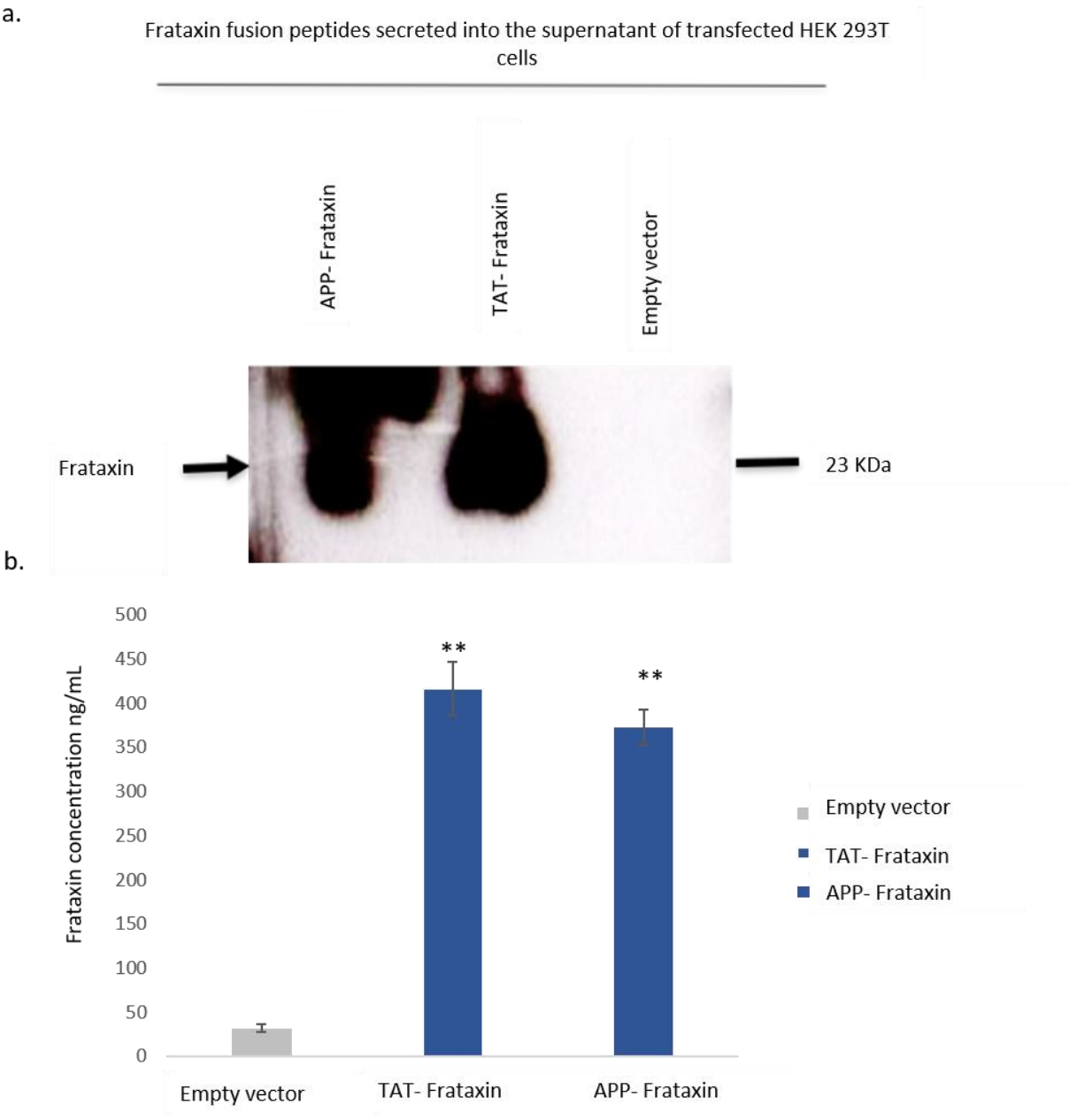

Figure 3-8 Western blot analysis and ELIZA frataxin quantification for protein precipitated from supernatant for transfected HEK 293T.

western blot analysis and ELIZA frataxin quantification for protein precipitated from supernatant collected from HEK 293T transfected with Frataxin fusion peptides or with empty vector as a negative control, frataxin bands were detected at 23 KDa in the protein precipitated from HEK 293T transfected with Frataxin fusion peptides. Columns represent mean values (mean± SEM) of two replicates of three independent experiments (n= 3, **p < 0.005).

3.5.2 Silver staining for polyacrylamide gel for APP-truncated frataxin fusion peptide construct

To investigate whether the transfected HEK 293T cells were able to secrete APP-truncated frataxin fusion peptide constructs into the supernatant and since there are no available antibodies to detect it, silver staining of the polyacrylamide gel was used to detect the truncated peptide. The supernatant of the transfected HEK 293T was collected 48 hours post-transfection with HEK 293T, APP-Truncated frataxin fusion peptide, and from cells transfected with APP-frataxin fusion peptide construct (used as a positive control) and empty vector (used as a negative control). The protein was acetone precipitated, and the samples separated on 4-20% PROTEAN TGX precast polyacrylamide gel from Bio-Rad and stained with a SilverXpress Silver Staining kit from Thermo Fisher. Frataxin bands were detected at 20 KDa in the supernatant collected from HEK 293T transfected with APP-frataxin fusion peptides, and at 14 KDa in supernatant collected from cells transfected with APP-truncated frataxin. There was no protein band detected from supernatant collected from HEK 293T transfected with the empty vector (Figure 3-9). The results indicated that the APP-Truncated frataxin fusion peptide was successfully secreted into the supernatant.

To summarise, frataxin fusion peptide constructs were able to transfect the HEK 293T efficiently, as shown by the GFP signal and the western blot analysis. Most importantly, the transfected cells were able to secrete the frataxin fusion peptide into the supernatant. This is an essential step because our aim is to deliver frataxin fusion peptide constructs to FRDA cells by incubating them with the supernatant from transfected HEK 293T.

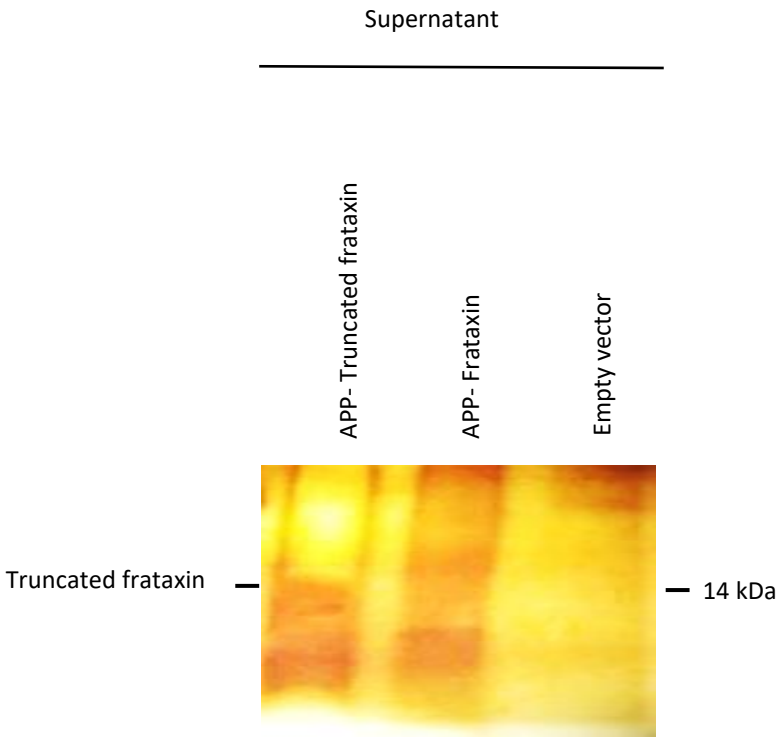

Figure 3-9. Silver staining of protein precipitated from supernatant collected from HEK 293T transfected with APP- Truncated frataxin.

Frataxin fusion peptides (positive control), APP-Truncated frataxin and with empty vector (negative control). Frataxin bands were detected at 20KDa in the protein precipitated from HEK 293T transfected with APP- Frataxin fusion peptides, and another band detected at 14KDa from HEK 293T transfected with APP- truncated Frataxin fusion peptides and no band detected in supernatant collected from cells transfected with empty vector**.**

3.6 Frataxin fusion peptide penetrates FRDA deficient human fibroblast

Cells derived from FRDA patients create the most appropriate frataxin-deficient cell model as they carry the GAA repeat expansions, and their viability is affected under stress situations (e.g., treatment with hydrogen peroxide or buthionine sulfoximine) (Pandolfo and Hausmann, 2013), which makes them suitable for studying the ability of our construct to prevent cellular damage

related to oxidative stress. Therefore, fibroblasts were used as a model to test the effect of frataxin fusion peptides on both human health and FRDA fibroblast patients (FA1).

To investigate the ability of constructs to penetrate and deliver frataxin into the FRDA fibroblast cells, and to test whether the delivered frataxin remains in the cells and does not translocate out of them, preliminary studies were carried out using TAT-frataxin fusion peptide. The fibroblast was treated with supernatant collected from HEK 293T transfected with TAT-frataxin fusion peptide for 4- and for 24-hours after which the cells have been collected for analysis.

Western blot and immunofluorescence analysis using the frataxin label antibody confirmed the delivery of frataxin to FRDA cells. The presence of a frataxin band at 14 KDa and 18 KDa indicates that the frataxin had been delivered into the mitochondria where it had been successfully processed by MPP. The presence of bands at 4- and 24-hours indicates that the CPP moiety has been removed successfully. This is considered an important step, otherwise, the CPP frataxin fusion peptide could potentially translocate out of the cell. Immunofluorescence analysis confirmed the same result (Figures 3-10 and 3-11).

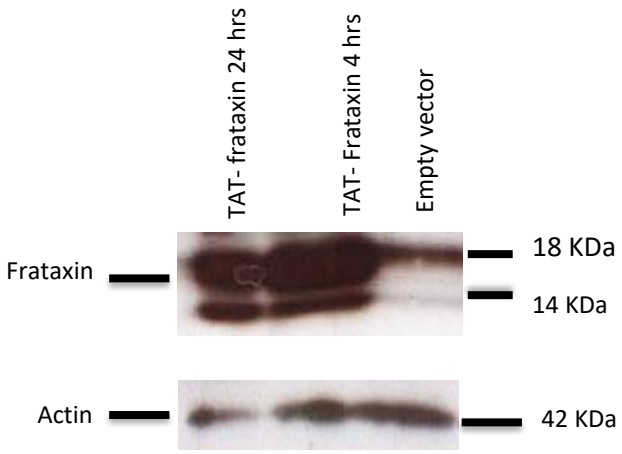

Figure 3-10. Western blot for FRDA fibroblast (FA1) incubated with the supernatant collected from HEK 293T transfected with TAT- Frataxin fusion peptide for 4 and 24 hrs.

Mature and intermediate frataxin bands were detected at 14 and 18 KDa respectively in the fibroblast incubated with the supernatant collected from HEK 293T transfected with TAT- Frataxin fusion peptide for 4 and 24 hrs, in comparison to faint bands at 14 and 18 KDa in cells incubated with the supernatant collected from HEK 293T transfected with empty vector.

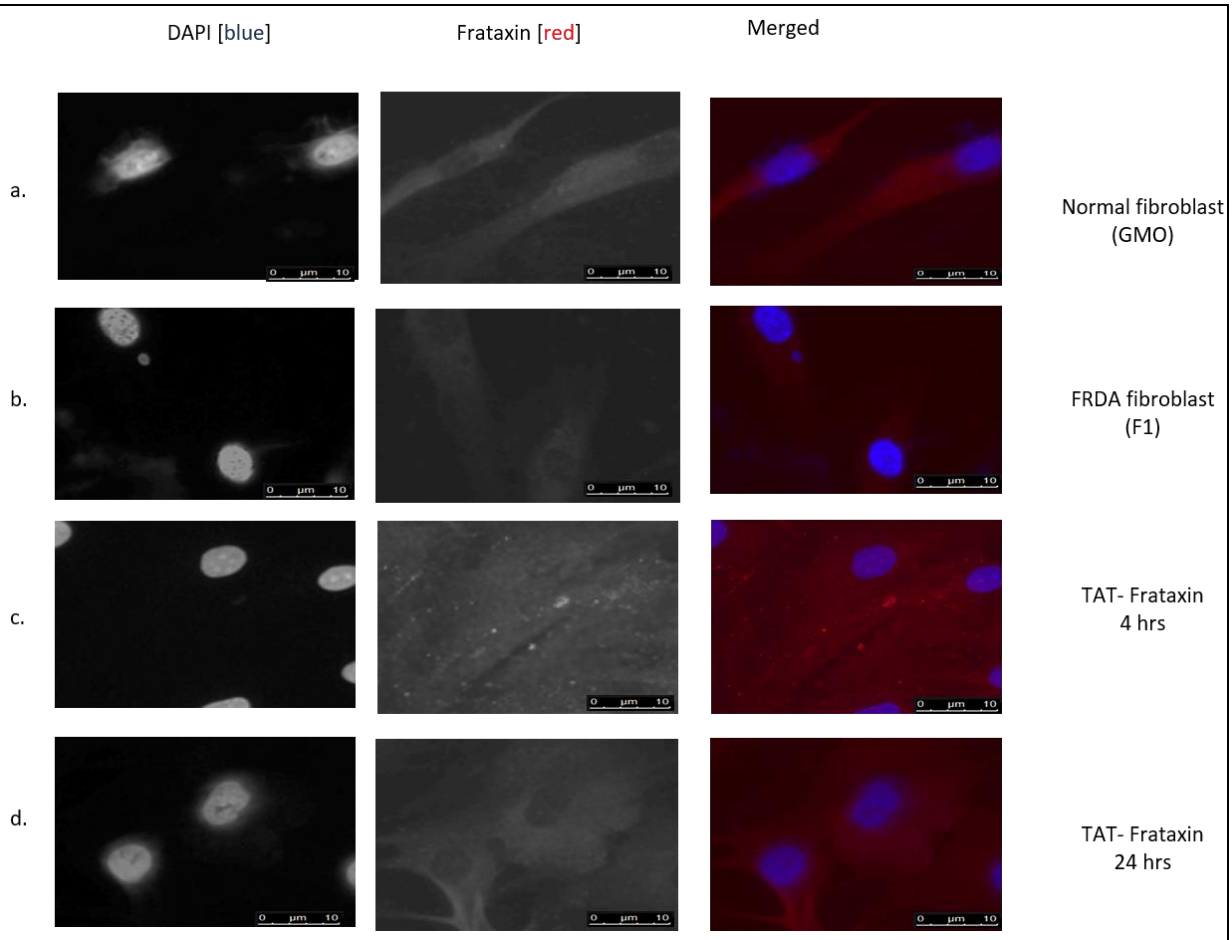

Figure 3-11. Immunofluorescence analysis of fibroblast incubated with the supernatant collected from HEK 293T transfected with TAT- Frataxin fusion peptide for 4 and 24 hrs.

a) Normal fibroblast (GMO) incubated with normal media and labelling frataxin with ab110328 at a dilution of 0.5 µg/ml (shown in red), nuclear DNA was labelled with DAPI (shown in blue) b) FRDA fibroblast incubated with normal media and labelling frataxin with ab110328, c) FRDA cells incubated with supernatant containing TAT- Frataxin fusion peptide for 4 hours labelling frataxin with ab110328, d) FRDA cells incubated with supernatant containing TAT- Frataxin fusion peptide for 24 hours labelling frataxin with ab110328. Scale bar: 10 µm

Once the system and the required incubation periods had been tested, the designated experiment was carried out. Human FRDA and healthy fibroblasts were treated with supernatant collected from HEK 293Tcells that had been transfected with Lipofectamine 3000 (Invitrogen) (see Chapter 2). After 4 hours the cells were harvested, labelled with frataxin ab110328 (Abcam) and analysed using Leica DM 4000 fluorescence microscopy. The result shows that frataxin was successfully detected in FA cells (Figure 3-12d and e) treated with supernatant with the frataxin

fusion peptide (shown in red), in comparison to FA1 (Figure 3-12b) and healthy fibroblast cells (Figure 3-12a) that had been treated with regular media.

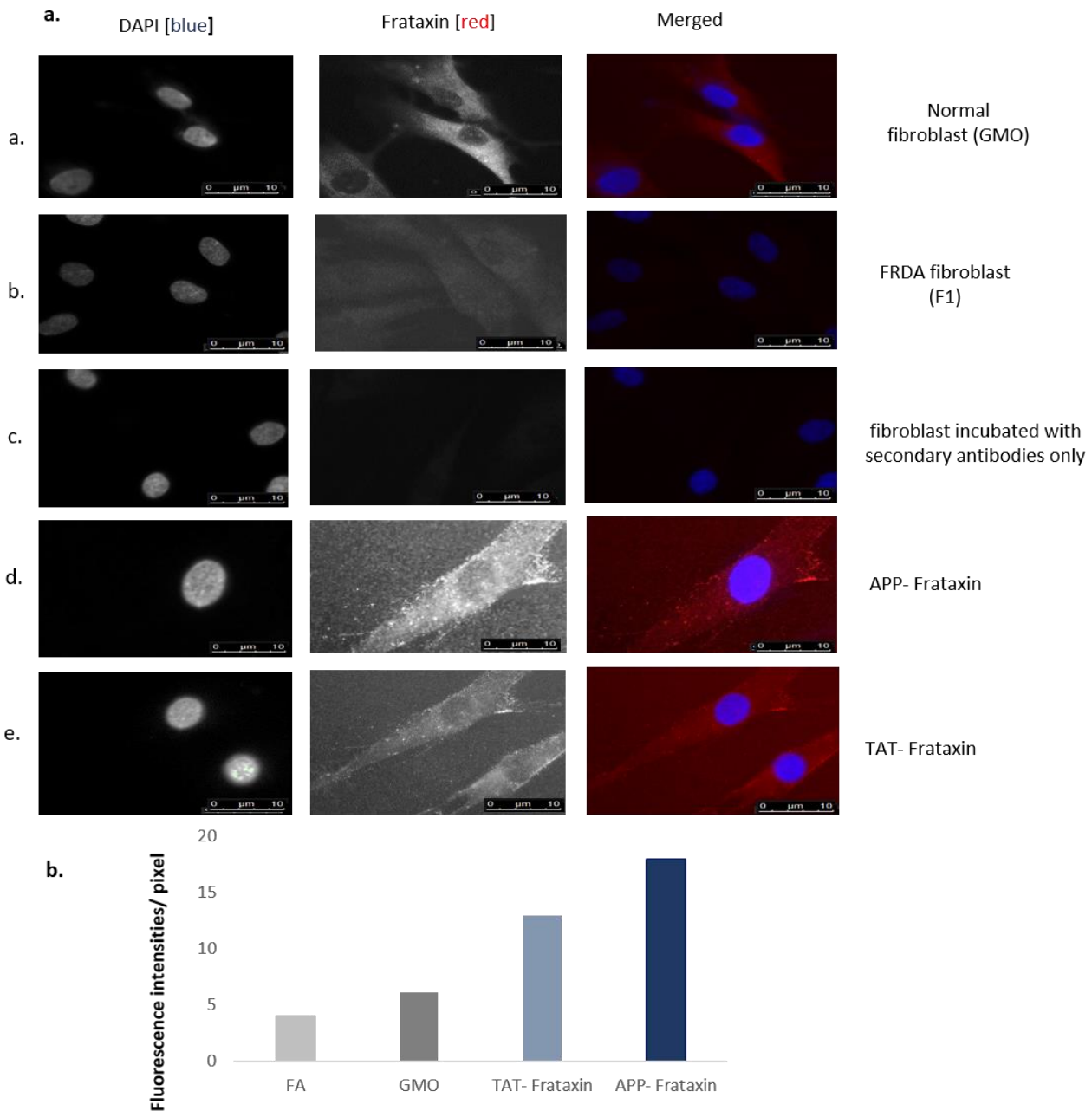

Figure 3-12. Immunofluorescence analysis of fibroblast and fluorescent intensities quantification of frataxin

a). Immunofluorescence staining and fluorescent intensities quantification of frataxin in fibroblast a) normal fibroblast (GMO) incubated with normal media and labelling frataxin with ab110328 (shown in red) at a dilution of 0.5 µg/ml. Nuclear DNA was labelled with DAPI (shown in blue), b) FRDA fibroblast (FA1) incubated with normal media and labelling frataxin with ab110328, c) normal fibroblast (GMO) cells incubated with normal media and secondary only AlexaFluor® 594 (2 µg/ml) to determine if the secondary antibodies have nonspecific binding d) FRDA cells incubated with supernatant containing APP- Frataxin fusion peptide labelling frataxin with ab110328, e) FRDA cells incubated with supernatant containing TAT- Frataxin fusion peptide labelling frataxin with ab110328.

b) Quantification of frataxin was performed using ImageJ quantification tool, Quantification performed from 2 experiments with 20 cells quantified for each condition. Quantification of frataxin is expressed as mean fluorescence intensities per pixel. Scale bar: 10 μm.

To determine if the frataxin fusion peptide can penetrate and deliver the frataxin to the mitochondria, the FRDA and normal fibroblast cells were double-stained with fluorophore-conjugated primary frataxin at 0.5μg/ml dilution and anti-mitochondria at dilution 1/800 and analysed using Leica DM 4000 fluorescence microscopy. Green signalled mitochondria panel, red frataxin panel, and yellow colocalisation signal panel. The result shows that frataxin fusion penetrating peptide could successfully penetrate into FRDA cells, and the frataxin was delivered to the mitochondria, as shown by colocalisation (yellow channel) (Figure 3-12c and d). By comparing the intensity of the signal in the frataxin (red) and colocalisation (yellow) channels, we can see that the APP is more efficient in comparison to TAT in delivering the frataxin (Figure 3-12d and e).

To summarise, based on the result of western blot and immunofluorescence, frataxin fusion peptides were able to successfully penetrate FRDA cells and deliver frataxin to the mitochondria as indicated by the presence of mature and intermediate frataxin isoforms and by double staining of the mitochondria.

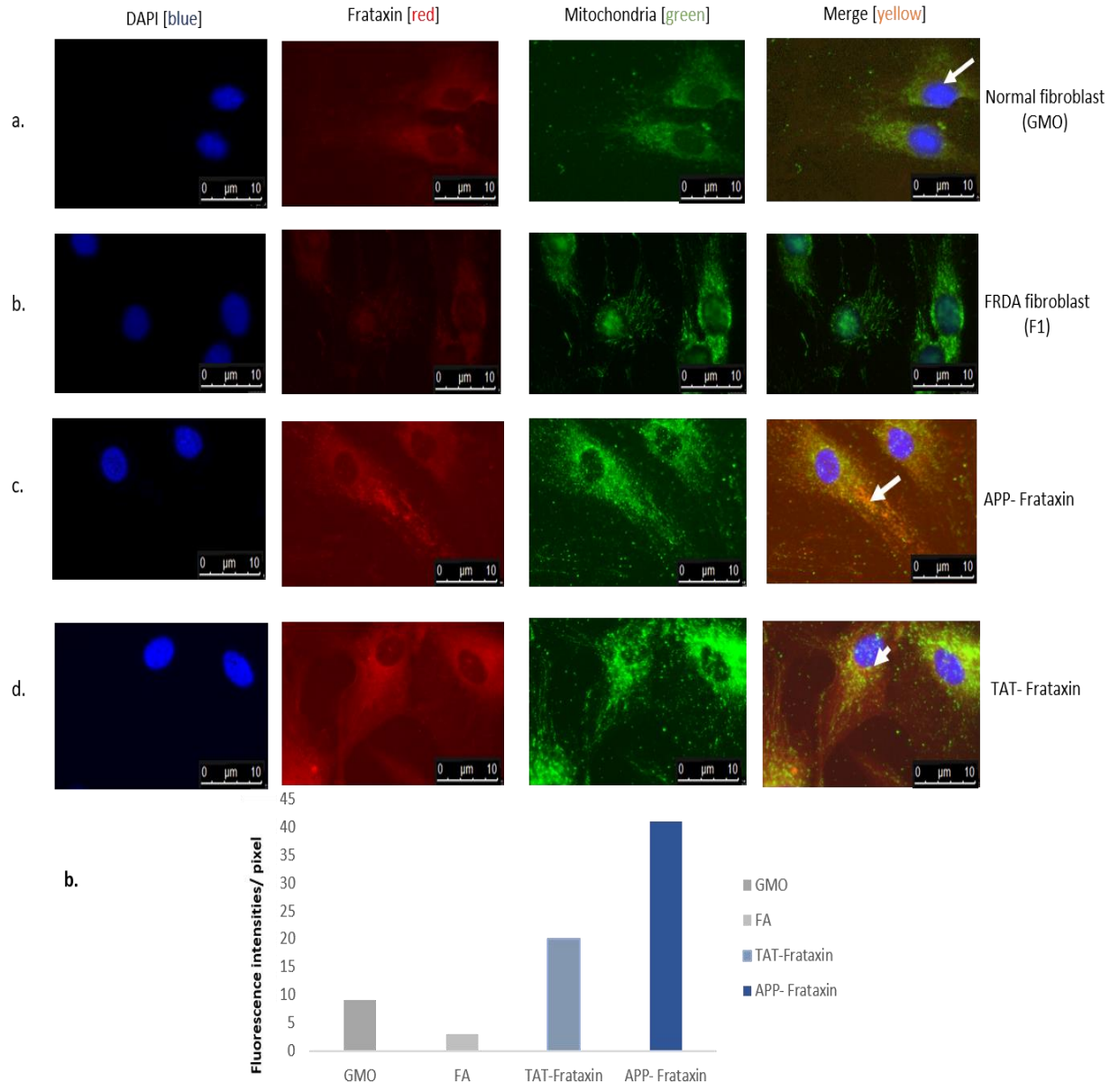

Figure 3-13. Double Immunofluorescence staining and fluorescent intensities quantification of mitochondrial frataxin.

Fibroblast double stained with frataxin ab110328 (shown in red) at a dilution of 0.5 µg/ml and anti-mitochondria antibody (ab92824) at dilution 1/800 (shown in green). Green/red signal overlap (yellow pattern), indicating colocalisation of frataxin in mitochondria. Nuclear DNA was labelled with DAPI (shown in blue). a) normal fibroblast cells (GMO) incubated with normal media; b) FRDA (FA1) incubated with normal media; c) FRDA cells incubated with supernatant containing APP-frataxin fusion peptide; d) analysis FRDA cells incubated with supernatant containing TAT-frataxin fusion peptide.

b) Quantification of frataxin was performed using ImageJ quantification tool, Quantification performed from 2 experiments with 20 cells quantified for each condition. Quantification of frataxin is expressed as mean fluorescence intensities per pixel. Scale bar: 10 µm

3.7 Discussion

The GAA expansion in FRDA does not alter the coding sequence of FXN. It results in reduced production of structurally normal frataxin; therefore, any increase in protein level is expected to be therapeutically beneficial. Recently, there has been increased interest in developing novel therapeutic applications like cell and/or gene therapies, which could provide effective treatment options for FRDA (Evans-galea *et al.*, 2014). Importantly, since individuals with FRDA produce frataxin at low levels, increased expression should not elicit an immune response (Evans-galea *et al.*, 2014). Previous studies have shown that a cell-penetrating peptide is efficient at delivering a protein to the mitochondria *in vivo* in quantities sufficient to rescue a fatal disease phenotype, in conjunction with other studies showing TAT-fusion proteins can restore mitochondrial enzyme activity in heterozygous mice , (Vyas *et al.*, 2012). This firmly supports the use of cell-penetrating peptides as a base for emerging novel therapeutic interventions for mitochondrial diseases (Vyas *et al.*, 2012).

The cationic peptide TAT was among the first CPPs to be discovered and, it has been widely used to promote cellular uptake of different cargos, both *in vitro* and *in vivo* (Patel *et al.*, 2019). Although the possibilities of CPPs for molecular delivery seem promising (Kim *et al.*, 2015b), they have several limitations such as poor serum stability, considerable cytotoxicity, immunogenicity and toxicity (Kim *et al.*, 2015b). All these difficulties arising from CPP sequences of non-human origin could be prevented by developing human protein sequences. If the CPPs of human proteins are non-cationic, challenges arising from traditional cationic CPPs can be avoided. Therefore, we have chosen APP as the CPP. APPs are calcium ion-regulated annexin proteins, which are membrane-associated and which regulate the actin dynamics through their membrane interaction and bind to negatively-charged head groups of phospholipids in the membrane (Kim

et al., 2015a). The frataxin fusion peptides have been cloned into the lentivirus vector, which would be used to infect CD34+ HSPC haematopoietic stem cells. Third-generation lentiviruses have been chosen in our study because they are thought to be nonpathogenic and non-immunogenic (Affleck and Stoll, 2018). Moreover, the third-generation lentiviral vectors are replication-incompetent and self-inactivating, which make them a safer option (Affleck and Stoll, 2018). In our studies, we have tried a novel cell and gene therapy, which showed promising results *in vitro* for Friedreich's ataxia.

Chapter 4.

Frataxin fusion peptides penetrate, are processed by MPP and increase aconitase level and rescue FRDA cells from oxidative stress

4.1 Introduction

Frataxin is a nuclear-encoded protein (Cook, 2010) which is produced in the cytosol as a 23 KDa 210 amino acid precursor. It is imported into the mitochondria where it undergoes proteolytic processing by mitochondrial processing peptidase (MPP) to produce the mature functional form through a two-step process: initial MPP-mediated cleavage of full-length frataxin to give an intermediate form, a 169-amino acid protein with an MW of 18,826 KDa; and then a second MPP-mediated cleavage to provide mature frataxin (81–210), as a 130-amino acid protein with an MW of 14,268 KDa (Figure 4-1) (Schmucker *et al.*, 2008). The mature type of the protein plays a crucial part in iron haemostasis, particularly for the *de novo* biosynthesis of the iron-sulphur cluster (ISC) protein and heme biosynthesis (Chiang *et al.*, 2016). Iron and Fe-S groups are necessary for metabolic processes, electron transport, DNA synthesis, redox, and non-redox reactions in addition to other cellular functions (Gonz, 2013; Pastore, 2013). Iron-sulfur-containing proteins have a vital role in cellular respiration and ATP production and reduced activity could considerably weaken mitochondrial function. Frataxin's role in iron-sulphur group formation makes it important for the activity of Fe-S-containing aconitase and respiratory chain complexes. Thus, reduced frataxin levels result in lower aconitase activity in cell culture models, *in vivo*, and in heart tissues and biopsies of FRDA patients (Walden, 2002). These effects on important enzymes of energy creation lead to a failure of ATP production in FRDA (Llorens *et al.*, 2019).

Aconitase is a citric acid enzyme responsible for the citrate-isocitrate conversion. the cytoplasm. Mitochondrial aconitase is highly sensitive to superoxide, peroxynitrite, and H_2O_2 (Lushchak *et al.*, 2014). Aconitase can be inactivated by superoxide and it has been shown that H_2O_2 also inhibited this enzyme at very low (less than 50 µM) H_2O_2 concentrations (Tretter and Adam-vizi, 2000). The most likely targets in aconitase for oxygen species (ROS) mediated inactivation are the iron-sulphur cluster (Tretter and Adam-vizi, 2000), which was shown to be primary sites for a ROS attack in other mitochondrial enzymes, as well (Tretter and Adam-vizi, 2000). The extreme sensitivity of aconitase to ROS permitted the measurement of aconitase activity to become a proper indicator for superoxide or H_2O_2 production in intact cells, synaptosomes, or in isolated mitochondria) (Tretter and Adam-vizi, 2000).

Frataxin deficiency is correlated with mitochondrial dysfunction through iron accumulation and production of reactive oxygen species (ROS). When ROS levels rise, oxidative damage can happen in the cell, in the mitochondria. Oxidative stress damages proteins and DNA, especially mitochondrial (mtDNA), as mtDNA lacks protection from histones and the complex nuclear repair system. Oxidative stress provokes apoptosis and has been linked to several neurodegenerative diseases such as Parkinson's disease (PD), Alzheimer's disease (AD), amyotrophic lateral sclerosis, and multiple sclerosis(Clark *et al.*, 2018).

It has been found that an elevated level of frataxin gene expression can rebuild cell viability. In a recent gene therapy study, correction of the FRDA heart pathology of a knockout mouse model with completely deleted frataxin in cardiac and skeletal muscle was accomplished where frataxin was overexpressed (Khonsari *et al.*, 2016); (Vyas *et al.*, 2012). Hence, delivering frataxin into these cells could provide a permanent correction to FRDA.

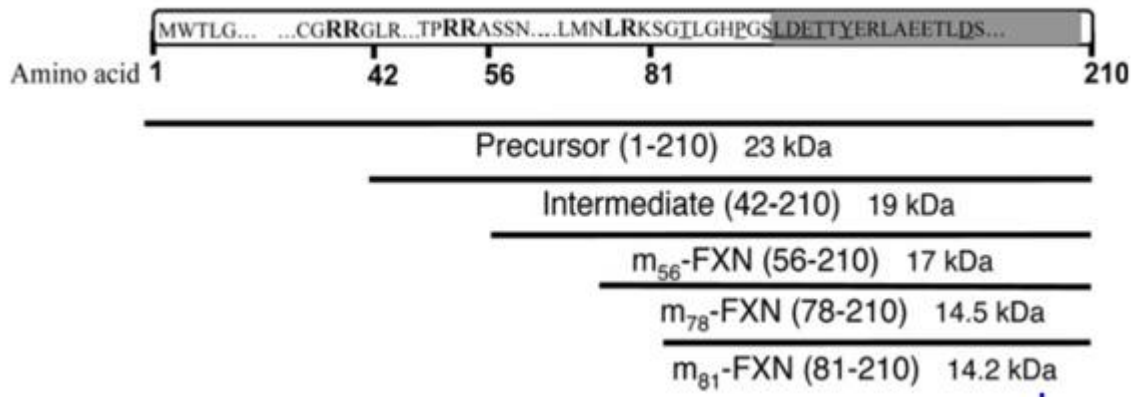

Figure 4-1. Graphic representation of the different forms of frataxin.

The pre-cursor of frataxin (encoded by amino acids 1–210) is targeted to the mitochondria and undergoes a two-step maturation process. The intermediate (i-FXN) and the three described mature forms beginning at the amino acids 56 (m56-FXN), 78 (m78-FXN) or 81 (m81-FXN) are represented (Schmucker et al., 2008).

The aims of the experiments described in this chapter are:

- To prove the ability of the delivered peptide to rescue the cells.
- To prove that cell rescue is related to delivered frataxin not to the effect of the cell-penetrating peptide.

4.2 Frataxin fusion peptide processed by MPP

The frataxin gene encodes for a 210 amino acid protein, which is the precursor of frataxin (Schmucker *et al.*, 2008). It contains an N-terminal transit sequence which directs its transference into the mitochondria, where it is processed by MPP (Mitochondrial processing peptidase) to produce the mature functional form of frataxin, which can functionally reconstitute aconitase activity and provide resistance to oxidative stress in frataxin-defective cells derived from FRDA patients (Walden, 2002). Therefore, we wanted to investigate the ability of the frataxin fusion peptide to penetrate and successfully deliver frataxin to mitochondria, and whether it would be successfully processed to its mature functional form.

The fibroblast from FRDA patients (FA1) was incubated with the supernatant collected from transfected HEK 293T cells for 4 hours, after which the FA cells were harvested, and western blot performed. The result showed a strong mature frataxin band at 14 KDa and intermediate band at 18 KDa, from sample lysate of cells treated with supernatant that had frataxin penetrating fusion peptides. Only a very faint band was observed in FRDA cells incubated with an empty vector. The presence of the intermediate and mature frataxin bands indicates that frataxin was delivered successfully into the mitochondria and was recognised and cleaved by the MPP (Figure 4-2).

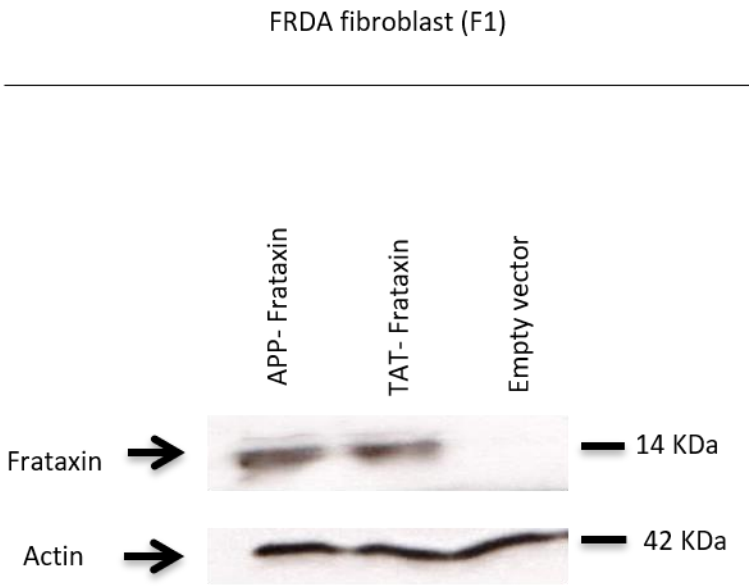

Figure 4-2. Western blot analysis of FA1 cells.

Western blot analysis of FA1 fibroblast incubated with the supernatant collected from HEK 293T transfected with Frataxin fusion peptide constructs and empty vector for 4 hours. Strong expressed mature frataxin bands were detected at 14KDa in comparing to FRDA cells incubated with empty vector where no band is detected.

4.3 Frataxin fusion peptides rescue cells from H_2O_2 induced oxidative stress

In Friedreich's ataxia, the decrease of the mitochondria protein frataxin causes the accumulation of iron and reactive oxygen species, and the increased sensitivity of cells to oxidative damage (A. Wong *et al.*, 1999). Therefore, we wanted to test the ability of frataxin fusion peptide constructs to rescue FRDA fibroblast cells that had been treated with an increased concentration of H_2O_2.

Normal and FRDA human fibroblasts were exposed to oxidative stress induced by increasing concentrations of H_2O_2 (50 and 200 µM) for 5 hours, after which cell viability was determined by MTS assay. FRDA cells exhibited significantly higher sensitivity compared to normal fibroblasts, and cell viability dropped from 80% at H_2O_2 50 µM to around 10% in FRDA fibroblasts, in comparison to normal fibroblasts were cell viability was around 80% at 50 µM and 50% at 200 µM (Figure 4-3). Cell viability improved in both FRDA and normal fibroblasts treated with frataxin fusion peptides. FRDA fibroblasts incubated with supernatant containing frataxin fusion peptides

showed a significant improvement in survival, especially with the APP-frataxin fusion peptides, where cell viability increased from 10% at 200 µM to around 60%. In comparison to TAT-frataxin fusion peptide, the cell viability increased from 10% at 200 µM with a cell incubated with supernatant containing the empty vector to around 50%.

These findings indicate that FRDA cells are more sensitive to oxidative damage in comparison to healthy cells and that frataxin fusion peptides construct were able to deliver frataxin into cells, which rescue the cells from oxidative stress.

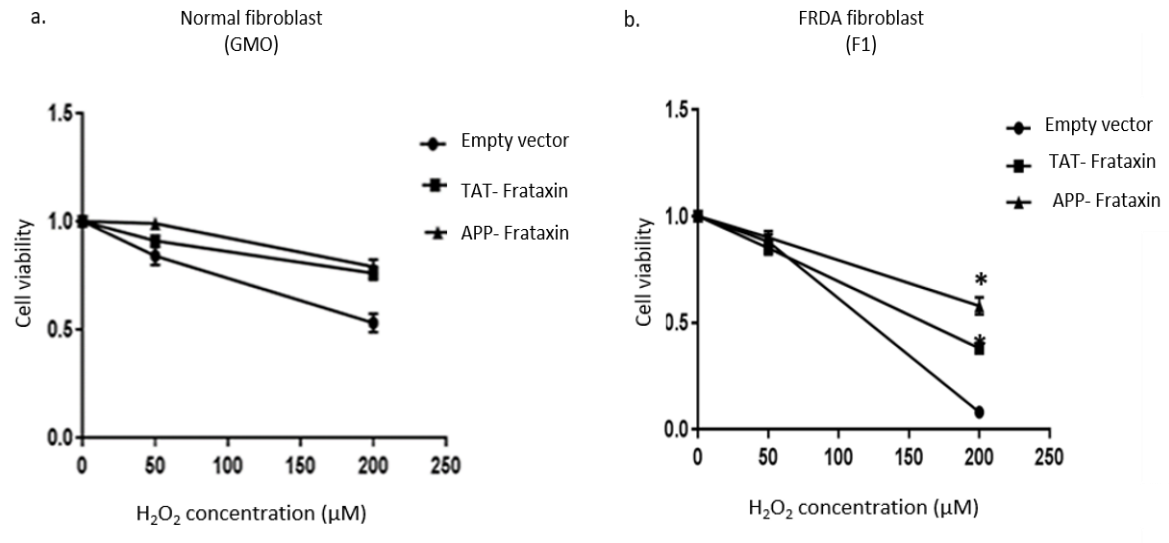

Figure 4-3. Sensitivity of normal fibroblast cells (GMO) and FRDA (FA1) cells to oxidative stress.

a) Illustrates the sensitivity of normal fibroblast cells (GMO) to oxidative stress in cells treated with frataxin fusion peptides (TAT-Frataxin, APP-Frataxin), versus cells treated with empty vector in three independent experiments. b) Illustrates the sensitivity of FA1 to H_2O_2 induced stress in cells treated with frataxin fusion peptides, versus cells treated with empty vector in three independent experiments**.** (n = 3, *p < 0.05) data reported as mean± SEM of three replicate of three independent experiments.

4.4 Aconitase activity increases in fibroblast treated with the frataxin fusion peptide

Early histological and biochemical study of the pathophysiology in patient's samples revealed that dysregulation of iron metabolism is a key feature of the FRDA (Clark *et al.*, 2018), mainly characterized by mitochondrial iron accumulation and by decreased activity of iron-sulfur cluster

enzymes such as aconitase (Clark *et al.*, 2018). The deletion of the frataxin gene has been associated with the accumulation of mitochondrial iron deposits (Llorens *et al.*, 2019) and resulted in deficiencies of aconitase and general Fe-S cluster protein deficiencies. This decrease of aconitase activity has been shown in both cell culture (Bru *et al.*, 2004) and *in vivo* models (Whitnall *et al.*, 2008; Puccio *et al.*, 2001). Since aconitase enzyme activity has been used as an indicator of low levels of frataxin protein and oxidative damage indicator. Therefore, we have tested the activity of this enzyme in fibroblast cells that are treated with frataxin fusion peptides treated and cells that are treated with empty vector.

Aconitase measurement was spectrophotometrically carried out in which citrate is converted by aconitase into isocitrate, which is further processed resulting in a product that converts a nearly colorless probe into an intensely colored form at 450 nm.

The aconitase activity was measured in healthy (Figure 4-4a) and FRDA fibroblasts treated with frataxin fusion peptide and empty vector (Figure 4-4b). The aconitase activity increased significantly more than 2.8-fold in the FRDA cells treated with APP-frataxin fusion peptide (n=3, **p<0.005), and 0.8 fold in the FRDA cells treated with TAT-frataxin fusion peptide in comparison to FRDA cells that were incubated with empty vector when compared to the negative controls (n = 3, *p<0.05) (Figure 4-4b).

The aconitase activity for the healthy human fibroblasts shows a significant increase in aconitase level in normal fibroblast that is treated with APP-frataxin fusion peptide by more than a 0.2-fold increase (n=3, **p<0.005) in comparison to the cells incubated with empty vector. There was a slight non- significant decrease in the level of aconitase activity in fibroblast that was treated with TAT-frataxin fusion peptide (Figure 4-4a).

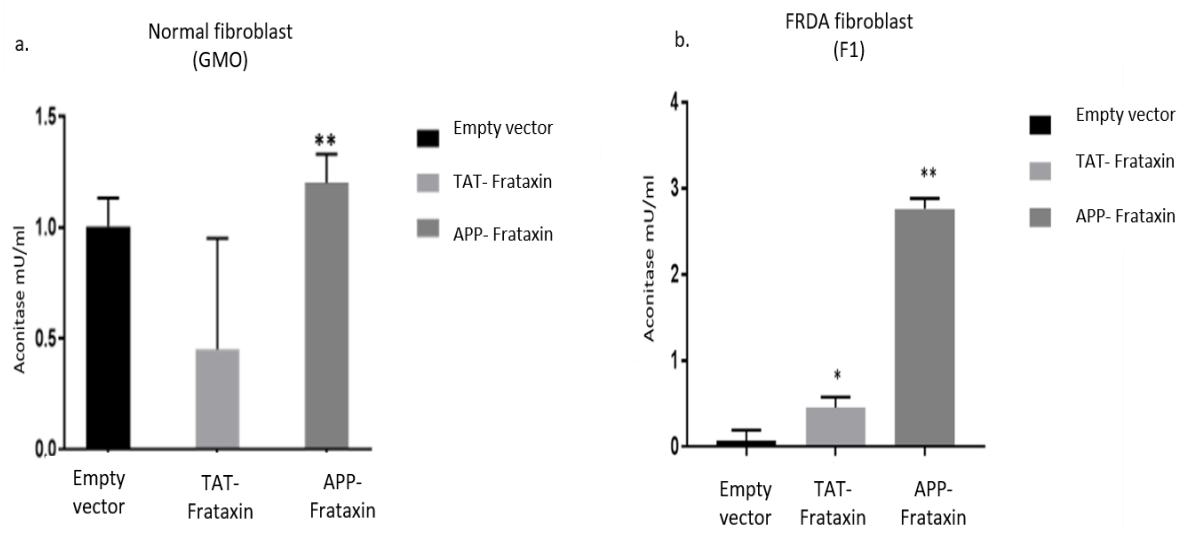

Figure 4-4. Aconitase level in the normal (GMO) and FRDA (FA1) fibroblasts.

a) Illustrate aconitase level in the normal human fibroblast, there's a significant increase in aconitase level in normal fibroblast that was treated with the supernatant that has APP- frataxin fusion peptide by more than 0.2 fold increase (n=3, **p< 0.005) in comparison to the cells treated with empty vector. There was also a slight insignificant decrease in the level of aconitase activity in fibroblast that was treated with TAT-frataxin fusion peptide in comparison to cells treated with empty vector (n=3, p>0.05). b) illustrate aconitase level in FRDA cells, there's a significant increase in aconitase level of more than 2.8 fold in the FRDA cells that were treated with APP- Frataxin fusion peptide (n=3, **p< 0.005), and 0.8 fold increase in the FRDA cells treated with TAT-frataxin fusion peptide in comparison to FRDA cells that were incubated with empty vector (n=3, *p< 0.05).

The results indicated that the aconitase level in FRDA cells was lower than that in normal fibroblasts and that the delivery of frataxin to cells was associated with the rescue of aconitase enzyme levels. Moreover, a comparison of the results obtained with both peptides suggested that APP is more efficient in delivering frataxin into the cells, as signified by the increased viability of FRDA cells in the oxidative stress test and the increased level of aconitase.

To summarise, FRDA cells were more sensitive to oxidative damage and had lower aconitase levels than healthy fibroblasts, and the treatment of cells with frataxin fusion peptide both rescued the FRDA cells and increased the aconitase levels significantly.

To investigate whether the cell-penetrating version of frataxin would have the same effect in a different cell line, a TAT-frataxin fusion peptide was tested using C4 and GMO 7492 fibroblasts from healthy individuals and FA1 and FA4 fibroblasts from patients with FRDA.

Cells were pre-treated with the supernatant from HEK 293T cells transfected with the TAT-frataxin fusion peptide and challenged with different concentrations of H_2O_2 (50 µM and 200 µM) for 5 h, after which cell viability was assessed using the MTS assay.

The results showed that FRDA fibroblasts were more sensitive to oxidative stress than healthy fibroblasts; at 200 µM of H_2O_2, the cell viability of FA1 and FA4 fibroblasts dropped to 18% and 16%, respectively, whereas the cell viability of C4 and GMO 7492 fibroblasts only dropped to 40% and 38%, respectively. Moreover, both transfected FRDA cell lines were significantly rescued by TAT-frataxin fusion peptide; the cell viability of transfected FA1 and FA4 fibroblasts increased to 80% and 60%, respectively. Fibroblasts from healthy individuals were also rescued by the TAT-frataxin fusion peptide treatment, and the cell viability of C4 and GMO 7492 fibroblasts increased to 60% and 57%, respectively; however, the difference was not statistically significant ($p > 0.05$; Figure 4-5 and 4-6).

To summarise, both FRDA and normal fibroblasts showed sensitivity to oxidative stress when challenged by H_2O_2; however, FRDA cells were more sensitive. Transfection with the TAT-frataxin fusion peptide was able to rescue the cells, and the cell viability of transfected cells increased significantly

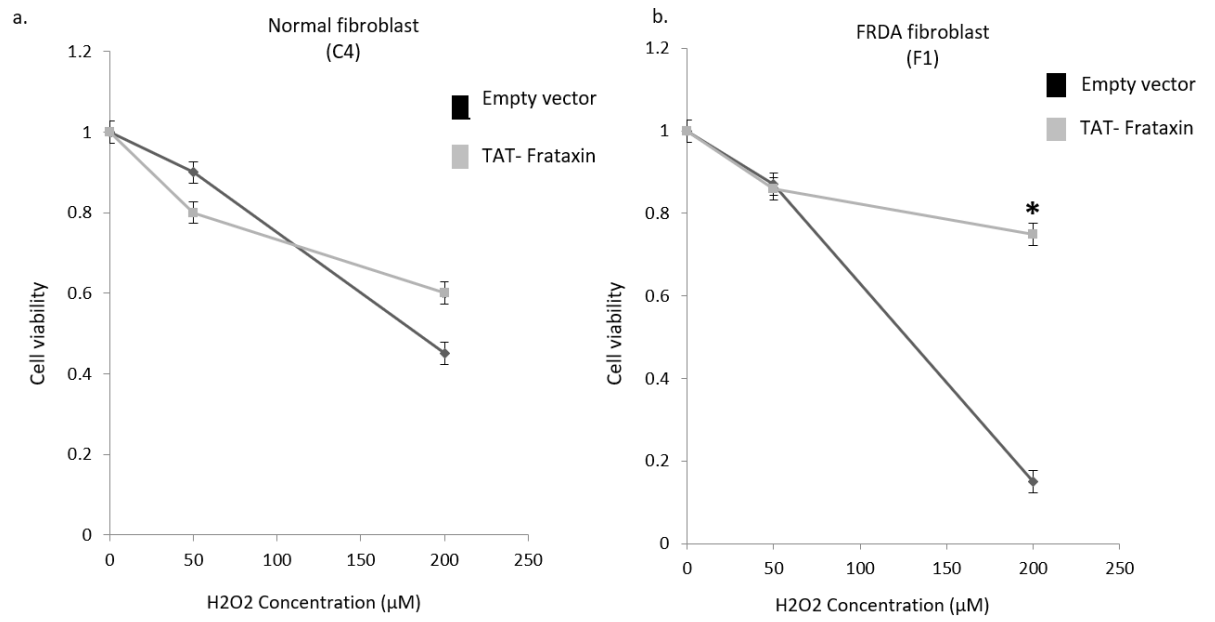

Figure 4-5. Sensitivity of normal fibroblast cells (C4) and FRDA (FA1) cells to oxidative stress.

a) Illustrates the sensitivity of normal fibroblast cells (C4) to oxidative stress in cells treated with TAT-Frataxin fusion peptide, versus cells treated with empty vector. The fibroblast cells show a mild sensitivity to oxidative stress, where cell viability dropped to only 40% in cells treated with empty vector in comparison to around 60% in cells treated with TAT-Frataxin fusion peptides at 200 µM of H_2O_2. b) Illustrates the sensitivity of FA1 to H_2O_2-induced stress in cells treated with `TAT- Frataxin fusion peptide in comparison to cells treated with empty vector. FA1 cells are sensitive to oxidative stress, where the viability of cells dropped to 18% in cells incubated with empty vector at H_2O_2 concentration of 200 µM, whereas FRDA fibroblast incubated with supernatant that has TAT-Frataxin fusion peptide showed an improvement in survival and the viability of the cells have been significantly increased to 80% at 200 µM concentration of H_2O_2 (n=3) $p<0.05$.

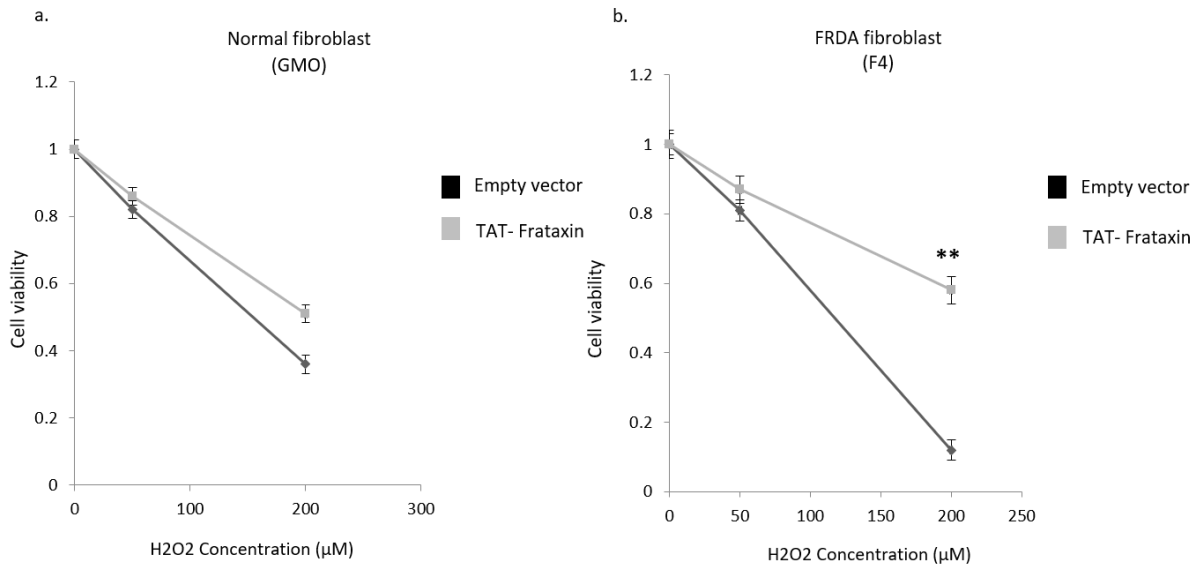

Figure 4-6. The sensitivity of normal fibroblast cells (GMO) and FRDA (FA4) cells to oxidative stress.

a). GMO fibroblast cells show a mild sensitivity to oxidative stress, where the cell viability had dropped to only 40 % in cells treated with empty vector versus around 57 % in cells treated with TAT-Frataxin fusion peptide at 200 µM concentration of H_2O_2. b) illustrate the sensitivity of FA4 to H_2O_2 induced oxidative stress in cells treated with empty vector in comparison to cells treated with TAT-Frataxin fusion peptide, FA4 cells were very sensitive to oxidative stress, where the viability of cells have been dropped to 18% at 200 µM in FRDA fibroblast incubated with supernatant that has an empty vector, the cell viability has been increased to 60% in cells treated with TAT-Frataxin fusion peptide at H_2O_2 of 200 µM (n=3)**p< 0.005.

Aconitase level has been compared in both FRDA cell lines and in both healthy fibroblasts. The fibroblasts were pre-treated by TAT-frataxin fusion peptide then collected for aconitase assay. The result shows that aconitase level is lower in both cell lines in FRDA then in normal fibroblasts and treating the cells with the TAT-frataxin fusion peptide increased the level in both healthy and FRDA cells (Figure 4-7 and 4-8).

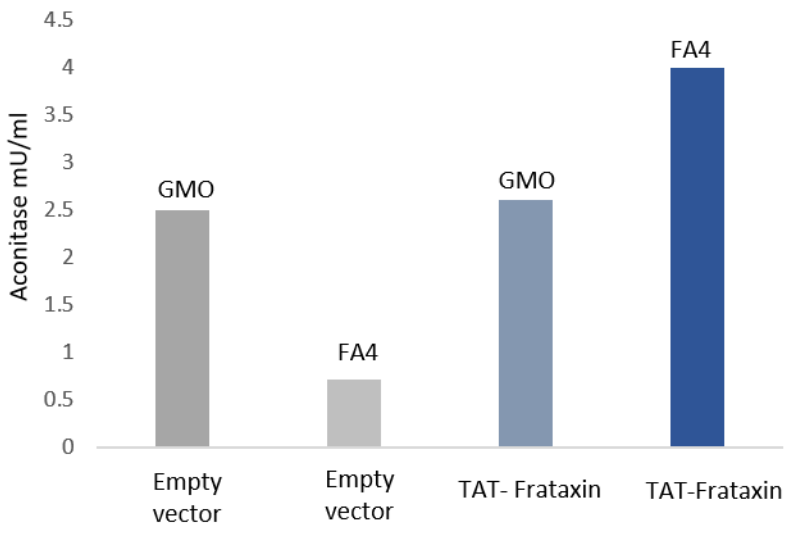

Figure 4-7. Aconitase level in the normal (GMO) and FRDA (FA4) fibroblasts.

The figure illustrates the aconitase level in cells treated with empty vector versus TAT-Frataxin in both normal human fibroblast (GMO) and FRDA cells (FA4). FRDA cells treated with empty vector have a lower aconitase level in comparison to empty vector treated normal fibroblast. However, after the cells treated with TAT-Frataxin the level of aconitase level in FA4 increased by more than 3 folds, in comparison to FA4 cells which treated only with an empty vector. Data reported as a mean of three replicates of 2 independent experiments (n= 2).

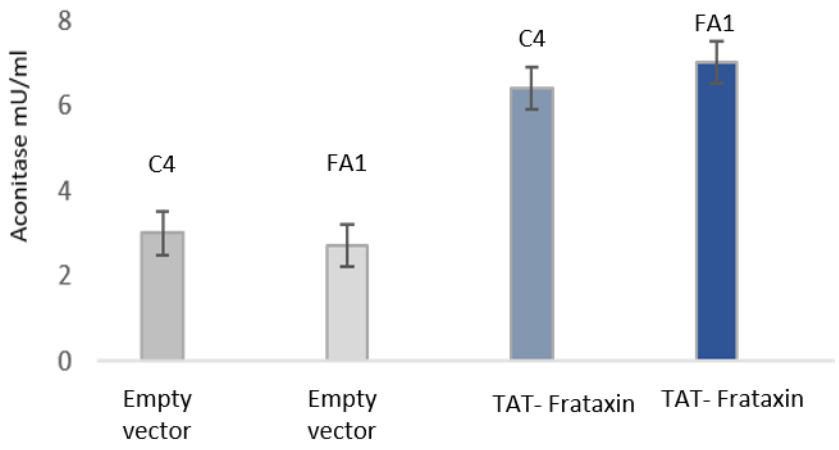

Figure 4-8. Aconitase level in the normal (C4) and FRDA (FA1) fibroblasts.

The figure illustrates the aconitase level in cells treated with empty vector versus TAT-Frataxin in both normal human fibroblast (C4) and FRDA cells (FA1). FRDA cells treated with empty vector have a lower aconitase level in comparison to normal fibroblast treated with empty vector. After the cells treated with TAT-Frataxin the level of aconitase level in FA4 increased by around 3 folds, and by more than 2-folds in C4 cells. in comparison to FA4 cells which treated only with empty vector. Data reported as mean± SEM of 3 replicate of three independent experiments (n= 3).

4.5 Cell rescue is related to delivered frataxin, not to the effect of cell-penetrating peptide

To test whether the effect that we have seen in fibroblast cells (oxidative fibroblast cell rescue and increased aconitase enzyme level) is caused by delivering of frataxin into deficient cells and not related to the APP effect, we designed a penetrating version of the construct with truncated frataxin.

FRDA fibroblasts were exposed to an increasing concentration of H_2O_2 (50 and 200 µM) for 5 hours, after which the viability of the cells was determined by MTS assay. It was found that FRDA fibroblast cells treated with the APP-truncated frataxin-penetrating fusion peptide construct and from GFP-vector construct are both more sensitive to oxidative stress than cells treated with APP-frataxin fusion peptide.

Cell viability dropped from 80% at 50 µM to less than 10% in FRDA fibroblast treated with GFP-vector constructs, to around 18% in FRDA cells treated with APP-truncated frataxin-penetrating fusion peptide (both results were statistically insignificant (n= 3, *p<0.05)). In comparison to FRDA fibroblasts treated with APP-Frataxin fusion peptides, the viability of the cells significantly increased from less than 10% in cells treated with empty vector to 75% at 200 µM (n= 3, *p<0.05) (Figure 4-9).

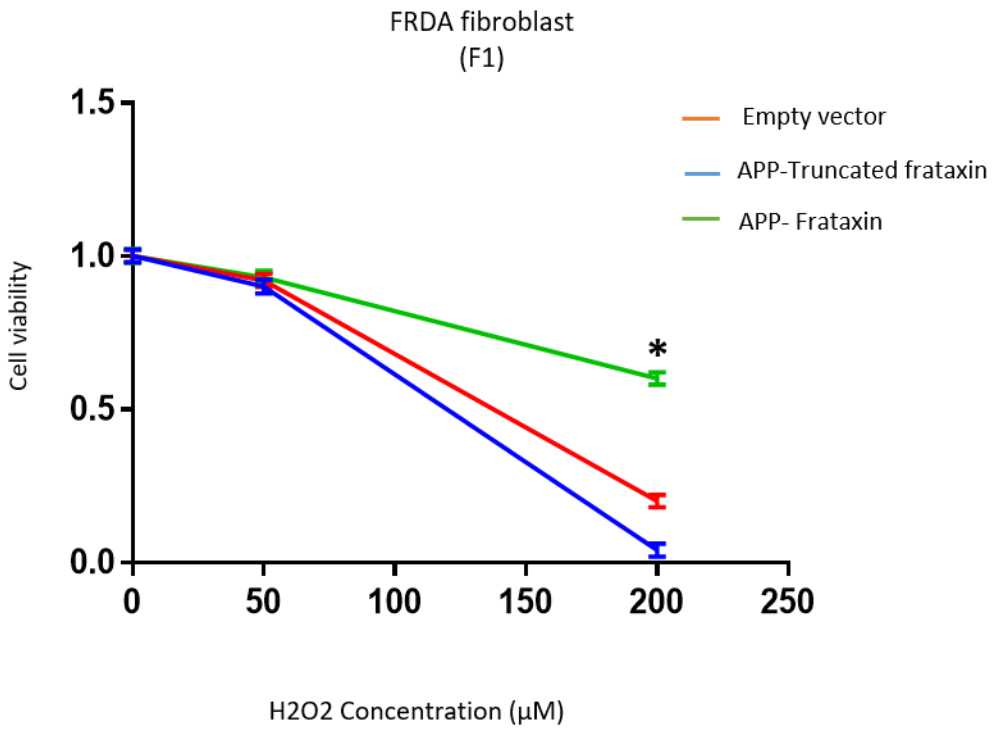

Figure 4-9. Sensitivity of FRDA cells (FA1) to H_2O_2 induced oxidative stress.

The figure illustrates the sensitivity of FA1 to H_2O_2 induced oxidative stress in cells treated with APP-truncated frataxin in comparison to cells treated with APP-frataxin fusion peptide and empty vector. The cells viability have been dropped from 80% at H_2O_2 50 µM to less 10% in FRDA fibroblast treated with empty vector, and to round 18% in FRDA cells treated with APP- truncated frataxin at 200 µM of H_2O_2 (both result are statistically insignificant (n= 3, *p < 0.05)). In comparison to FRDA cells treated with APP-Frataxin, where the cells viability at 200 µM of H_2O_2 is around 75% (n= 3, *p < 0.05). Data reported as mean± SEM of three replicate of three independent experiments

The aconitase activity was again measured in FRDA fibroblasts treated with frataxin fusion peptide, truncated frataxin fusion peptide, and empty vector (Figure 4-10). The aconitase activity was increased significantly more than 5- fold in the FRDA cells treated with APP-frataxin fusion peptide, and 0.8- fold in comparison to FRDA cells that were incubated with empty vector. These effectors were compared to the negative controls, where there was no significant change in aconitase activity in FRDA cells treated with the truncated version of the frataxin fusion peptide ($n = 3$, $*p < 0.05$).

These results showed a significant increase in cell viability after challenging the cells with H_2O_2, and the increase in aconitase activity is related to increased frataxin expression in FRA fibroblast cells, and not because of APP.

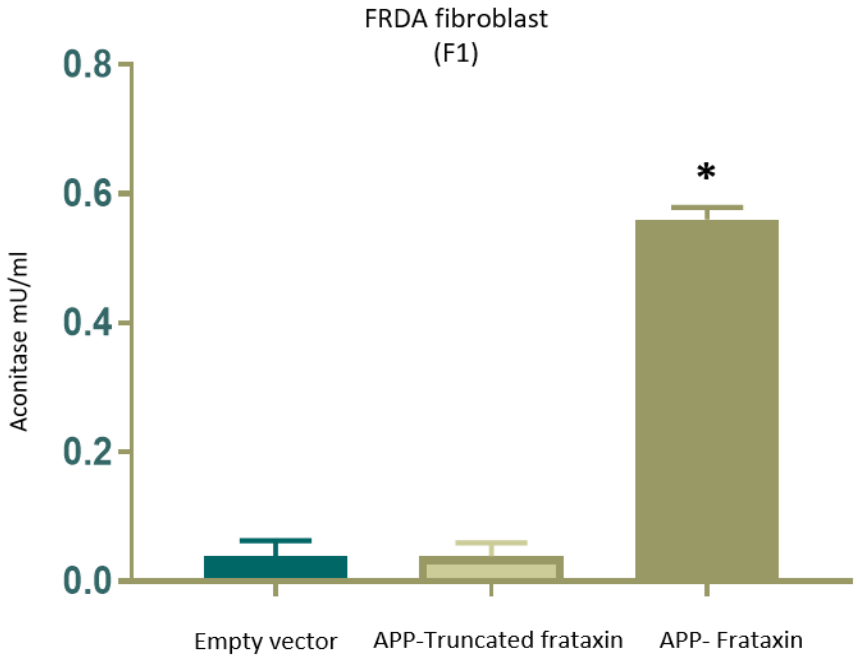

Figure 4-10. Aconitase level in FRDA (FA1) fibroblast.

The figure illustrates the aconitase level in cells treated with APP-truncated frataxin in comparison to cells treated with APP-frataxin fusion peptide and empty vector. There was a significant increase in aconitase level by more than 5-fold in the FRDA cells treated with APP- Frataxin fusion peptide, where there was no significant change in the aconitase level in cells treated with APP-truncated frataxin. (n = 3, *$p < 0.05$) data reported as mean± SEM of three replicate of three independent experiments.

4.6 Discussion

In previous studies, TAT frataxin fusion peptide has been delivered successfully to the mitochondria, where it has been processed by the MPP (Vyas *et al.*, 2012). The key finding from these experiments is that a cell-penetrant peptide is capable of delivering a replacement protein to mitochondria *in vivo* in amounts sufficient to rescue a very severe (fatal) disease phenotype

(Vyas *et al.*, 2012). These results, in conjunction with our findings showing cell penetrating -fusion proteins, can restore mitochondrial enzyme activity (Rapoport, Salman and Sabag, 2011), strongly support the use of cell-penetrant peptides as a platform for developing novel therapeutic interventions for mitochondrial diseases.

Aconitase is a mitochondrial enzyme with Fe–S clusters. The loss of FXN has been shown to decrease its activity in both cell culture models (Cantu, Schaack and Patel, 2009), and *in vivo* (Whitnall *et al.*, 2008). Studies have proven that the mature form of frataxin can functionally reconstitute aconitase activity and provide resistance to oxidative stress in frataxin-defective cells derived from FRDA patients (Walden, 2002) and this has been shown also in our results where FRDA cells treated with frataxin fusion peptides constructs were more resistant to oxidative stress and showed an increase in their aconitase levels.

The MTS assay showed that FRDA fibroblasts were more sensitive to H_2O_2-induced oxidative stress in comparison to the control, and the kinetics of fibroblast death were related to the concentration of H_2O_2. Treating cells with frataxin had a protective role. The oxidative stress hypothesis could explain this in FRDA. Declines in hydrogen peroxide scavenging enzymes have been described in cells originated from patients with FA and are believed to add to increased sensitivity to oxidative stress in these models (Kemp *et al.*, 2017). It has also been shown that frataxin deficiency could result in an ineffective use of iron through ISC (iron-sulfur cluster) synthesis, which would result in the build-up of the iron and faults in ISC-containing enzymes such as aconitase and complexes I, II and III of the mitochondrial respiratory pathway and lead to defects in mitochondria respiration, lower ATP production and iron accumulation. Hydrogen peroxide will be changed into an extremely toxic hydroxyl radical in the presence of iron through Fenton's reaction, and then react with mitochondrially-produced superoxide anions to produce a free radical reaction (a Wong *et al.*, 1999). Numerous studies have shown that death in FRDA cells happens through an intrinsic pathway of apoptosis and that the pro-apoptotic Bcl-2 family members Bad, DP5 and Bim are the critical mediators of the intrinsic pathway of apoptosis (Kemp et al., 2017; Palomo, et al., 2011). Other studies have demonstrated that low frataxin levels may induce autophagy, which is a phenomenon that provides amino acid supplies during starvation

by controlled degradation of the intracellular protein. Autophagy, in this case, can be in response to the presence of free radicals to remove depolarised mitochondria and other injured cells. However, reactive oxygen species attenuate lysosomal membranes and consequently impair the mechanism of autophagy. In this case, apoptosis represents an alternative mechanism to autophagy (a Wong *et al.*, 1999).

Chapter 5.

Viral titration, infecting human haematopoietic stem cells with frataxin lentiviruses

5.1 Introduction

Cell and gene therapy for FRDA is being considered as a hopeful treatment approaches, which have been currently being tested for potential efficacy (Evans-galea *et al.*, 2014). A significant advantage in developing cell and gene therapy for FRDA is that affected individuals already produce frataxin, although, at deficient levels, so therapeutic introduction of frataxin will not elicit an immune response. We hypothesised that the transplantation of genetically modified HSPCs could provide a long-term delivery vehicle for functional frataxin and therefore, could stop the progression of the disease and reverse some of the pathological events. Furthermore, since FRDA could be genetically tested, consequently, delivering the genetically modified HSPCs, could provide a way not only to stop the disease progression but also to stop a disease manifestation in suspected individuals who are tested positive by genetic analysis.

The aims of the experiments described in this chapter are to:

- Genetically modify the HSPC by transducing it with a lentivirus vector carrying the penetrating version of frataxin.
- Test the ability of genetically modified HSPCs to secrete the penetrating fusion peptide of frataxin into the supernatant.
- Test the ability of genetically modified cells to differentiate.
- Test the ability of differentiated cells to continue carrying the modified gene and the ability to secrete the peptide.

5.2 Viral titration

The lentivirus carrying frataxin-fusion peptides and empty vector were produced at the UCL Institute of Child Health. Since the lentivirus carrying empty vector gene was produced in parallel with the lentivirus-carrying frataxin fusion peptide gene, this allowed us to use it to calculate Transducing Units and later to estimate the transduction efficiency.

K-562 has been used as a model for a broad variety of investigations including the study of human erythroid differentiation, the biology of factors regulating the expression of the embryonic and adult globin genes, immunotherapy of leukaemia and the study of the differentiation of haematopoietic cells (Clegg and Thompson, 1981; Lozzio *et al.*, 1981), therefore, we chose K-562 for viral titration. The titration of the GFP-expressing lentivirus vector was carried out by the

transduction of K-562 cells with LV carrying an empty vector. Seventy-two hours post-transduction, the GFP expressing cells were evaluated using fluorescent activated cell sorting (FACS) for each dilution (figure 5-1). The titre was calculated based on the following formula: (% GFP+ve of the 100,000 cells) x 1/virus dilution. The dilution of virus that gave about 3-10% GFP +ve was chosen (Charrier *et al.*, 2011). The reason for is that the titration calculation depends on any GFP positive cell being representative of a single vector integration event. It has been shown previously that in a cell population showing 10-30% transduction rate, any GFP+ cell will contain only one vector integration (Charrier *et al.*, 2011).

.

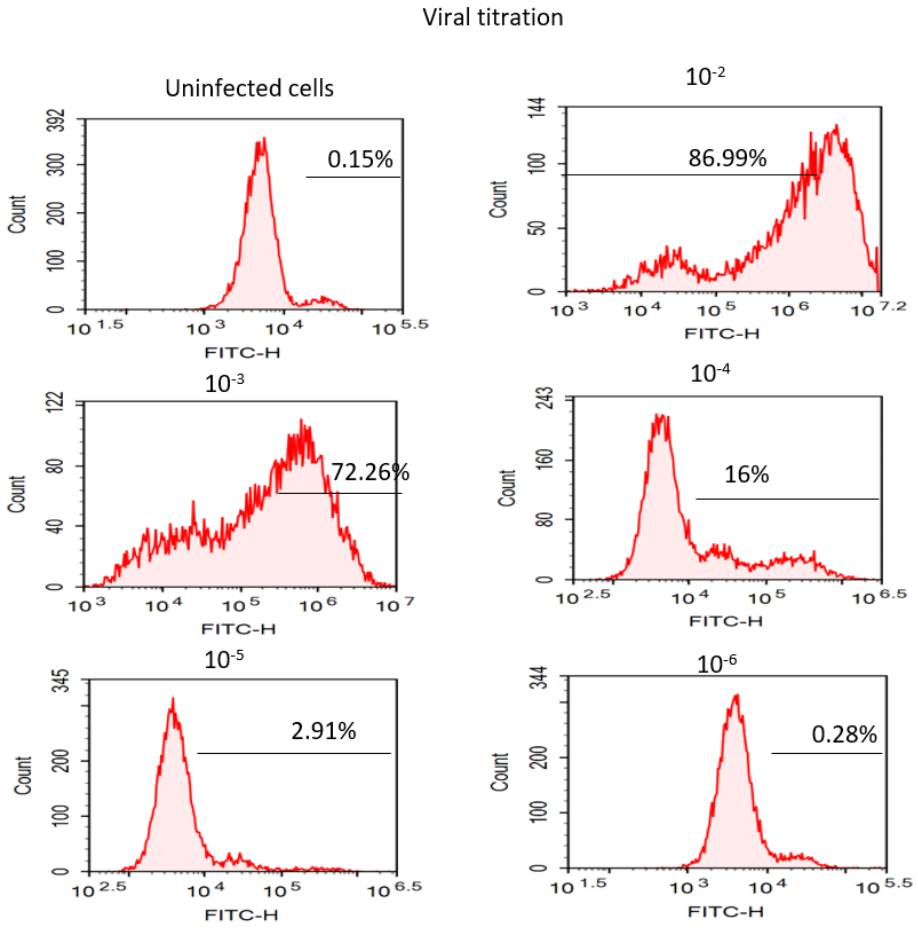

Figure 5-1. Viral titration.

The titration of the GFP-expressing lentivirus vector was carried out by the transduction of K-562 cells with a 5-fold dilution of LV carrying an empty vector. Histograms showing GFP-positive cells 72 hours post-transduction. Uninfected cells were 0.15% GFP positive, at a dilution of 10^{-2} 86.99% of cells were GFP positive, at a dilution of 10^{-3} 72.26% of cells were GFP positive, at a dilution of 10^{-4} 16% of cells were GFP positive, at a dilution of 10^{-5} 2.91% of cells were GFP positive and at a dilution of 10^{-6} 0.28% of cells were GFP positive.

5.2.1 Transduction of K-562 cells with LV carrying FXN fusion protein gene

To investigate the ability of lentivirus carrying frataxin fusion peptide to transduce cells efficiently and to compare it with the FACS result, K-562 cells were transduced serial dilution of the lentivirus, 10^{-2}, 10^{-3}, and 10^{-5}. Seventy-two hours post-transduction, cell lysates were prepared,

and a western blot was performed. Samples lysate of cells transduced with lentivirus carrying empty vector genes were also prepared to be used as a control.

A frataxin band of both full-length (23 KDa) and intermediate form (18 KDa) were detected in sample lysate of cells transduced with lentivirus carrying TAT and APP-frataxin constructs at 10^{-2} concentration. There was no detection of protein expression with other concentrations or with the cells transduced with the control (Figure 5-2).

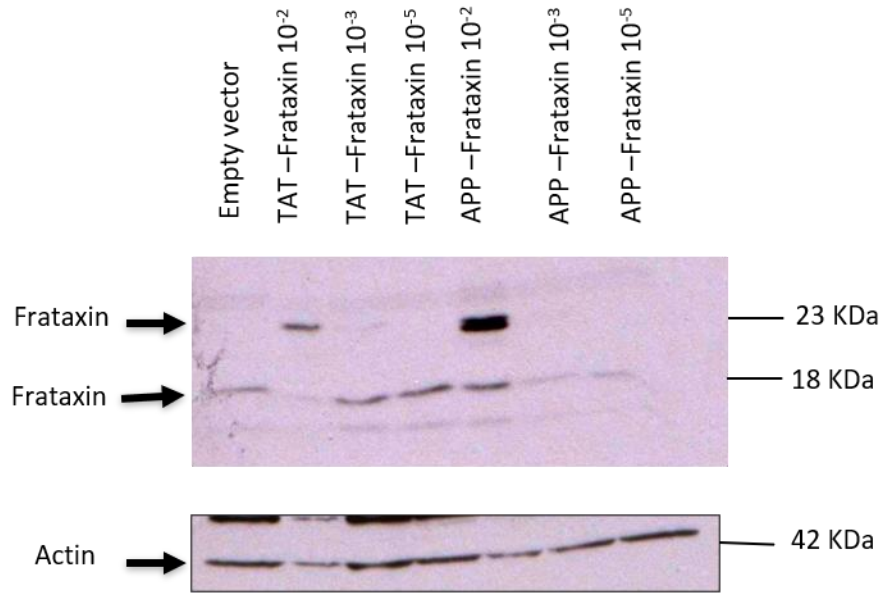

Figure 5-2. Western blot analysis for sample lysate of K-562.

Western blot analysis for sample lysate of K-562, 72-hour post-transduction with 3- fold serial dilution of lentivirus vector, which carrying TAT, APP –Frataxin construct. Arrows indicate 23 and 18KDa frataxin. Actin was used as a loading control.

5.3 Transduction of CD34+ HSPC stem cells (MOI 20)

Despite the success of retrovirus- based CD34+ HSPC gene therapy for several haematopoietic and non-haematopoietic indications, HSPC transduction remains difficult and cannot be accomplished across all patients and disorders. Some diseases need high copy numbers or a high quantity of gene-modified cells. High MOIs (Multiplicity of Infection), which indicates the number of vector particles per cell used in a transduction are applied to overcome these difficulties. Therefore we have chosen an MOI = 20 to transduce CD34+ HSPC cells (Schott *et al.*, 2019).

Also, it has been demonstrated that pre-stimulation can enhance the transduction efficiency of reconstituting stem cells(Miller, Adam and Miller, 1990; Roe *et al.*, 1993). Therefore, an overnight pre-stimulation of human CD34+ HSPC cells has been carried out first before the adding of the virus.

To determine whether CD34+ HSPC cells were successfully transduced with lentivirus carrying the frataxin penetrating peptides constructs, 24 hours post-transduction, 100,000 CD34+ HSPC haematopoietic cells were harvested, and proteins were separated on 12% SDS-polyacrylamide gel.

Frataxin was strongly overexpressed in CD34+ HSPC cells transduced with TAT and APP and full-length frataxin bands were detected were at 25 KDa, in comparison to cells transduced with empty vector as control, where only a faint band was detected. These results suggest that the CD34+ HSPC cells were effectively transduced (Figure 5-3).

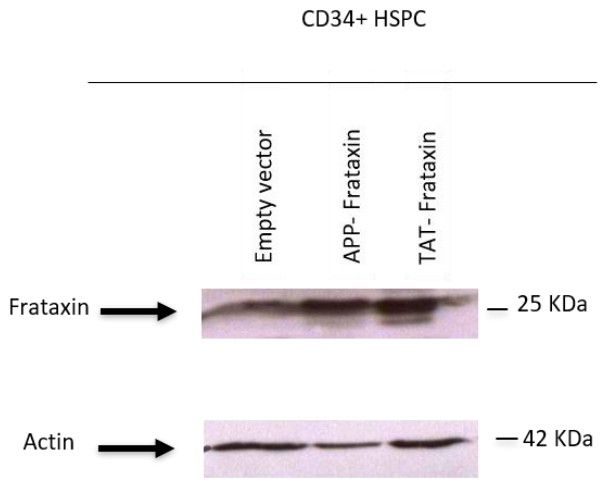

Figure 5-3. Western blot for transduced CD34+ HSPC with lentiviruses that caring penetrating frataxin fusion peptide and empty vector genes.

Western blot for transduced CD34+ HSPC with lentiviruses that caring penetrating frataxin fusion peptide genes (APP- Frataxin fusion peptides, TAT- Frataxin fusion peptide and empty vector). Frataxin bands were strongly expressed at 25 KDa with cells transduced with lentivirus carrying APP- frataxin fusion peptides, TAT- frataxin fusion peptide, in comparison to the empty vector which showed a faint band of frataxin at 25 kDa.

5.4 Frataxin fusion peptide has been secreted into the supernatant

To determine whether the penetrating fusion peptide construct was secreted into the supernatant, the supernatant of the transduced CD34+ HSPC was collected 24 hours post-transduction and centrifuged. The protein was acetone-precipitated. The sample was loaded in 12% SDS-polyacrylamide gel.

The results showed that frataxin was strongly overexpressed in the supernatant collected from CD34+ HSPC cells transduced with TAT and APP, as strong frataxin bands were detected at 28 KDa, in comparison to cells transduced with empty vector as control, where only faint bands were detected. This indicates that the frataxin fusion peptide constructs were successfully secreted into the supernatant (Figure 5-4). It's also noted that the frataxin band was detected at 28 KDa in comparison to the western blot of the supernatant collected from HEK 293T transfected with cell penetrating peptides in the previous image in which the frataxin band was detected at 23 KDa, which could be related to the post- translational modification.

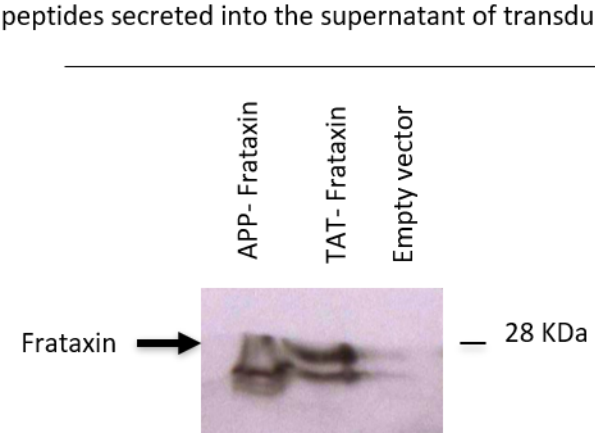

Figure 5-4. Western blot analysis for protein precipitated from the supernatant of transduced CD34+ HSPC.

Frataxin bands were strongly detected at 28 KDa in the protein precipitated from CD34+ HSPC transduced with lentivirus carrying TAT and APP-Frataxin fusion peptides genes, in comparison to cells transduced with an empty vector, which showed a faint band of frataxin at 28 kDa.

5.5 Frataxin peptides are expressed and secreted by differentiated myeloid cells

A recent study carried on by Rocc *et al.* (2015) showed that a solo transplant of wild-type mouse haematopoietic stem cells into young adult YG8R mice prevented the development of FRDA pathology, including neurobehavioral deficits, degeneration of DRG sensory neurons and muscle weakness. This supports the main idea behind our research, the ability of the haematogenic stem cells to repopulate the bone marrow and migrate from their niche to differentiate into various cells lineage including phagocytic cells (Mahla, 2016), and the ability of the differentiated cells to continuously express the frataxin The phagocytic cells would be able to cross the blood-brain barrier and engraft within the CNS as microglia, where they can deliver the frataxin to target cells. Therefore, we wanted to test the ability of the transduced CD34+ HSPC cells to propagate and differentiate and, most importantly, if the frataxin peptide is still expressed and secreted by the differentiated cells.

To demonstrate that the cells were differentiated into granulocytes (liquid culture), cell differentiation was carried out for 20 days and checked by FACS with anti-CD11B-APC (Thermofisher). The result showed that around 54.83%, 46.74%, and 52.65% of CD34+ HSPC cells transuded with lentivirus carrying the empty vector, TAT and APP, were successfully differentiated into granulocytes (Figure 5-5). The percentage of differentiation between the CD34+ HSPC cells transduced with the frataxin penetrating version of the peptide and the empty vector are approximately equal to each other, and so we conclude that transducing the haematopoietic stem cells with the frataxin penetrating version of the peptide does not affect the ability of the cells to differentiate. However, further *in vivo* studies need to be carried out to confirm this.

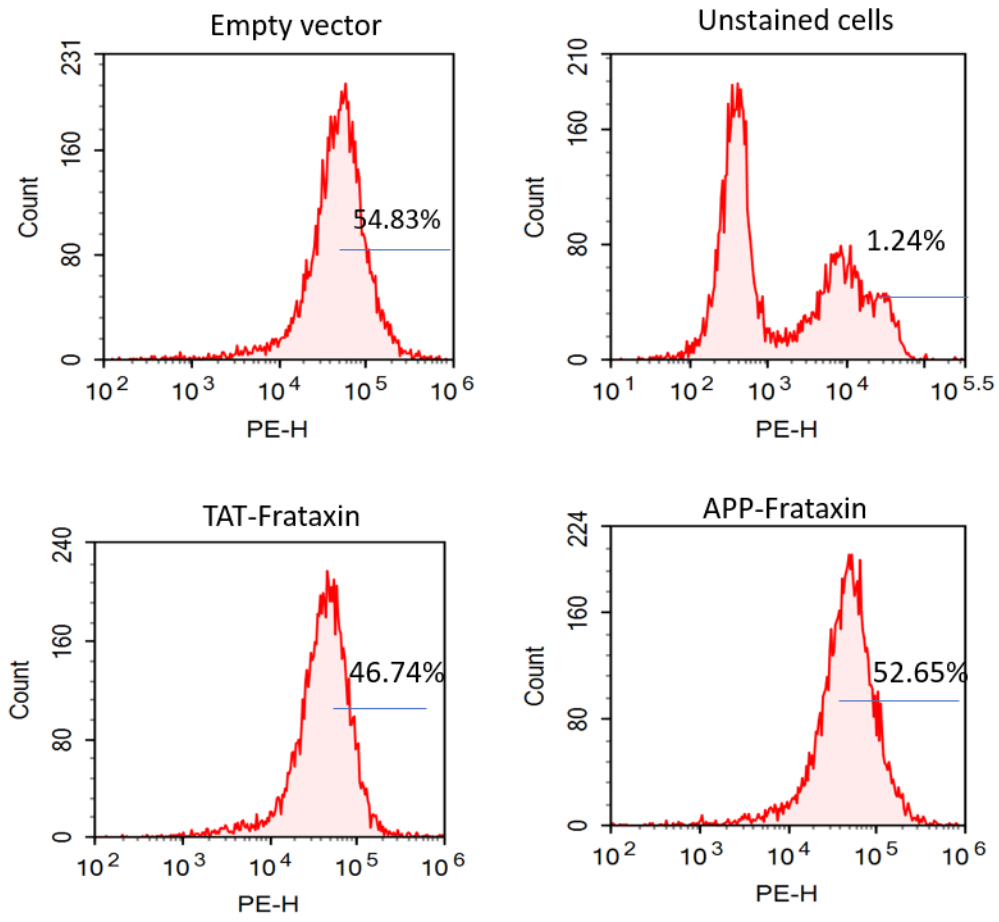

Figure 5-5. FACS cells sorting of cd11b positive and negative population.

The FACS result showed that around 54.83%,46.74%, and 52.65% of CD34+ HSPC transuded with lentivirus carrying the empty vector, TAT, and APP, were successfully differentiated into granulocyte.

To investigate whether the differentiated cells still express frataxin, around 100,000 differentiated leukocytic cells were harvested, and proteins were then separated on 12% SDS-polyacrylamide gel.mWestern blot analysis showed that frataxin continued to be strongly overexpressed in the differentiated cells transduced with TAT and APP. Frataxin bands were detected were at 23 KDa and 25 KDa, in comparison to cells transduced with empty vector as control, where only faint bands were detected (Figure 5-6).

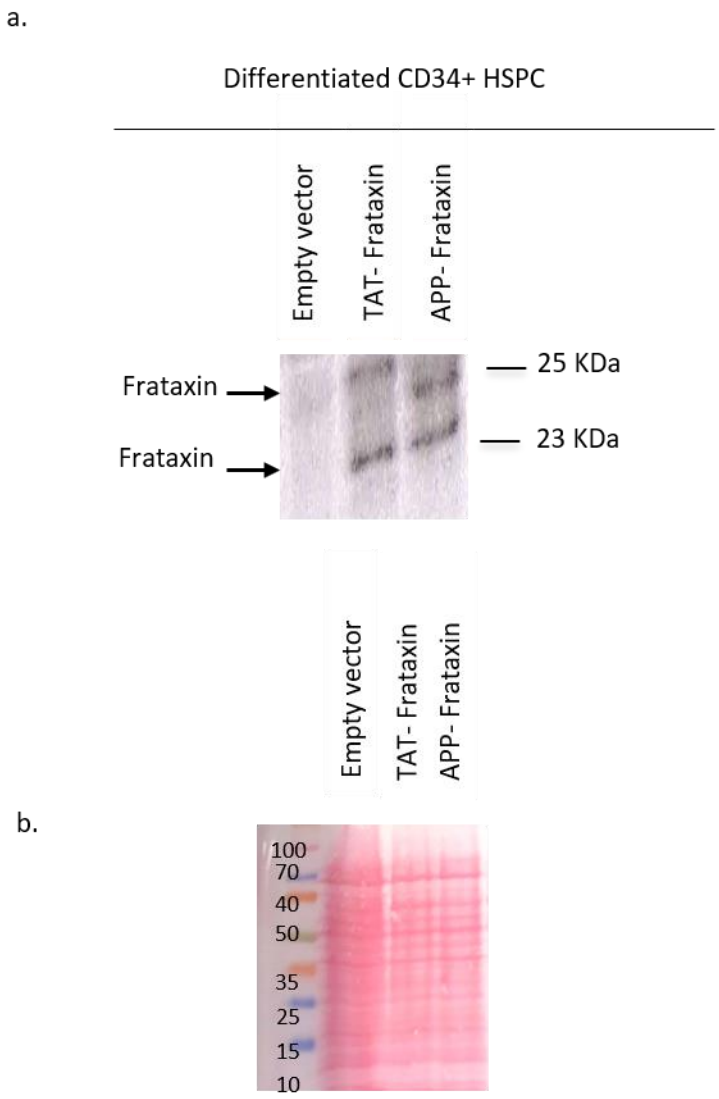

Figure 5-6. Western blot for differentiated CD34+ HSPC.

a). Western blot for transduced CD34+ HSPC with lentiviruses that caring APP-frataxin fusion peptides, TAT-frataxin fusion peptide, and empty vector genes. The CD34+ HSPC has been differentiated into leukocyte for 20 days after which they have been collected for analysis. Frataxin bands were strongly expressed at 23 KDa and 25 KDa in cells transduced with lentivirus carrying APP--frataxin fusion peptides and TAT-frataxin fusion peptide, in comparison to the empty vector in which there's no band detected. It's also to be noted that the frataxin bands detected at 23 and 25 KDa and at 28 KDa in the supernatant this inconsistency in the size of the frataxin band could be related to the posttranslational modification of the peptide b). Ponceau stain is used as normalisation of protein.

To determine whether the differentiated cells continued to secrete the fusion peptide constructs, the supernatant of the differentiated cells was collected 20 days post-transduction, and the proteins separated on 12% SDS-polyacrylamide gel.

The results showed that differentiated cells transduced with a virus carrying the APP-frataxin constructs gene were both overexpressing the frataxin and secreting it into the supernatant. A strong frataxin band was detected at 23 KDa, in comparison to cells transduced with an empty vector as the control, where only a faint band was detected. Although the differentiated cells that were originally transduced with TAT-frataxin fusion peptide were overexpressing the peptide in the sample lysate, there was no frataxin band from the collected supernatant. A conclusion about the ability of transduced cells to continuously secrete the TAT-frataxin peptide construct could not be reached because the cells are difficult to get, and it was not possible to get more cells to repeat the experiment and investigate why there was no band detected (Figures 5-7).

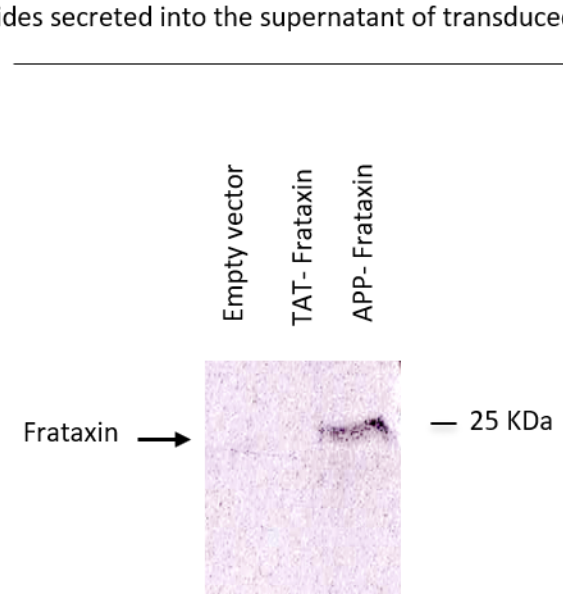

Figure 5-7. Western blot analysis for supernatant of differentiated CD34+ HSPC.

Western blot analysis for protein precipitated from supernatant collected from differentiated CD34+ HSPC transduced with lentivirus carrying penetrating TAT and APP-frataxin fusion peptide constructs and empty vector. Frataxin bands were strongly detected at 25 KDa (the frataxin band was detected at 28 KDa in the supernatant collected from CD34+ HSPC, this discrepancy again in frataxin band could be related to post-translational modification as mentioned previously) in the protein precipitated from differentiated CD34+ HSPC transduced with APP-frataxin fusion peptides, whereas no frataxin bands were detected with the cells transduced with TAT- frataxin fusion peptide control.

To summarise, CD34+ HSPC were successfully transduced at MOI= 20; the transduced cells were successfully secreting the peptide, as shown from the protein precipitated from the transduced cells. Most importantly, the differentiated CD34+ HSPC expressed and secreted the frataxin; this is the most crucial part of this research. *In vivo*, the differentiated CD34+ HSPC can deliver the frataxin fusion peptide cell to target cells everywhere in the body, including the heart and the nervous system.

5.6 Ectopic frataxin expression does not change haematopoietic differentiation

Insertional mutagenesis is a significant downside for the use of γ-retroviral vectors in human gene therapy. Although the lentivectors similarly show insertional mutagenesis in animal models and cellular-based systems prone to oncogenesis (Bokhoven *et al.*, 2009), third-generation lentivirus vectors are thought to be replication-incompetent and self-inactivating vectors, and have numerous further safety features over the second-generation: the viral *tat* gene, which is crucial for wild-type human immunodeficiency virus type 1 (HIV-1) replication (Affleck and Stoll, 2018), has been removed; vector packaging functions have been divided into three separate plasmids as an alternative of two in order to decrease danger of recombination during plasmid amplification and viral vector manufacture; an altered 3' LTR renders the vector "self-inactivating" in order to stop integrated genes from being repackaged; and a heterologous coat protein (*e.g.*, VSV-G) is used in position of the native HIV-1 envelope protein (Affleck and Stoll, 2018) Therefore, we wanted to investigate further if the lentivirus or the ectopic frataxin overexpression could have any effect on haematopoietic stem cells differentiation.

The CD34+ cells were plated in Methocult media and the colonies scored after 14 days. The total number of colonies with an empty vector (as control) was 97, of which 55 were BFU-E, 19 were GFU-GM and 24 were CFU-GEMM. The total number of colonies from the cells infected with lentivirus carrying TAT Frataxin constructs was 101, of which are around 54 were BFU-E, 23 were GFU-GM and 21 were CFU-GEMM. The total number of colonies from cells infected with lentivirus carrying APP Frataxin construct was 99 colonies of which 55 were BFU-E 55, 23 GFU-GM, and 19 CFU- GEMM (see Table 5-2 and Figure 5-8). CFU-E colonies are usually counted at medium magnification (40X - 60X magnification). Large BFU-E, CFU-GM, and CFU-GEMM colonies are usually counted at low magnification (4X objective), the high power to help with colony identification if necessary. There was a small cluster of cells, usually between 8 and 20, that were considered to be colonies; however, a higher magnification is required to confirm whether the small colony was derived from a BFU-E or a CFU-E. Therefore, they were included in the counting as a colony; however, they have not been added to the differentiation blot.

.The number of repeats of this experiment was only one since the CD34+ HSPC cells are scarce and it was not possible to have more cells to repeat the experiment. Although a statistically significant result could not be calculated, we can conclude that the ectopic expression of frataxin or the virus transduction doesn't affect the haematopoietic cells' differentiation, if we compare the cells infected with lentivirus carrying empty vector construct and cells infected with lentivirus carrying frataxin construct. However, further experiments need to be carried on *in vivo* to support these results.

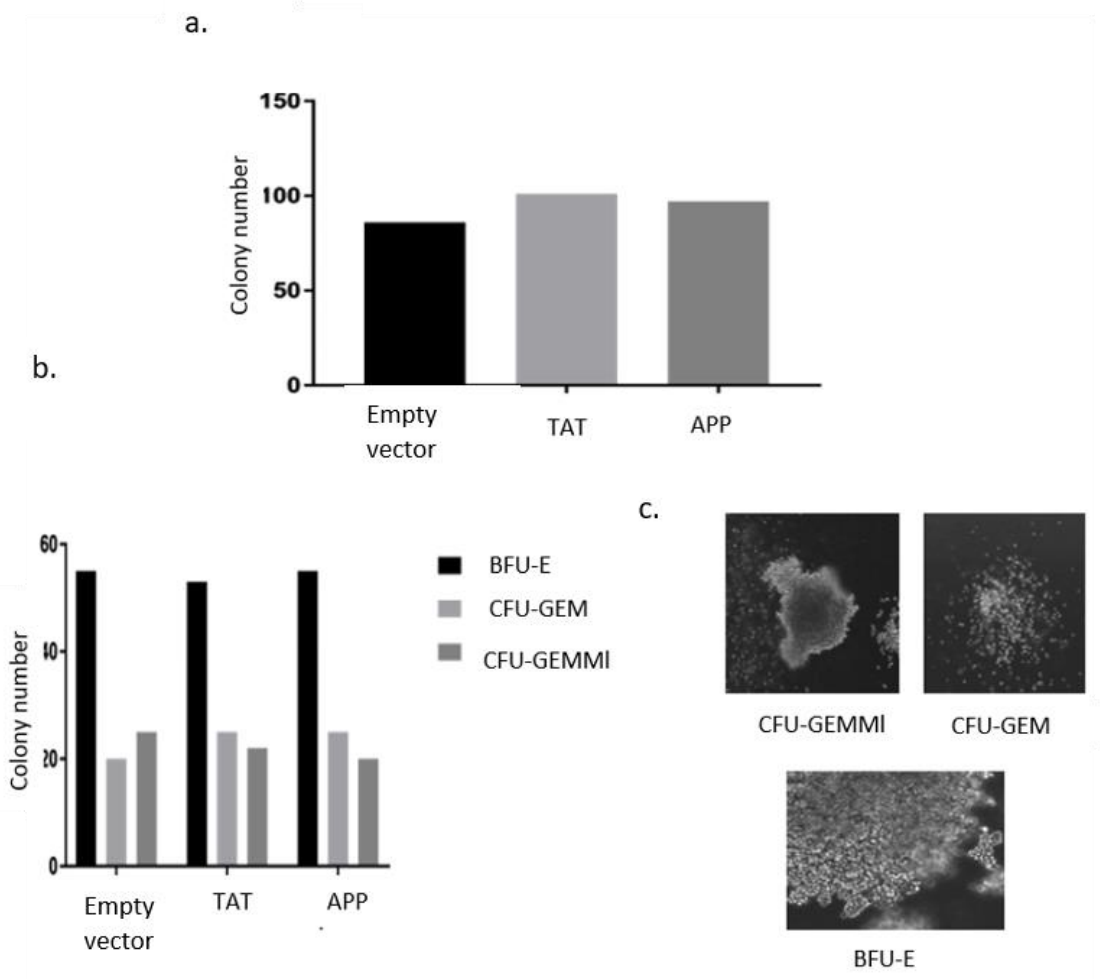

Figure 5-8. CD34+ HSPC colony formation after 15 days of differentiation in Methoccult media.

a). demonstrates the total number of colonies in CD34+ HSPC that transduced with lentivirus vectors containing the frataxin cDNA fused to the sequences encoding tissue penetrating peptides and empty vector as a control. b). The number of colonies that were differentiated to BFU-E, GFU-GM, and CFU-GEMM. c). Bright field of different colonies. CFU-E colonies are usually counted at medium magnification (40X - 60X magnification). Large BFU-E, CFU-GM, and CFU-GEMM colonies are usually counted at low magnification (4X objective), with which to high power to help with colony identification if necessary. There was a small cluster of cells, usually between 8 and 20, that were considered to be colonies; however, a higher magnification is required to confirm whether the small colony was derived from a BFU-E or a CFU-E. Therefore, they were included in the counting as a colony; however, they have not been added to the differentiation blot.

Table 5-1. CD34+ HSPC colony formation after 15 days of differentiation of the cells in Methoccult media.

	Total number of colonies	BLFU- E	CFU- GM	CFU- GEMM
Lenti-Empty vector	97	55	19	24
Lenti-TAT	101	54	23	21
Lenti-APP	99	55	23	19

5.7 Discussion

Until now, FRDA has been considered to be an incurable, debilitating neurodegenerative disease. Therapeutic gene transfer could offer the promise of lasting therapies and even a cure for diseases believed to be incurable or for which only suboptimal or temporary therapies were accessible, FRDA among them (Kumar *et al.*, 2016b).

There is new *in vivo* research that has reported the prevention and reversal of serious cardiomyopathy in a frataxin-knockout mouse model following intravenous injection of AAV9 (adeno-associated virus serotype 9 human frataxin cDNA (Perdomini *et al.*, 2014), Adeno-associated viral (AAV) vectors have been found to provide for sustained, long-term gene expression in a wide variety of tissues and cause minimal immunological complications compared to other viral vectors being tested for gene therapy (Konkalmatt *et al*, 2014). In recent years, a variety of new AAV serotypes have been isolated (Konkalmatt *et al*, 2014) that exhibit a wide range of tissue tropisms and provide for efficient transduction and long-term gene expression (Konkalmatt *et al*, 2014). In particular, serotypes AAV6, AAV8 and AAV9 transduce cardiomyocytes preferentially following systemic administration and provide uniform gene delivery throughout the myocardium (Konkalmatt *et al*, 2014). An additional study has shown that a single transplant of wild-type mouse HSPCs into young adult YG8R mice stopped the development of FRDA pathology, including neurobehavioral deficits, muscle weakness, and degeneration of DRG sensory neurons (Celine J Rocca *et al.*, 2017). It has been shown that a cell-penetrating peptide can deliver a protein to the mitochondria *in vivo* in quantities that were

adequate to rescue a fatal disease phenotype and restore mitochondrial enzyme activity in heterozygous mice (Vyas *et al.*, 2012). All this supports the use of genetically modified stem cells as a basis for developing novel therapeutic interventions for FRDA. The critical advantage using HSPC transplantation is the ability of these cells to repopulate the bone marrow permanently, and from there migrate to differentiate into phagocytic cell types within various tissues (Naphade *et al.*, 2016). Therefore, there would be no need to repeatedly inject the patient to deliver the therapeutic peptide. HSPCs might even be able to transmigrate through the blood-brain barrier and engraft within the CNS as differentiated microglia (Eglitis and Mezey, 1997; Gregory *et al.*, 2000; Priller *et al.*, 2001).

In our approach, we have used an autologous stem transplant, in which the transplanted stem cells are derived from the patient's own bone marrow, which is safer than allogeneic transplantation in which the stem cells are collected from another donor, and so there will be no need for immunosuppressive medication or risk of graft versus host disease.

We demonstrated that the transduced haematopoietic stem cells were able to secrete the cell-penetrating version in the supernatant, and the cell-penetrating version of the peptides was expressed and secreted by differentiated myeloid cells. Ectopic frataxin expression does not change haematopoietic differentiation. Our work suggests that this strategy could be a potential approach for treating FRDA; this would be further supported by the result of the *in vivo* animal work that is being carried currently out.

Chapter 6.

General discussion

FRDA is still considered to be an incurable disease in which rehabilitation is the primary treatment, although there have been a few clinical trials that have made some limited progress (Zhao *et al.*, 2017). Some of the therapy options under research include mitochondrial function enhancers, antioxidant and neuroprotection agents, enhancers of frataxin gene expression and frataxin replacement. The latter involves delivering frataxin to cells using the HIV-trans-activator of transcription (TAT) as a cargo molecule (Vyas *et al.*, 2012). Using a conditional-KO mouse model in which Frataxin was depleted in the brain (Vyas *et al.*, 2012), intraperitoneal (IP) TAT-FXN injections showed evidence of mitochondrial localisation and rescued the lethal phenotype. Studies have shown that TAT-FXN has also been able to traverse the blood-brain barrier and protect dopaminergic neurons in a conditional mice model after intraperitoneal injections(IP injections) (Britti, Tamarit and Ros, 2018).

Gene and cell therapies are being established as likely treatments for several genetic diseases. A significant advantage in emerging cell and gene therapy for FRDA is that affected persons already make frataxin, even though at minimal amounts; therefore, therapeutic delivery of frataxin will not develop an immune response. Returning function to even a minor percentage of cells could have a positive impact on the adjacent microenvironment and increase overall clinical outcomes (Evans-galea *et al.*, 2014).

There are currently numerous lines of data clearly showing that FRDA is responsive to gene therapy, where a recent study proves the strong potential of AAV transfer to restore frataxin expression in dorsal root ganglia and rescue the ganglionopathy as well as sensory neuropathy accompanied by frataxin deficiency, even in severely affected animals (Piguet *et al.*, 2018). Another study demonstrated the ability of gene therapy to prevent as well as reverse the severe mitochondrial cardiomyopathy in a mouse model of Friedreich's ataxia (Perdomini *et al.*, 2014)

Human haematopoietic stem and progenitor cells (HSPCs) from the bone marrow are considered to be an ideal candidate for use in regenerative medicine and cell replacement therapy (Mahla, 2016). A recent study has shown that transplantation of wild-type mouse HSPCs into young YG8R mice saved various aspects of the FRDA phenotype, such as coordination and locomotion deficits and vascular degeneration of DRG neurons (Celine J Rocca *et al.*, 2017).

Our findings show that frataxin fusion cell-penetrating peptides were able to penetrate and deliver frataxin efficiently to FRDA cells, and functionally reconstitute aconitase activity and provide resistance to oxidative stress in frataxin-defective cells derived from FRDA patients. Oxidative stress has lately been shown to encourage DNA damage and increase poly (adenosine 5'-diphosphate–ribose) polymerase 1 (PARP1) expression in frataxin-deficient microglial cells, which resulted in increased microglial activation (Rocca *et al*., 2017). As PARP1 activation causes increased inflammatory cytokine expression in microglial cells, these results indicate that oxidative stress may induce neuroinflammatory-mediated neurodegeneration in FRDA (Celine J Rocca *et al.*, 2017). In our study, we tested the possibility of using the APP as CPP. APP is a calcium ion-regulated annexin protein that is membrane-associated and which controls actin dynamics through their membrane interaction and attaches to the negatively-charged head groups of phospholipids in the membrane (Kim *et al.*, 2015a). That means it would have a higher serum availability and less immunogenicity and cytotoxicity than CPP of non-human origin. We also demonstrated that the transduced haematopoietic stem cells were able to secrete the cell-penetrating version in the supernatant, and the cell-penetrating version of peptides is expressed and secreted by differentiated myeloid cells.

Our results show that the ectopic frataxin expression does not change haematopoietic differentiation, and our findings indicate that genetically modified stem cells could be used as a basis for developing novel therapeutic interventions for FRDA patients. The main advantage of using HSPC transplantation is its capacity to permanently repopulate the bone marrow and migrate from its niche to differentiate into phagocytic cell types within various tissues (Naphade *et al.*, 2016). Therefore, there will be no need to repeatedly inject the patient to deliver the therapeutic peptide.

Genetically modified HSPCs could even be able to migrate across the blood-brain barrier and engraft within the CNS as differentiated microglia (Eglitis and Mezey, 1997; Gregory *et al.*, 2000; Priller *et al.*, 2001). That means that HSPCs would be able to deliver the cell-penetrating frataxin fusion peptide continuously to diseased tissues. Our approach depend on the use of an autologous stem transplant, in which the transplanted stem cells are derived from the patients'

own bone marrow. This is safer than allogeneic transplantation, in which the stem cells are collected from another donor.

In our studies, we have tried a novel cell and gene therapy, which showed promising results *in vitro* studies; however, these results need to be further confirmed by *in vivo* studies that are currently taking place in our lab.

Bibliography

Adamec, J. *et al.* (2000) 'Iron-Dependent Self-Assembly of Recombinant Yeast Frataxin: Implications for Friedreich's ataxia', *The American Journal of Human Genetics*, 67(3), pp. 549–562. doi: 10.1086/303056.

Affleck, V. and Stoll, E. A. (2018) 'Manufacture of Third-Generation Lentivirus for Preclinical Use, with Process Development Considerations for Translation to Good Manufacturing Practice', *Human Gene Therapy Methods*, 29(1), pp. 1–15. doi: 10.1089/hgtb.2017.098.

Aiuti, A. *et al.* (2015) 'Lentiviral haematopoietic stem cell gene therapy in patients with Wiskott-Aldrich syndrome', *Science*, 341(6148). doi: 10.1126/science.1233151.

Alves, I. D. *et al.* (2008) 'Membrane interaction and perturbation mechanisms induced by two cationic cell-penetrating peptides with distinct charge distribution', *Biochimica et Biophysica Acta - General Subjects*, 1780(7–8), pp. 948–959. doi: 10.1016/j.bbagen.2008.04.004.

Alviña, K. and Khodakhah, K. (2008) 'Selective regulation of spontaneous activity of neurons of the deep cerebellar nuclei by N-type calcium channels in juvenile rats', *Journal of Physiology*, 586(10), pp. 2523–2538. doi: 10.1113/jphysiol.2007.148197.

Aranca, T. V *et al.* (2016) 'Emerging therapies in Friedreich' s ataxia', *Neurodegenerative Disease Management*, 6, pp. 49–65. doi:10.2217/nmt.15.73

Bannister, A. J. *et al.* (2001) 'Selective recognition of methylated lysine 9 on histone H3 by the HP1 chromo domain', *Nature*, 410(6824), pp. 120–124. doi: 10.1038/35065138.

Beisel, C. and Paro, R. (2011) 'Silencing chromatin: comparing modes and mechanisms', *Nature Review Genetics,* 12(2), pp. 123–135. doi: 10.1038/nrg2932.

Belancio, V. P., Hedges, D. J. and Deininger, P. (2008) 'Mammalian non-LTR retrotransposons: For better or worse, in sickness and in health', *Genome Research*, 18(3), pp. 343–358. doi: 10.1101/gr.5558208.

Bentin, T. *et al.* (2005) 'Transcription arrest caused by long nascent RNA chains', *Biochimica et Biophysica Acta - Gene Structure and Expression*, 1727(2), pp. 97–105. doi: 10.1016/j.bbaexp.2004.12.006.

Benz, J. and Hofmann, A. (1997) 'Annexins: From structure to function', *Biological Chemistry*, 378(3–4), pp. 177–183. doi: 10.1152/physrev.00030.2001

De Biase, I. *et al.* (2009) 'Epigenetic silencing in Friedreich's ataxia is associated with depletion of CTCF (CCCTC-binding factor) and antisense transcription', *PLoS ONE,* 4(11). doi: 10.1371/journal.pone.0007914.

Bidichandani, S. I., Ashizawa, T. and Patel, P. I. (1998) 'The GAA Triplet-Repeat Expansion in Friedreich's ataxia Interferes with Transcription and May Be Associated with an Unusual DNA Structure', *The American Journal of Human Genetics*, 62(1), pp. 111–121. doi: 10.1086/301680.

Biffi, A. *et al.* (2013) 'Lentiviral Haematopoietic Stem Cell Gene Therapy Benefits Metachromatic Leukodystrophy'. *science*, 341(6148). doi: 10.1126/science.1233158.

Boesch, S. *et al.* (2007) 'Friedreich's ataxia: Clinical pilot trial with recombinant human erythropoietin', *Annals of Neurology*, 62(5), pp. 521–524. doi: 10.1002/ana.21177.

Boesch, S. *et al.* (2014) 'Safety and tolerability of carbamylated erythropoietin in Friedreich's ataxia', *Movement Disorders*, 29(7), pp. 935–939. doi: 10.1002/mds.25836.

Boisguerin, P. *et al.* (2011) 'Systemic delivery of BH4 anti-apoptotic peptide using CPPs prevents cardiac ischemia-reperfusion injuries in vivo', *Journal of Controlled Release*, 156(2), pp. 146–153. doi: 10.1016/j.jconrel.2011.07.037.

Bokhoven, M. *et al.* (2009) 'Insertional Gene Activation by Lentiviral and Gammaretroviral Vectors', *Journal of Virology*, 83(1), pp. 283–294. doi: 10.1128/jvi.01865-08.

Borsello, T. *et al.* (2003) 'A peptide inhibitor of c-Jun N-terminal kinase protects against excitotoxicity and cerebral ischemia', *Nature Medicine*, 9(9), pp. 1180–1186. doi: 10.1038/nm911.

Bou-Abdallah, F. *et al.* (2004) 'Iron binding and oxidation kinetics in frataxin CyaY of Escherichia coli', *Journal of Molecular Biology*, 341(2), pp. 605–615. doi: 10.1016/j.jmb.2004.05.072.

Bright, R. (2004) 'Protein Kinase C Mediates Cerebral Reperfusion Injury In Vivo', *Journal of Neuroscience*, 24(31), pp. 6880–6888. doi: 10.1523/JNEUROSCI.4474-03.2004.

Britti, E. *et al.* (2017) 'Frataxin-deficient neurons and mice models of Friedreich's ataxia are improved by TAT-MTScs-FXN treatment', *Journal of Cellular and Molecular Medicine*, 22(2), pp. 834–848. doi: 10.1111/jcmm.13365

Bru, B. *et al.* (2004) 'Iron – sulphur protein maturation in human cells: evidence for a function of frataxin', *Human Molecular Genetics*, 13(23), pp. 3007–3015. doi: 10.1093/hmg/ddh324.

Bulteau, A. L. *et al.* (2004) 'Frataxin acts as an iron chaperone protein to modulate mitochondrial aconitase activity', *Science*, 305(5681), pp. 242–245. doi: 10.1126/science.1098991.

Buratowski, S. (2011) 'Progression through the RNA polymerase II CTD cycle', *Molecular cell*, 36(4), pp. 541–546. doi: 10.1016/j.molcel.2009.10.019.

Bürk, K. (2017) 'Friedreich's ataxia: current status and future prospects', *Cerebellum & Ataxias*, 4(1). doi: 10.1186/s40673-017-0062-x.

Burnight, E. R. *et al.* (2015) 'Gene therapy using stem cells', *Cold Spring Harbor Perspectives in Medicine*, 5(4), pp. 1–11. doi: 10.1101/cshperspect.a017434.

Campuzano, V. *et al.* (1996) 'Repeat Expansion', *Science*, 271, pp. 1423–1427. doi: 10.1126/science.271.5254.1423.

Cantu, D., Schaack, J. and Patel, M. (2009) 'Oxidative inactivation of mitochondrial aconitase results in iron and H2O2-mediated neurotoxicity in rat primary mesencephalic cultures', *PLoS ONE*, 4(9), pp. 3–11. doi: 10.1371/journal.pone.0007095.

Cao, Y. J. *et al.* (2002) 'Modulation of recombinant and native neuronal SK channels by the neuroprotective drug riluzole', *European Journal of Pharmacology*, 449(1–2), pp. 47–54. doi: 10.1016/S0014-2999(02)01987-8.

Castaldo, I. *et al.* (2008) 'DNA methylation in intron 1 of the frataxin gene is related to GAA repeat length and age of onset in Friedreich's ataxia patients', *Journal of Medical Genetics*, 45(12) pp. 808–812. doi: 10.1136/jmg.2008.058594.

Cavadini, P. *et al.* (2002) 'Assembly and iron-binding properties of human frataxin, the protein deficient in Friedreich's ataxia', *Human molecular genetics*, 11(3), pp. 217–227. doi: 10.1093/hmg/11.3.217.

Cavazzana-calvo, M. (2012) 'Gene Therapy of Human Severe Combined Immunodeficiency (SCID)– X1 Disease', *Science*, 288(5466), pp. 669-672. doi: 10.1126/science.288.5466.669.

Chan, P. K. *et al.* (2013) 'Heterochromatinisation induced by GAA-repeat hyperexpansion in Friedreich' s ataxia can be reduced upon HDAC inhibition by vitamin B3', *Human Molecular Genetics*, 22(13), pp. 2662–2675. doi: 10.1093/hmg/ddt115.

Charrier, S. *et al.* (2011) 'Quantification of lentiviral vector copy numbers in individual hematopoietic colony-forming cells shows vector dose-dependent effects on the frequency and level of transduction', *Gene Therapy*, 18(5), pp. 479–487. doi: 10.1038/gt.2010.163.

Chevronnay, H. P. G. *et al.* (2016) 'Haematopoietic stem cells transplantation can normalise thyroid function in a cystinosis mouse model', *Endocrinology*, 157 (4), pp. 1363–1371. doi: 10.1210/en.2015-1762.

Chiang, S. *et al.* (2016) 'Frataxin and the molecular mechanism of mitochondrial iron-loading in Friedreich' s ataxia', *Science*, 130(11), pp. 853–870. doi: 10.1042/CS20160072.

Chou, S. H., Chin, K. H. and Wang, A. H. J. (2003) 'Unusual DNA duplex and hairpin motifs', *Nucleic Acids Research*, 31(10), pp. 2461–2474. doi: 10.1093/nar/gkg367.

Cideciyan, A. V *et al.* (2009) 'Human RPE65 Gene Therapy for Leber Congenital and Safety at 1 Year', *Human gene therapy*, 20(9), pp. 999–1004. doi:10.1089/hum.2009.086.

Clark, E. *et al.* (2018) 'Role of frataxin protein deficiency and metabolic dysfunction in Friedreich ataxia, an autosomal recessive mitochondrial disease', *Neuronal signaling*, *2*(4), pp. 1-11.doi.org/10.1042/NS20180060

Clegg, J. B. and Thompson, J. (1981) 'Embryonic erythroid differentiation in the human leukemic cell line K562', *Proceedings of the National Academy of Sciences of the United States of America*, 78(1), pp. 348–352. doi:10.1073/pnas.78.1.348

Clément, F. *et al.* (2017) 'Stem cell manipulation, gene therapy and the risk of cancer stem cell emergence', *Stem cell investigation,* 4(67). doi: 10.21037/sci.2017.07.03

Cnop, M., Mulder, H. and Igoillo-esteve, M. (2013) 'Diabetes in Friedreich's ataxia', *Journal of Neurochemistry*,126(1), pp. 94-102. doi: 10.1111/jnc.12216.

Coppola, G. *et al.* (2009) 'Functional genomic analysis of frataxin deficiency reveals tissue-specific alterations and identifies the PPARγ pathway as a therapeutic target in Friedreich's ataxia', *Human Molecular Genetics*, 18(13), pp. 2452–2461. doi: 10.1093/hmg/ddp183.

Cossee, M. *et al.* (1997) 'Evolution of the Friedreich's ataxia trinucleotide repeat expansion: Founder effect and premutations', *Proceedings of the National Academy of Sciences*, 94(14), pp. 7452–7457. doi: 10.1073/pnas.94.14.7452.

Delatycki, M. B. *et al.* (1999) 'Clinical and genetic study of Friedreich's ataxia in an Australian population', *American Journal of Medical Genetics*, 87(2), pp. 168–174. doi: 10.1002/(SICI)1096-8628(19991119)87:2<168: AID-AJMG8>3.0.CO;2-2.

Delatycki, M. B., Williamson, R. and Forrest, S. M. (2000) 'Friedreich's ataxia: an overview', *Journal of medical genetics*, 37(1), pp. 1–8. doi: 10.1136/jmg.37.1.1.

Derakhshankhah, H. and Jafari, S. (2018) 'Cell penetrating peptides: A concise review with emphasis on biomedical applications', *Biomedicine and Pharmacotherapy*. Elsevier, 108(June), pp. 1090–1096. doi: 10.1016/j.biopha.2018.09.097

Dhe-Paganon, S. *et al.* (2000) 'Crystal Structure of Human Frataxin', *Journal of Biological Chemistry*, 275(40), pp. 30753–30756. doi: 10.1074/jbc.C000407200.

Domhan, S. *et al.* (2011) 'Intercellular Communication by Exchange of Cytoplasmic Material via Tunneling Nano-Tube Like Structures in Primary Human Renal Epithelial Cells'*, PLoS ONE,* 6(6), pp. 1–8. doi: 10.1371/journal.pone.0021283.

Dull, T. *et al.* (1998) 'A third-generation lentivirus vector with a conditional packaging system', *Journal of virology*, 72(11), pp. 8463–71. Available at: http://www.ncbi.nlm.nih.gov/pubmed/9765382

Eglitis, M. A. and Mezey, É. (1997) 'Haematopoietic cells differentiate into both microglia and macroglia in the brains of adult mice', *Proceedings of the National Academy of Sciences of the United States of America*, 94(8), pp. 4080–4085. doi: 10.1073/pnas.94.8.4080.

Entezam, M. *et al.* (2017) 'Comparison of Two Different PCR-based Methods for Detection of GAA Expansions in Frataxin Gene', *Iranian journal of public health,* 46(2), pp. 222–228. Available at: http://www.ncbi.nlm.nih.gov/pubmed/ 28451558

Evans-galea, M. V *et al.* (2012) 'FXN Methylation Predicts Expression and Clinical Outcome in Friedreich's ataxia', *Annals of Neurology,* 71(4), pp. 487–497. doi: 10.1002/ana.22671.

Evans-galea, M. V *et al.* (2014) 'Cell and Gene Therapy for Friedreich's ataxia', *Human gene therapy,* 693(August), pp. 684–693. doi: 10.1089/hum.2013.180.

Escors, D. and Breckpot, K. (2011) 'Lentiviral vectors in gene therapy: their current status and future potential', *Archivum Immunologiae et Therapiae Experimentalis*, 58(2), pp. 107–119. doi: 10.1007/s00005-010-0063-4.Lentiviral.

Fahey, M. C. *et al.* (2008) 'Vestibular, saccadic and fixation abnormalities in genetically confirmed Friedreich's ataxia'. *Brain*, 31(4), pp. 1035–1045. doi: 10.1093/brain/awm323.

Fleming, J. *et al.* (2005) 'Partial Correction of Sensitivity to Oxidant Stress in Friedreich Ataxia Patient Fibroblasts by Frataxin-Encoding Adeno-Associated Virus and Lentivirus Vectors', *Human gene therapy,* 956(August), pp. 947–956. doi: 10.1089/hum.2005.16.947.

De Figueiredo, I. R. *et al.* (2014) 'Cell-penetrating peptides: A tool for effective delivery in gene-targeted therapies', *IUBMB Life*, 66(3), pp. 182–194. doi: 10.1002/iub.1257.

Fisher, A. G. and Merkenschlager, M. (2002) 'Gene silencing, cell fate and nuclear organisation', *Current Opinion in Genetics and Development*, 12(2), pp. 193–197. doi: 10.1016/S0959-437X (02)00286-1.

Del Gaizo, V., MacKenzie, J. A. and Payne, R. M. (2003) 'Targeting proteins to mitochondria using TAT', *Molecular Genetics and Metabolism*, 80(1–2), pp. 170–180. doi: 10.1016/j.ymgme.2003.08.017.

Gakh, O. *et al.* (2006) 'Mitochondrial iron detoxification is a primary function of frataxin that limits oxidative damage and preserves cell longevity', *Human Molecular Genetics*, 15(3), pp. 467–479. doi: 10.1093/hmg/ddi461.

Gellera, C. *et al.* (2007) 'Frataxin gene point mutations in Italian Friedreich's ataxia patients', *Neurogenetics*, 8(4), pp. 289–299. doi: 10.1007/s10048-007-0101-5.

Gerke, V., Creutz, C. E. and Moss, S. E. (2005) 'Annexins: Linking Ca2+ signalling to membrane dynamics', *Nature Reviews Molecular Cell Biology*, 6(6), pp. 449–461. doi: 10.1038/nrm1661.

Giugliano, G. R. (2007) 'Friedreich' s Ataxia as a Cause of Premature Coronary Artery Disease', Friedreich's ataxia as a cause of premature coronary artery disease. Texas Heart Institute journal, 34(2), 214–217.34(2), pp. 2–5. Available at: http://www.ncbi.nlm.nih.gov/pubmed/ 17622372.

Gonçalves, G. A. R. and Paiva, R. de M. A. (2017) 'Gene therapy: advances, challenges and perspectives', *Einstein (Sao Paulo, Brazil)*, 15(3), pp. 369–375. doi: 10.1590/S1679-45082017RB4024.

Gonz, P. (2013) 'Mitochondrial pathophysiology in Friedreich's ataxia', *Journal of Neurochemistry,* 126, pp. 53–64. doi: 10.1111/jnc.12303.

Gottesfeld, J. M., Rusche, J. R. and Pandolfo, M. (2013) 'Increasing frataxin gene expression with histone deacetylase inhibitors as a therapeutic approach for Friedreich's ataxia', *Journal of Neurochemistry*, 126(SUPPL.1), pp. 147–154. doi: 10.1111/jnc.12302.

Grabczyk, E. and Usdin, K. (2000) 'The GAA • TTC triplet repeat expanded in Friedreich' s ataxia impedes transcription elongation by T7 RNA polymerase in a length and supercoil dependent manner', *Nucleic acids research*, 28(14), pp. 2815–2822.

Gräslund, A. *et al.* (2011) 'Mechanisms of cellular uptake of cell-penetrating peptides', *Journal of Biophysics*, 2011, pp. 1–10. doi: 10.1155/2011/414729.

Grice, J., Willmott, H. and Taylor, H. (2016) '(Assessment and management of cavus foot deformity', *Orthopaedics and Trauma*. Elsevier Ltd, 30(1), pp. 1–7. doi: 10.1016/j.mporth.2016.02.001.

Groh, M. *et al.* (2014) 'R-loops Associated with Triplet Repeat Expansions Promote Gene Silencing in Friedreich's ataxia and Fragile X Syndrome', *PLoS Genetics*, 10(5), e1004318. doi: 10.1371/journal.pgen.1004318.

Guidotti, G., Brambilla, L. and Rossi, D. (2017) 'Cell-Penetrating Peptides: From Basic Research to Clinics', *Trends in Pharmacological Sciences*. Elsevier Ltd, 38(4), pp. 406–424. doi: 10.1016/j.tips.2017.01.003.

Harada, K. *et al.* (2002) 'Hypothermia inhibits translocation of CaM kinase II and PKC-α, β, γ isoforms and fodrin proteolysis in rat brain synaptosome during ischemia-reperfusion', *Journal of Neuroscience Research*, 67(5), pp. 664–669. doi: 10.1002/jnr.10159.

Harding, A. E. (1981) 'Friedreich's ataxia: A clinical and genetic study of 90 families with an analysis of early diagnostic criteria and a familial clustering of clinical features', *Brain*, 104 (3), pp. 589–620. doi:10.1093/brain/104.3.589

Herman, D. *et al.* (2006) 'Histone deacetylase inhibitors reverse gene silencing in Friedreich's ataxia', *Nature Chemical Biology*, 2(10), pp. 551–558. doi: 10.1038/nchembio815.

Hosseini, A. *et al.* (2012) 'Efficacy of a Phosphorodiamidate Morpholino Oligomer Antisense Compound in the Inhibition of Corneal Transplant Rejection in a Rat Cornea Transplant Model', *Journal of Ocular Pharmacology and Therapeutics*, 28(2), pp. 194–201. doi: 10.1089/jop.2011.0135.

Hu, X. *et al.* (2017) 'Cerebral Vascular Disease and Neurovascular Injury in Ischemic Stroke', *Circulation Research ,*120(3), pp. 449–472. doi: 10.1161/CIRCRESAHA.116.308427.

Huang, G.-Q. *et al.* (2011) 'The combined transduction of copper, zinc-superoxide dismutase and catalase mediated by cell-penetrating peptide, PEP-1, to protect myocardium from ischemia-reperfusion injury', *Journal of Translational Medicine*, 9(1), p. 73. doi: 10.1186/1479-5876-9-73.

Huang, M. L.-H., Lane, D. J. R. and Richardson, D. R. (2011) 'Mitochondrial Mayhem: The Mitochondrion as a Modulator of Iron Metabolism and Its Role in Disease', *Antioxidants & Redox Signaling*, 15(12), pp. 3003–3019. doi: 10.1089/ars.2011.3921.

Igoillo-Esteve, M. *et al.* (2015) 'Unveiling a common mechanism of apoptosis in β-cells and neurons in Friedreich's ataxia', *Human Molecular Genetics*, 24(8), pp. 2274–2286. doi: 10.1093/hmg/ddu745.

Ilg, W. *et al.* (2009) 'Intensive coordinative training improves motor performance in degenerative cerebellar disease', *Neurology*, 73(22), pp. 1823–1830. doi: 10.1212/WNL.0b013e3181c33adf.

Kohwi, Y., and Kohwi-Shigematsu, T. (1991) 'Altered gene expression correlates with DNA structure', *Genes & Development*, 5(12b), 2547–2554. doi:10.1101/gad.5.12b.2547

Kemp, K. *et al.* (2017) 'Mesenchymal Stem Cell-Derived Factors Restore Function to Human Frataxin-Deficient Cells', *Cerebellum*. The Cerebellum, 16(4), pp. 840–851. doi: 10.1007/s12311-017-0860-y.

Khalil, A. M. *et al.* (2008) 'A novel RNA transcript with antiapoptotic function is silenced in fragile X syndrome', *PLoS ONE*, 3(1). doi: 10.1371/journal.pone.0001486.

Khonsari, H. *et al.* (2016) 'Lentivirus-meditated frataxin gene delivery reverses genome instability in Friedreich's ataxia patient and mouse model fibroblasts', Nature Publishing Group, 23(12), pp. 846–856. doi: 10.1038/gt.2016.61.

Kim, H. Y. *et al.* (2015) 'Discovery of a non-cationic cell penetrating peptide derived from proteins and its potential as a protein delivery carrier', *Scientific Reports*, 5(1), p.11719. doi: 10.1038/srep11719.

Koeppen, A. H. *et al.* (2007) 'The dentate nucleus in Friedreich' s ataxia: the role of iron-responsive proteins', *Acta Neuropathologica*, 114(2), pp. 163–173. doi: 10.1007/s00401-007-0220-y.

Koeppen, A. H. (2011) 'Journal of the Neurological Sciences Friedreich' s ataxia: Pathology, pathogenesis, and molecular genetics', *Journal of the Neurological Sciences*, 303(1–2), pp. 1–12. doi: 10.1016/j.jns.2011.01.010.

Koeppen, A. H. and Mazurkiewicz, J. E. (2013) 'Friedreich Ataxia: Neuropathology Revised', *Journal of neuropathology and experimental neurology,* 72(2), pp. 78–90. doi:10.1097/NEN.0b013e31827e5762.

Konkalmatt, P. R. *et al*. (2012) 'Adeno-associated virus serotype 9 administered systemically after reperfusion preferentially targets cardiomyocytes in the infarct border zone with

pharmacodynamics suitable for the attenuation of left ventricular remodeling', *The journal of gene medicine*, *14*(9-10), 609–620. https://doi.org/10.1002/jgm.2673

Kouzarides, T. (2007) 'Chromatin Modifications and Their Function', *Cell*, 128(4), pp. 693–705.

Kumar, S. R. P. *et al.* (2016a) 'Clinical development of gene therapy: results and lessons from recent successes', *Molecular Therapy - Methods & Clinical Development, 3*(December) , pp. 1–11. doi: 10.1038/mtm.2016.34.

Kumar, S. R. P. *et al.* (2016b) 'Clinical development of gene therapy: results and lessons from recent successes', *Molecular Therapy - Methods and Clinical Development*, 3(April), p. 16034. doi: 10.1038/mtm.2016.34.

Lamberson, R. C. (2015) 'Unusual Kinetic Isotope Effects of Deuterium Reinforced Polyunsaturated Fatty Acids in Tocopherol-Mediated Free Radical Chain Oxidations', *Journal of the American Chemical Society,* ,136(3), pp. 838–841. doi: 10.1021/ja410569g.

Lane, D. J. R. *et al.* (2013) 'Biochemistry of cardiomyopathy in the mitochondrial disease Friedreich's ataxia', *Biochemical Journal*, 453(3), pp. 321–336. doi: 10.1042/BJ20130079.

Lane, D. J. R. and Richardson, D. R. (2010) 'Frataxin, a molecule of mystery: trading stability for function in its iron-binding site', *Biochemical Journal*, 426(2), pp. e1–e3. doi: 10.1042/BJ20091959.

LeProust, E. M. *et al.* (2000) 'Unexpected formation of parallel duplex in GAA and TTC trinucleotide repeats of Friedreich's ataxia', *Journal of Molecular Biology*, 302(5), pp. 1063–1080. doi: 10.1006/jmbi.2000.4073.

Li, L. *et al.* (2013) 'Pharmacological Screening Using an FXN-EGFP Cellular Genomic Reporter Assay for the Therapy of Friedreich's ataxia', *PLoS ONE, 8(2), e55940*. doi: 10.1371/journal.pone.0055940.

Li, Y. *et al.* (2015) 'Excision of expanded GAA repeats alleviates the molecular phenotype of Friedreich's ataxia', *Molecular Therapy*, 23(6), pp. 1055–1065. doi: 10.1038/mt.2015.41.

Libri, V. *et al.* (2014) 'Epigenetic and neurological effects and safety of high-dose nicotinamide in patients with Friedreich's ataxia: An exploratory, open-label, dose-escalation study', *The Lancet*. Elsevier Ltd, 384(9942), pp. 504–513. doi: 10.1016/S0140-6736(14)60382-2.

Lim, F. *et al.* (2007) 'Functional Recovery in a Friedreich' s Ataxia Mouse Model by Frataxin Gene Transfer Using an HSV-1 Amplicon Vector', *Molecular Therapy,* 15(6), pp. 1072–1078. doi: 10.1038/sj.mt.6300143.

Llorens, J. V. *et al.* (2019) 'The Role of Iron in Friedreich' s Ataxia: Insights from Studies in Human Tissues and Cellular and Animal Models', *Frontiers in neuroscience*, 13(February), p. 75. doi: 10.3389/fnins.2019.00075.

Lodi, R. *et al.* (2001) 'Antioxidant Treatment Improves In Vivo Cardiac and Skeletal Muscle Bioenergetics in Patients with Friedreich' s Ataxia', Annals *of Neurology,* 49(5), pp. 590–596. doi:10.1002/ana.1001

Lozzio, B. B. et al. (1981) 'A Multipotential Leukemia Cell Line (K-562) of Human Origin', *Proceedings of the Society for Experimental Biology and Medicine*, 166(4), pp. 546–550. doi: 10.3181/00379727-166-41106.

Lundstrom, K. (2018) 'Viral Vectors in Gene Therapy'. *Diseases, 6(2),* pp*. 42.* doi: 10.3390/diseases6020042.

Lushchak, O. V. *et al.* (2014) 'Aconitase post-translational modification as a key in linkage between Krebs cycle, iron homeostasis, redox signaling, and metabolism of reactive oxygen species', *Redox Report*, 19(1), pp. 8–15. doi: 10.1179/1351000213Y.0000000073.

Lynch, D. R. *et al.* (2012) 'A0001 in Friedreich's ataxia: Biochemical Characterisation and Effects in a Clinical Trial', 27(8), pp. 1026–1033. doi: 10.1002/mds.25058.

Lynch, D. R., Perlman, S. L. and Meier, T. (2010) 'A Phase 3, Double-blind, Placebo-Controlled Trial of Idebenone in Friedreich Ataxia', *Archives of Neurology*, 67(8), pp. 941–947. doi:10.1001/archneurol.2010.168.

Mahla, R. S. (2016) 'Stem Cells Applications in Regenerative Medicine and Disease Therapeutics'. *International Journal of Cell Biology,* 2016, pp. 1–24. doi: 10.1155/2016/6940283.

Mali, S. (2013) 'Delivery systems for gene therapy', *Indian Journal of Human Genetics*, 19(1), pp. 3–8. doi: 10.4103/0971-6866.112870.

Marmolino, D. *et al.* (2009) 'PPAR-γ agonist azelaoyl PAF increases frataxin protein and mRNA expression', *Cerebellum*, 8(2), pp. 98–103. doi: 10.1007/s12311-008-0087-z.

Mccarty, D. M. (2008) 'Self-complementary AAV Vectors; Advances and Applications THE PROBLEM WITH A SINGLE-STRANDED', *YMTHE*. The American Society of Gene Therapy, 16(10), pp. 1648–1656. doi: 10.1038/mt.2008.171.

Milbrandt, T. A., Kunes, J. R. and Karol, L. A. (2008) 'Friedreich's ataxia and scoliosis: the experience at two institutions', *Journal of Pediatric Orthopaedics*, 28(2), pp. 234–238. doi: 10.1097/BPO.0b013e318164fa79\r01241398-200803000-00019 [pii].

Miller, D. G., Adam, M. A. and Miller, A. D. (1990) 'Gene transfer by retrovirus vectors occurs only in cells that are actively replicating at the time of infection.', *Molecular and Cellular Biology*, 10(8), pp. 4239–4242. doi: 10.1128/mcb.10.8.4239.

Miller, D. G., Petek, L. M. and Russell, D. W. (2004) 'Adeno-associated virus vectors integrate at chromosome breakage sites', *Nature Genetics,* 36(7), pp. 767–773. doi: 10.1038/ng1380.

Mingozzi, F. and High, K. A. (2016) ‘Review Article Immune responses to AAV vectors: overcoming barriers to successful gene therapy’, *Blood,* 122(1), pp. 23–37. doi: 10.1182/blood-2013-01-306647.

Mouse, A. Y. G. R. *et al.* (2013) ‘Frataxin Deficiency Leads to Defects in Expression of Antioxidants and Nrf2 Expression in Dorsal Root Ganglia’, 19(13). doi: 10.1089/ars.2012.4537.

Nachbauer, W. *et al.* (2012) ‘Skeletal Muscle Involvement in Friedreich Ataxia and Potential Effects of Recombinant Human Erythropoietin Administration on Muscle Regeneration and Neovascularization’, *Journal of Neuropathology & Experimental Neurology,* 71(8), pp. 708-715.doi:10.1097/nen.0b013e31825fed76

Nakai, H. *et al.* (2003) ‘AVV serotype 2 vectors preferentially integrate into active genes in mice’, *Nature Genetics,* 34(3), pp. 297–302. doi: 10.1038/ng1179.

Vallabhaneni, Krishna C *et al.* (2012) ‘Vascular Smooth Muscle Cells Initiate Proliferation of mesenchymal stem cells by mitochondrial transfer via tunneling nanotubes', *Stem cells and developmen*t, 21(17), 3104–3113. doi:10.1089/scd.2011.0691

Naphade, S. *et al.* (2016) ' Lysosomal Cross-Correction by Haematopoietic Stem Cell-Derived Macrophages Via Tunneling Nanotubes', *STEM CELLS*, 33(1), 301–309. doi:10.1002/stem.1835

Ohno, M., Fukagawa, T. and Lee, J. S. (2002) ‘Triplex-forming DNAs in the human interphase nucleus visualized in situ by polypurine / polypyrimidine DNA probes and antitriplex antibodies’, *Chromosoma*, 111(3), pp. 201–213. doi: 10.1007/s00412-002-0198-0.

Stehling, O., and Lill, R. (2013) 'The role of mitochondria in cellular iron-sulfur protein biogenesis: mechanisms, connected processes, and diseases', *Cold Spring Harbor perspectives in biology*, 5(8), pp. 1–17. doi:10.1101/cshperspect.a011312.

Palomo, G. M. *et al.* (2011) ‘Silencing of frataxin gene expression triggers p53- dependent apoptosis in human neuron-like cells’, *Human Molecular Genetics*, 20(14), pp. 2807–2822. doi: 10.1093/hmg/ddr187.

Pandolfo, M. and Hausmann, L. (2013) ‘Deferiprone for the treatment of Friedreich’s ataxia’, *Journal of Neurochemistry*, 126(SUPPL.1), pp. 142–146. doi: 10.1111/jnc.12300.

Palomo, G. M. *et al.* (2011) ‘Silencing of frataxin gene expression triggers p53- dependent apoptosis in human neuron-like cells’, *Human Molecular Genetics*, 20(14), pp. 2807–2822. doi: 10.1093/hmg/ddr187.

Pandolfo, M. and Hausmann, L. (2013) ‘Deferiprone for the treatment of Friedreich’s ataxia’, *Journal of Neurochemistry*, 126(01), pp. 142–146. doi: 10.1111/jnc.12300.

Papers, J. B. C. *et al.* (2001) 'Sticky DNA, a Self-associated Complex Formed at Long GAA·TTC Repeats in Intron 1 of the Frataxin Gene, Inhibits Transcription', *Journal of Biological Chemistry*, 276(29), pp. 27171–27177. doi:10.1074/jbc.m101879200

Pastore, A. (2013) 'Frataxin: a protein in search for a function', J*ournal of Neurochemistry*, 126, pp. 43—52. doi:10.1111/jnc.12220

Patel, S. G. *et al.* (2019) 'Cell-penetrating peptide sequence and modification dependent uptake and subcellular distribution of green florescent protein in different cell lines', *Scientific Reports*, (January), pp. 1–9. doi: 10.1038/s41598-019-42456-8.

Paul, B. T. *et al.* (2017) 'Mitochondria and Iron: current questions', *Expert Review of Hematology*, 10(1), pp. 65–79. doi: 10.1080/17474086.2016.1268047.

Paupe, V. *et al.* (2009) 'Impaired nuclear Nrf2 translocation undermines the oxidative stress response in Friedreich's ataxia', *PLoS ONE*, 4(1). doi: 10.1371/journal.pone.0004253.

Payne, R. M. and Wagner, G. R. (2012) 'of Child Neurology Cardiomyopathy in Friedreich Ataxia', *Journal of Child Neurology*, (July). doi: 10.1177/0883073812448535.

Peng, C. *et al.* (2019) 'Factors influencing recombinant protein secretion efficiency in gram-positive bacteria: Signal peptide and beyond', *Frontiers in Bioengineering and Biotechnology*, 7(JUN), pp. 1–9. doi: 10.3389/fbioe.2019.00139.

Perdomini, M. *et al.* (2014) 'Prevention and reversal of severe mitochondrial cardiomyopathy by gene therapy in a mouse model of Friedreich' s ataxia', *Nature Medicine,* 20(5), pp. 542–547. doi: 10.1038/nm.3510

Peters, J. M., Tedeschi, A. and Schmitz, J. (2008) 'The cohesin complex and its roles in chromosome biology', *Genes and Development*, 22(22), pp. 3089–3114. doi: 10.1101/gad.1724308

Peters, J. M., Tedeschi, A. and Schmitz, J. (2008) 'The cohesin complex and its roles in chromosome biology', *Genes and Development*, 22(22), pp. 3089–3114. doi: 10.1101/gad.1724308.

Piguet, F. et al. (2018) 'Rapid and Complete Reversal of Sensory Ataxia by Gene Therapy in a Novel Model of Friedreich Ataxia', Molecular Therapy, 26(8), pp. 1940–1952. doi: 10.1016/j.ymthe.2018.05.006.

Potaman, V. N. *et al.* (2004) 'Length-dependent structure formation in Friedreich ataxia (GAA) n ´ (TTC) n repeats at neutral pH', *Nucleic Acids Research*, 32(3), pp. 1224–1231. doi: 10.1093/nar/gkh274.

Pousset, F. *et al.* (2015) 'A 22-Year Follow-up Study of Long-term Cardiac Outcome and Predictors of Survival in Friedreich Ataxia', JAMA Neurology, pp. 1–8. doi: 10.1001/jamaneurol.2015.1855.

Press, P. and Doi, R. (2017) 'Iron – sulfur cluster biogenesis and trafficking in mitochondria', 292, pp. 12754–12763. doi: 10.1074/jbc.R117.787101.

Priller, J. *et al.* (2001) 'Targeting gene-modified haematopoietic cells to the central nervous system: Use of green fluorescent protein uncovers microglial engraftment', *Nature Medicine*, 7(12), pp. 1356–1361. doi: 10.1038/nm1201-1356.

Puccio, H. *et al.* (2001) 'Mouse models for Friedreich ataxia exhibit cardiomyopathy, sensory nerve defect and Fe-S enzyme deficiency followed by intramitochondrial iron deposits', *Nature Genetics,* 27(february), pp. 181–186. doi:10.1038/84818

Rapoport, M., Salman, L. and Sabag, O. (2011) 'Successful TAT-mediated enzyme replacement therapy in a mouse model of mitochondrial E3 deficiency', pp. 161–170. doi: 10.1007/s00109-010-0693-3.

Richardson, D. R. *et al.* (2010) 'Mitochondrial iron trafficking and the integration of iron metabolism between the mitochondrion and cytosol', *Proceedings of the National Academy of Sciences*, 107(24), pp. 10775–10782. doi: 10.1073/pnas.0912925107.

Ristori, G., Romano, S. and Visconti, A. (2010) 'Riluzole in cerebellar ataxia', *Neurology*, 74, pp. 839–845. doi: 10.1212/WNL.0b013e3181d31e23.

Robertson, K. D. (2001) 'DNA methylation, methyltransferases, and cancer', *Oncogene*, 20(24), pp. 3139–3155. doi:10.1038/sj.onc.1204341

Rocca, C. J. *et al.* (2015) 'Treatment of Inherited Eye Defects by Systemic Haematopoietic Stem Cell Transplantation', *Investigative Opthalmology & Visual Science,* 56(12), pp. 7214-7223. doi: 10.1167/iovs.15-17107.

Rocca, Celine J. *et al.* (2017) 'Transplantation of wild-type mouse haematopoietic stem and progenitor cells ameliorates deficits in a mouse model of Friedreich's ataxia', *Science Translational Medicine*, 9(413). doi: 10.1126/scitranslmed.aaj2347.

Roe, T. *et al.* (1993) 'Integration of murine leukemia virus DNA depends on mitosis.', *The EMBO Journal*, 12(5), pp. 2099–2108. doi: 10.1002/j.1460-2075.1993. tb05858.x.

Rouault, T. A. (2012) 'Biogenesis of iron-sulfur clusters in mammalian cells: New insights and relevance to human disease', *DMM Disease Models and Mechanisms*, 5(2), pp. 155–164. doi: 10.1242/dmm.009019.

Rouault, T. a and Tong, W.-H. (2005) 'Iron-sulphur cluster biogenesis and mitochondrial iron homeostasis.', *Nature reviews. Molecular cell biology*, 6(4), pp. 345–351. doi: 10.1038/nrm1620.

Rufini, A. *et al.* (2011) 'Preventing the ubiquitin-proteasome-dependent degradation of frataxin, the protein defective in Friedreich's ataxia', *Human Molecular Genetics*, 20(7), pp. 1253–1261. doi: 10.1093/hmg/ddq566.

Sakamoto, N. *et al.* (1999) 'Sticky DNA: Self-Association Properties of Long GAA · TTC Repeats in R · R · Y Triplex Structures from Friedreich' s Ataxia', *Molecular Cell,* 3(4), pp. 465–475. doi:10.1016/s1097-2765(00)80474-8.

Santos, R. *et al.* (2010) 'Friedreich Ataxia: molecular mechanisms, redox considerations, and therapeutic opportunities', *Antioxidants & redox signaling*, 13(5), pp. 651–690. doi:10.1089/ars.2009.3015

Sanz-gallego, I., Torres-aleman, I. and Arpa, J. (2014) 'IGF-1 in Friedreich' s Ataxia – proof-of-concept trial'. *Cerebellum & ataxias*, 1 (July), p. 10. doi:10.1186/2053-8871-1-10

Saveliev, A., Everett, C. and Sharpe, T. (2003) 'DNA triplet repeats mediate variegated gene silencing', *Nature*, 3528(1998) pp. 909-913. doi:10.1038/nature01596.

Schmucker, S. *et al.* (2008) 'The in vivo mitochondrial two-step maturation of human frataxin', *Human Molecular Genetics*, 17(22), pp. 3521–3531. doi: 10.1093/hmg/ddn244.

Schöls, L. *et al.* (1997) 'Friedreich's ataxia. Revision of the phenotype according to molecular genetics', *Brain*, 120(12), pp. 2131–2140. doi: 10.1093/brain/120.12.2131.

Schott, J. W. *et al.* (2019) 'Enhancing Lentiviral and Alpharetroviral Transduction of Human Haematopoietic Stem Cells for Clinical Application', *Molecular Therapy - Methods and Clinical Development*. Elsevier Ltd., 14(9), pp. 134–147. doi: 10.1016/j.omtm.2019.05.015.

Schulz, J. B. *et al.* (2009) 'Diagnosis and treatment of Friedreich's ataxia: a European perspective', *Nature Reviews Neurology*, 5(4), pp. 222–234. doi: 10.1038/nrneurol.2009.26.

Schulz, W. A., Steinhoff, C. and Florl, A. R. (2006) 'Methylation of endogenous human retroelements in health and disease', *Current Topics in Microbiology and Immunology*, 310, pp. 211–250. doi: 10.1007/3-540-31181-5_11.

Sclip, a *et al.* (2014) 'c-Jun N-terminal kinase has a key role in Alzheimer disease synaptic dysfunction in vivo.', *Cell death & disease*. Nature Publishing Group, 5(1), p. e1019. doi: 10.1038/cddis.2013.559.

Sisakhtnezhad, S. and Khosravi, L. (2015) 'Emerging physiological and pathological implications of tunneling nanotubes formation between cells', *European Journal of Cell Biology*, 94(10), pp. 429–443. doi: 10.1016/j.ejcb.2015.06.010.

Snyder, E. L. *et al.* (2004) 'Treatment of terminal peritoneal carcinomatosis by a transducible p53-activating peptide', *PLoS Biology*, 2(2), pp. 186–193. doi: 10.1371/journal.pbio.0020036.

Sorbi, S. *et al.* (2000) 'Double-Blind, Crossover, Placebo-Controlled Clinical Trial with L-Acetylcarnitine in Patients with Degenerative Cerebellar Ataxia', *Clinical Neuropharmacology,* 23(2), pp. 114–118. doi:10.1097/00002826-200003000-00010

Stewart, K. M., Horton, K. L. and Kelley, S. O. (2008) 'Cell-penetrating peptides as delivery vehicles for biology and medicine', *Organic and Biomolecular Chemistry*, 6(13), pp. 2242–2255. doi: 10.1039/b719950c.

Sturm, B. *et al.* (2005) 'Recombinant human erythropoietin: Effects on frataxin expression in vitro', *European Journal of Clinical Investigation*, 35(11), pp. 711–717. doi: 10.1111/j.1365-2362.2005.01568.x.

Sung, Y. K. (2019) 'Recent advances in the development of gene delivery systems', Biomaterials *Research*, 23(1), p. 8). doi:10.1186/s40824-019-0156-z

Syres, K. *et al.* (2016) 'Successful treatment of the murine model of cystinosis using bone marrow cell transplantation', *Blood*, 114(12), pp. 2542–2553. doi: 10.1182/blood-2009-03-213934.

Thennarasu, S. *et al.* (2010) 'Antimicrobial and membrane disrupting activities of a peptide derived from the human cathelicidin antimicrobial peptide ll37', *Biophysical Journal*. Biophysical Society, 98(2), pp. 248–257. doi: 10.1016/j.bpj.2009.09.060.

Ting, D. T. *et al.* (2013) 'Aberrant Overexpression of Satellite Repeats in Pancreatic and Other Epithelial Cancers', Science, 331(6017), pp. 593–596. doi:10.1126/science.1200801

Tretter, L. and Adam-vizi, V. (2000) 'Inhibition of Krebs Cycle Enzymes by Hydrogen Peroxide : A Key Role of α -Ketoglutarate Dehydrogenase in Limiting NADH Production under Oxidative Stress', *The Journal of Neuroscience*20(24), pp. 8972–8979.

Tripathi, P. P. *et al.* (2018) 'Cell penetrating peptides in preclinical and clinical cancer diagnosis and therapy', *Oncotarget,* 9(98), pp. 37252–37267. doi:10.18632/oncotarget.26442

Tsai, C. L. and Barondeau, D. P. (2010) 'Human frataxin is an allosteric switch that activates the Fe-S cluster biosynthetic complex', *Biochemistry*, 49(43), pp. 9132–9139. doi: 10.1021/bi1013062.

Tsirikos, A. I. and Smith, G. (2008) 'Scoliosis in patients with Friedreich' s ataxia', *The Journal of Bone and Joint Surgery,* 94(5), pp*. 684–689. doi: 10.1302/0301-620X.94B5.28391.*

Tsou, A. Y. *et al.* (2011) 'Mortality in Friedreich Ataxia', *Journal of the Neurological Sciences*, 307(1–2), pp. 46–49. doi: 10.1016/j.jns.2011.05.023.

Vallabhaneni, Krishna C *et al.* (2012) 'Vascular Smooth Muscle Cells Initiate Proliferation of mesenchymal stem cells by mitochondrial transfer via tunneling nanotubes', *Stem cells and developmen*t, 21(17), 3104–3113. doi:10.1089/scd.2011.0691

Vannucci, L. *et al.* (2013) 'Viral vectors: a look back and ahead on gene transfer technology', *New Microbial*, 36(1):1-22. pp. 1–22. Available at: http://www.ncbi.nlm.nih.gov/pubmed/ 23435812

Villa, R. F. *et al.* (1988) 'Action of L-Acetylcarnitine on Age-Dependent Modifications of Mitochondrial Membrane Proteins from Rat Cerebellum', *Neurochemical Research,* 13(10), pp. 909–916. doi:10.1007/bf00970761

Vivès, E., Schmidt, J. and Pèlegrin, A. (2008) 'Cell-penetrating and cell-targeting peptides in drug delivery', *Biochimica et Biophysica Acta - Reviews on Cancer*, 1786(2), pp. 126–138. doi: 10.1016/j.bbcan.2008.03.001.

Vyas, P. M. *et al.* (2012) 'A TAT-frataxin fusion protein increases lifespan and cardiac function in a conditional Friedreich's ataxia mouse model', *Human Molecular Genetics*, 21(6), pp. 1230–1247. doi: 10.1093/hmg/ddr554.

Walden, W. E. (2002) 'From bacteria to mitochondria: aconitase yields surprises', Proceedings of the National Academy of Sciences of the United States of America, 99(7), pp. 4138–4140. doi:10.1073/pnas.082108799.

Wang, F. et al. (2012) 'Biodistribution and Safety Assessment of Bladder Cancer Specific Recombinant Oncolytic Adenovirus in Subcutaneous Xenografts Tumor Model in Nude Mice', Current Gene Therapy, (82), pp. 67–76. doi: 10.2174/156652312800099599.

Wang, X. and Rivière, I. (2017) 'Genetic Engineering and Manufacturing of Haematopoietic Stem Cells', *Molecular Therapy - Methods & Clinical Development*, 5(June), pp. 96–105. doi: 10.1016/j.omtm.2017.03.003.

Whitnall, M. *et al.* (2008) 'The MCK mouse heart model of Friedreich ' s ataxia : Alterations in iron-regulated proteins and cardiac hypertrophy are limited by iron chelation', *Proceedings of the National Academy of Sciences of the United States of America,* 105(28), 9757–9762. doi:10.1073/pnas.0804261105

Wong, a *et al.* (1999) 'The Friedreich's ataxia mutation confers cellular sensitivity to oxidant stress which is rescued by chelators of iron and calcium and inhibitors of apoptosis.', *Human molecular genetics*, 8(3), pp. 425–430. doi: 10.1093/hmg/8.3.425.

Yang, D. *et al.* (2013) 'Intranasal delivery of cell-penetrating anti-NF-??B peptides (Tat-NBD) alleviates infection-sensitized hypoxic-ischemic brain injury', *Experimental Neurology*, 247, pp. 447–455. doi: 10.1016/j.expneurol.2013.01.015.

Yeagy, B. A. *et al.* (2011) 'Kidney preservation by bone marrow cell transplantation in hereditary nephropathy', *Kidney International*. Nature Publishing Group, 79(11), pp. 1198–1206. doi: 10.1038/ki.2010.537.

Yoder, J. A., Walsh, C. P. and Bestor, T. H. (1997) 'Cytosine methylation and the ecology of intragenomic parasites', *Trends in Genetics*, 13(8), pp. 335–340. doi: 10.1016/S0168-9525(97)01181-5.

Yoon, T. and Cowan, J. A. (2003) 'Iron-sulphur cluster biosynthesis. Characterisation of frataxin as an iron donor for assembly of [2Fe-2S] clusters in ISU-type proteins', *Journal of the American Chemical Society*, 125(20), pp. 6078–6084. doi: 10.1021/ja027967i.

Yoon, T. and Cowan, J. A. (2004) 'Frataxin-mediated iron delivery to ferrochelatase in the final step of heme biosynthesis', *Journal of Biological Chemistry*, 279(25), pp. 25943–25946. doi: 10.1074/jbc.C400107200.

Zange, J. *et al.* (2005) 'L-carnitine and creatine in Friedreich' s ataxia. A randomized, placebo-controlled crossover trial', *Journal of Neural Transmission,* 112(6), pp. 789–796. doi: 10.1007/s00702-004-0216-x.

Zhao, H. *et al.* (2017) 'Peptide SS-31 upregulates frataxin expression and improves the quality of mitochondria: implications in the treatment of Friedreich's ataxia', *Scientific Reports*. Springer US, (August), pp. 1–11. doi: 10.1038/s41598-017-10320-2.